MIT
Open Access Articles

Concentrating Solar Power

Citation	Weinstein, Lee A. et al. "Concentrating Solar Power." Chemical Reviews 115.23 (2015): 12797–12838.
As Published	http://dx.doi.org/10.1021/acs.chemrev.5b00397
Publisher	American Chemical Society (ACS)
Version	Author's final manuscript
Accessed	Sat Mar 30 09:34:03 EDT 2019
Citable Link	http://hdl.handle.net/1721.1/106513
Terms of Use	Article is made available in accordance with the publisher's policy and may be subject to US copyright law. Please refer to the publisher's site for terms of use.
Detailed Terms	

Concentrating Solar Power

Lee A. Weinstein,[1] James Loomis,[1,2] Bikram Bhatia,[1] David M. Bierman,[1] Evelyn N. Wang,[1] and Gang Chen*,[1]

[1]*Department of Mechanical Engineering, Massachusetts Institute of Technology, Cambridge, MA, 02139, USA.*

[2]*Department of Mechanical Engineering, University of Auckland, Auckland 1010, New Zealand.*

Table of Contents

1. INTRODUCTION

Solar energy is a bountiful renewable energy resource: the energy in the sunlight which reaches Earth in an hour exceeds the energy consumed by all of humanity in a year.[1] While the phrase "solar energy conversion" probably brings photovoltaic (PV) cells to mind first, PV is not the only option for generating electricity from sunlight. Another promising technology for solar energy conversion is solar-thermal conversion, commonly referred to as concentrating solar power (CSP).[2] The first utility-scale CSP plants were constructed in the 1980s, but for the following two decades CSP saw little expansion.[3,4] More recent

3

years, however, have seen a CSP renaissance due to unprecedented growth in the adoption of CSP.[3,5] Photos of two operating CSP plants, a parabolic trough collector plant and a central receiver (or "power tower"), are shown in Figure 1.
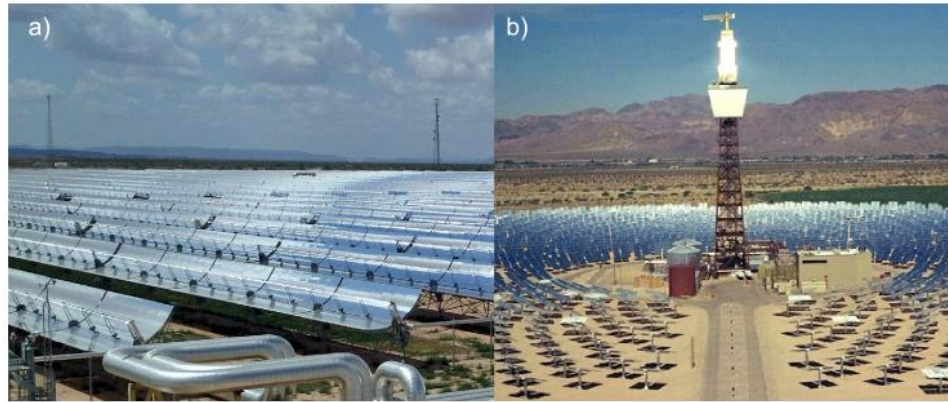
Figure 1 Photos of two CSP plants: a) Solana Generating Station (proprietary technology of Abengoa Solar, S.A.), a parabolic trough collector plant in Phoenix, Arizona (original photo by James Loomis) and b) Solar Two, a "power tower" plant near Barstow, California. Reprinted with permission from reference [6]. Copyright 2015 Elsevier.

There are five steps to a conventional CSP system (illustrated in Figure 2):

1. Concentration: sunlight incident on a large concentrator is redirected to a much smaller receiver
2. Absorption: sunlight incident on the receiver is converted to heat by an absorber
3. Transfer: heat is carried away from the absorber by a heat transfer fluid (HTF)
4. Storage: heat can be stored in a thermal energy storage (TES) tank for later use
5. Generation: the HTF delivers heat to a heat engine which generates electricity

It is worth noting that there are many uses for thermal energy and solar thermal systems are not limited to electricity generation,[7] however this review will be limited in scope to address technologies which generate electricity. Transfer, the third step on this list, is not strictly necessary for CSP systems (e.g., the absorber can be directly coupled to the heat engine), however all currently operating utility-scale CSP plants use heat transfer fluids. Storage, the fourth step on this list, is optional for CSP systems, however it is one of the primary advantages compared to other renewable electricity technologies, and as such is an important step to cover.
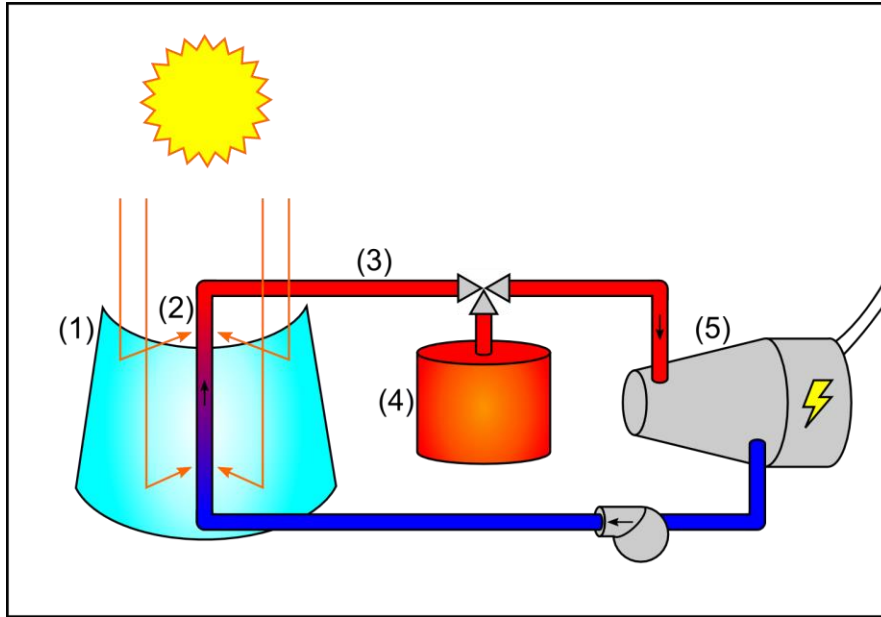
Figure 2 Illustrated components of a conventional CSP system: 1) concentrator 2) receiver 3) heat transfer fluid 4) thermal energy storage and 5) heat engine

Similar to most renewable energy technologies at the time of writing, CSP is not cost-competitive with conventional fossil-fuel technologies without the aid of governmental subsidies or regulatory advantages.[8] To reach cost parity with conventional energy sources (i.e., fossil fuels), advances which reduce CSP plant construction costs and improve CSP plant efficiency are needed.[9] Given current cost estimates for CSP generated electricity, reaching parity would require about half the current plant cost or double the current efficiency (realistically a combination of both reduced cost and increased efficiency will be pursued).[10] An important piece of the economics of CSP plants is system design (e.g., navigating the tradeoff between the size of the plant power block and the size of the concentrator field),[9] however this review will not focus on these issues. Rather, this review will provide a brief overview of the main types of CSP plants, cover basic CSP operating principles, and focus on materials issues concerning the performance of CSP components. Since cost is the primary driver of utility-scale CSP technology, improvements purely in performance are not sufficient for commercial adoption. Rather than efficiency, the primary figure of merit for a CSP plant is the Levelized Cost Of Energy (LCOE, sometimes also called Levelized Cost Of Electricity or Levelized Energy Cost), which represents the cost of electrical

energy produced from the plant (typically given in units of cents/kWhr) including capital costs and operations and maintenance costs.[11,12] Thus, in addition to efficiency, affordability and reliability are very important to the feasibility of new CSP solutions.

1.1.   CSP Configurations

There are a number of configurations which are commonly used as concentrators for CSP systems. The first step of concentrating sunlight from a concentrator to a receiver is not necessary for all solar-thermal applications, however for electricity generation it is almost always a requirement. CSP systems require concentration to be efficient, as otherwise system losses would be dominated by the large receiver areas at the high temperatures required to drive a heat engine efficiently. The level of concentration can be characterized by the concentration ratio, which is the ratio of the concentrator aperture area (the large mirror area intercepting sunlight) to the receiver aperture area (the small receiver area where the sunlight is redirected). Because concentration is required, CSP can only use the direct portion of sunlight (diffuse sunlight cannot be concentrated easily) which limits the best locations for CSP plants to areas with high average annual direct normal irradiation.[13] Due to the solar progression across the sky (daily in the east-west direction and both daily and seasonally in the north-south direction) two-axis tracking is required to maintain a concentrator normal to the sun. With two-axis tracking sunlight can be focused approximately to a point ("point-focus"). While the sun has both east-west and north-south movement, most of its daily movement is in the east-west direction. If one only tracks a concentrator in the east-west direction, sunlight can be focused approximately to a line ("line-focus"). Both line-focus and point-focus concentrators can be found in commercial use.[14] Point-focus systems can achieve higher concentration ratios (~1,000×), but the required two-axis solar tracking is more complex and more expensive to implement. Line-focus systems have lower concentration ratios (~80×) but use simpler, less expensive one-axis solar tracking.

Another distinction between different types of concentrators is whether the collecting surface is continuous or made up of discrete facets. Concentrators with continuous surfaces can achieve higher

concentration ratios, as there is no sunlight lost between facets, and tracking is simpler since only one surface needs to be actuated. When using a continuous surface, the focal axis should always intersect both the receiver and the sun, so the receiver is typically mounted with the reflector in one assembly, limiting the receiver size. Concentrators with discrete facets can cover a greater area since the receivers can be stationary (they do not need to be tracked with the reflecting surfaces). Additionally, wind loading is typically a smaller concern for discrete facets since they can be kept closer to the ground (the stationary receivers in this case are still elevated so wind loading should be considered, but they are less susceptible to damage than reflector elements).

The four combinations of these two distinctions (point-focus vs. line-focus and continuous surface vs. discrete facets) result in the four primary concentrators for CSP systems: Parabolic trough collectors (PTC), linear Fresnel reflectors (LFR),[15,16] parabolic dish reflectors and heliostat fields, which are all shown in Figure 3. In a parabolic trough collector, a long, curved, trough-shaped mirror tracks the sun from east to west and concentrates sunlight on a pipe at the focus of the curved mirror, with the whole assembly rotating together. In a linear Fresnel reflector, long mirrors tracking the sun from east to west reflect sunlight onto a fixed, raised receiver. The "Fresnel" in this concentrator's name originates from the many reflector elements approximating a continuous curve, as in a Fresnel lens. With a parabolic dish, the sun is tracked on both axes across the sky, and sunlight is focused on a receiver which moves with the dish, such that it is always on-axis with the sun. In a heliostat field, individual mirrors track the sun across the sky to reflect sunlight to a central, raised receiver. Thus, PTCs and LFRs are line-focus systems, while parabolic dish reflectors and heliostat fields are point-focus, and PTCs and parabolic dishes use continuous surfaces, while LFRs and heliostat fields use discrete facets. It should be noted that parabolic dish systems sometimes have discrete reflector facets which form the overall parabolic shape, but since these facets are fixed in position relative to each other, they can be effectively considered a continuous reflective surface. While these characteristics in principle only determine the concentrator of the CSP

system, in practice the concentrator type determines many of the operating conditions of the overall system.

This connection between concentrator type and plant operating conditions is a result of the concentrator being paramount in determining the receiver concentration ratio and the overall plant size. As an example, parabolic dish plants are almost ubiquitously referred to as dish Stirling systems, due to how commonly they are paired with a Stirling engine to convert heat to electricity.[17] Similarly, plants which use a heliostat field as the concentrator are often called power tower or central receiver systems, referring to the large tower where sunlight is focused at the center of the field.
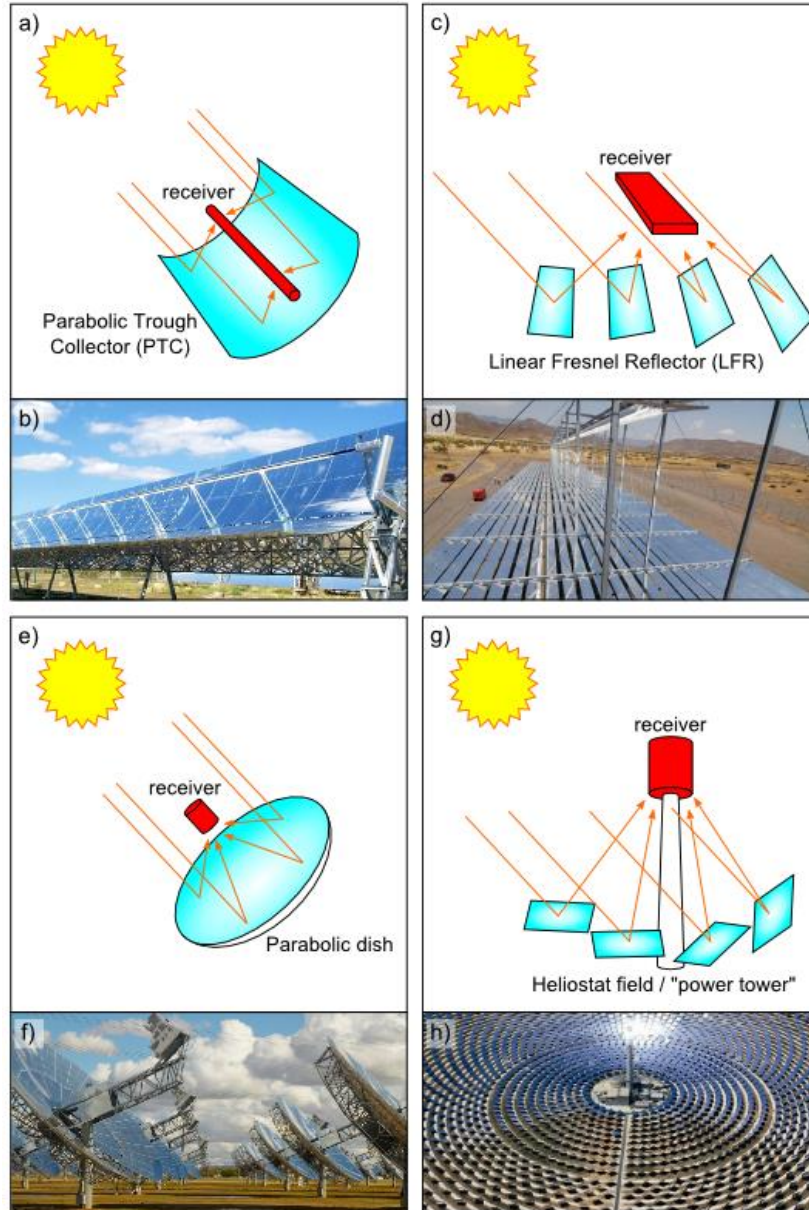
Figure 3 Illustrations and photos of CSP plant configurations: a) illustration of a parabolic trough collector, b) photo of a PTC reprinted with permission from reference [18]. Copyright 2012 Elsevier. c) illustration of a linear Fresnel reflector, d) photo of the FRESDEMO LFR project demonstration at Plataforma Solar de Almeria in Spain reprinted with permission from reference [16]. Copyright 2014 Elsevier. e) illustration of a parabolic dish, f) photo of Maricopa Solar project in Arizona reprinted with permission from reference [6]. Copyright 2015 Elsevier. g) illustration of a heliostat field ("power tower") plant and h) photo of Solar Tres in Sevilla, Spain reprinted with permission from reference [6]. Copyright 2015 Elsevier

While in principle lenses can also be used as the concentrating element in a solar concentrator, there has been limited deployment in CSP primarily due to higher cost per area than reflector systems, and difficulties in making precise lenses at the large scales required for CSP. Significant progress has been

made in optical designs of Fresnel lenses, and Fresnel lenses have seen use in commercial concentrated PV (CPV) systems.[19] However, in order for Fresnel lenses to achieve substantial adoption in CSP, they would need to be made larger and cheaper.

To give an idea of the basic characteristics of the different types of CSP plants, Table 1 has typical LCOE, annual efficiency, peak efficiency, operating temperature, and concentration ratio of the four types of CSP systems. It should be noted that the values reported here are characteristic of the concentrator type, but individual plants may have different values. Here peak efficiency refers to the highest instantaneous solar to electricity efficiency achieved (typically during solar noon) while annual efficiency (annual electrical energy output divided by annual solar energy incident on the solar concentrators during operating hours) considers the effect of daily and seasonal variation on performance, and is a more relevant to LCOE than peak efficiency. It is difficult to assign characteristic LCOE values, as estimated LCOE values for the different CSP technologies vary widely by reference, even when only considering the LCOE of electricity generated by utility-scale plants currently in operation.[13,14,20,21] This uncertainty is somewhat exacerbated by the limited number of plants operating for all the technologies besides parabolic trough collectors. While the current cost of electricity from CSP is greater than the cost from conventional sources, many parties are optimistic about significant LCOE reduction in the next decade for CSP.[13,21,22]

Table 1 Typical performance metrics for the four primary CSP plant configurations[10,13,14,21,23–26]

	LCOE [USD/kWh]	Annual efficiency [%]	Peak efficiency [%]	Operating temperature [°C]	Concentration ratio
PTC	0.16 – 0.40	14	25	400	80
Heliostat / Power Tower	0.13 – 0.30	16	22	400 – 600	1000
LFR	0.14 – 0.45	13	18	300 – 400	30

Parabolic Dish	No commercial plants	20	32	550 – 750	1500

PV currently has the largest deployment among solar electricity technologies, with the LCOE of electricity from PV quickly dropping over the past decade,[3] but there are a few differences between CSP and PV that make CSP worth pursuing even given the lower cost of PV. Many of the practical differences arise due to the fact that CSP plants use well-established turbine technologies to generate electricity. Turbines have much different scaling than PV systems, and become more efficient and cost effective with increasing size, so CSP can excel in large installations. On the other hand, this limits small plants, and there are effectively no options for residential scale CSP installations (an area where PV shines). A large hurdle for constructing CSP plants is financing them, as capital costs are very high (typical plant construction costs are in excess of $1 billion USD) and payback periods are long for CSP projects.[27] If CSP could operate efficiently and cost effectively in small-scale plants, it would lower the capital costs required to undertake a CSP project and accelerate the learning cycles for CSP technologies. Another interesting opportunity for CSP that arises from its use of conventional turbine generators is that CSP can be retrofitted onto existing fossil fuel plants to reduce their fuel consumption and replace that input with solar energy.[28,29] A significant advantage that CSP has over PV, which arises from its intermediary use of heat, is the potential for thermal storage.[30] With a PV system, electricity is only produced when the sun is shining on the PV cells. Production of electricity is interrupted when a cloud passes over the PV panels and when the sun sets. For a PV system, if electricity is desired when the sun is not shining then collected electricity must be stored, but rechargeable battery technology is very expensive, which limits the potential to use PV with storage in practice. In contrast, CSP systems can store the thermal energy they collect inexpensively, which can be converted to electricity later on demand. By using thermal storage, electricity can be produced from solar thermal systems reliably even when the sun is no longer shining on the collector, which increases the value of CSP plants.[31] A recent study by Jorgenson, et al. found that

electricity produced by CSP with storage could be more than twice as valuable to a utility provider than electricity produced from PV.[32] Additionally, while the price of PV and batteries are dropping, CSP with thermal storage is predicted to be cheaper than PV with battery storage.[33]

While CSP has not seen as widespread adoption as PV, it does account for a non-trivial amount of current global renewable electricity generation. By 2013, there were about 3.4 GW of installed CSP operational capacity worldwide, with the great majority in the USA and Spain.[3] Most of the current installed capacity uses parabolic trough collectors, however the CSP technologies being installed are diversifying. As an example, the largest CSP plant in operation (both in terms of land area and peak power output) is the BrightSource Ivanpah plant, which uses a heliostat field concentrator. Some of the most notable plants currently operating are listed in Table 2. As it is the most mature technology, many of the largest companies in CSP work with PTCs (sometimes in addition to other technologies) such as Abengoa Solar, Acciona, Rioglass, Schott Solar, and Torresol Energy. There are also large companies that work with power tower plants (e.g., BrightSource and SolarReserve), as well as LFR technologies (e.g., Areva Solar and Novatec Solar), driven by the potential for lower LCOE. While there are no commercial scale parabolic dish plants currently operating, a few companies are working with this technology – such as Ripasso Energy for dish Stirling systems and Heliofocus for hybridization with coal plants.

Table 2 Large and notable operating CSP plants[34]

Name	Gross capacity (MW)	Location	Concentrator type	Operational since	Notes
Ivanpah	392	San Bernardino, CA, USA	Heliostat / Power Tower	2014	
SEGS	354	Mojave Desert, CA, USA	PTC	1984	
Mojave Solar	280	Barstow, CA,	PTC	2014	

Project		USA			
Solana Generating Station	280	Gila Bend, AZ, USA	PTC	2013	6 h thermal storage
Genesis Solar Energy Project	250	Blythe, CA, USA	PTC	2014	
Solaben	200	Logrosan, Spain	PTC	2012	
Solnova	150	Sanlucar la Mayor, Spain	PTC	2010	
Andasol	150	Guadix, Spain	PTC	2008	7.5 h thermal storage
Extresol	150	Torre de Miguel Sesmero, Spain	PTC	2010	7.5 h thermal storage
Dhursar	125	Dhursar, India	LFR	2014	
Martin Next Generation Solar Energy Center	75	Indiantown, FL, USA	PTC	2010	Integrated solar combined cycle
Puerto Errado	31.4	Murcia, Spain	LFR	2009	

1.2. Maximum efficiency of a CSP system

A natural question which arises when considering CSP is "what is the highest efficiency a CSP system can achieve?" While LCOE is more important in practice, efficiency is a strong lever of LCOE, and finding maximum efficiency is a tractable thermodynamics problem (whereas finding minimum LCOE is not). The maximum efficiency can be determined most easily by separating system efficiency into two

sub-efficiencies: the sunlight to heat conversion process (receiver efficiency) and the heat to electricity conversion process. The receiver efficiency is calculated as the absorbed heat minus any losses divided by the solar power incident on the receiver. A simplified version of receiver efficiency η_{rec} (which will be discussed further in section 3) assuming the only loss is radiation from the absorbing surface (the only thermodynamically required loss) is given by:

$$\eta_{rec} = \alpha - \frac{\epsilon\sigma(T_H^4 - T_{amb}^4)}{\eta_{coll}CG} \tag{1}$$

where α is receiver absorptance, ϵ is receiver emittance, σ is the Stefan-Boltzmann constant, T_H is the receiver temperature, T_{amb} is the ambient temperature, η_{conc} is the concentrator efficiency (ratio of sunlight directed to the receiver by the concentrator divided by sunlight incident on the concentrator), C is concentration ratio, and G is the solar insolation. The efficiency of the heat to electricity conversion process is well known to be limited at the Carnot efficiency. In the case where the heat engine converts at Carnot efficiency, the total efficiency is thus given by the product of the receiver efficiency and Carnot efficiency:

$$\eta = \left(\alpha - \frac{\epsilon\sigma(T_H^4 - T_{amb}^4)}{\eta_{conc}CG}\right)\left(1 - \frac{T_{amb}}{T_H}\right) \tag{2}$$

One ideal receiver would be a blackbody absorber with the maximum possible concentration ratio incident on it. While it may not be immediately clear why a maximum concentration ratio exists, from a thermodynamics standpoint this arises because arbitrarily high concentration ratios could lead to arbitrarily high temperatures.[35] At some point this would lead to heat flowing from the sun to an absorber hotter than the sun, violating the second law of thermodynamics. From an optical standpoint, the limited concentration ratio arises from the finite solid angle of the sun in the sky on Earth, leading to a non-zero divergence angle of sunlight at the Earth's surface. If, by contrast, there was an infinitesimal point source illuminating the Earth with perfectly collimated radiation, it would be possible to concentrate that light to an arbitrarily high ratio. The maximum value of $\eta_{coll}CG$ is thus the flux at the surface of the sun (σT_{sun}^4),

which assumes a concentrator efficiency of unity and the maximum concentration ratio. The efficiency of such an ideal system can therefore be given by

$$\eta = \left(1 - \frac{T_H^4 - T_{amb}^4}{T_{sun}^4}\right)\left(1 - \frac{T_{amb}}{T_H}\right) \tag{3}$$

It is typical to take T_{amb} to be 300 K (27 °C) and T_{sun} to be 5800 K (~5500 °C, the apparent sun surface temperature). Using these values, efficiency is maximized when T_H is set at 2480 K (~2200 °C) which yields an efficiency of about 85%. Systems today fall short of this efficiency for a number of reasons. An obvious reason is that the Carnot limit cannot be reached for practical heat engines. Another reason is that current systems do not operate at ~2200 °C, due to the limited stability of absorbers, heat transfer fluids, and heat engines. Finally, current solar receivers are not perfect. There are other ways to achieve a perfect receiver besides the maximum concentration that was explored in this exercise, but all current technologies fall short of ideal performance (other techniques for improving receiver efficiency will be discussed in section 3). This review addresses research areas where performance can be brought closer to ideal, and some of the associated challenges.

This review paper will discuss different subcomponents of a CSP system in the order that energy transfers through the CSP system: concentrator/reflector (section 2), receiver/absorber (section 3), heat transfer fluid (section 4), thermal storage (section 5) and heat engine (section 6). Each section will cover the properties required for high performance, the current state of the art used in the field, and current research directions to improve performance even further.

2. CONCENTRATOR/REFLECTOR

The concentrator of a CSP system uses reflector facets to optically concentrate solar energy and direct this concentrated flux to the receiver. The concentrator consists of a combination of reflector, structural or

supporting elements, and a one-axis (for PTC and LFR) or two-axis (for dish and helisostat) tracking system.[36] Concentrators are used in CSP systems because concentration is required for efficient conversion at high operating temperatures,[37] however there are additional benefits such as reducing the amount of costly receiver materials needed. While mirror materials are usually much less expensive than the materials used for the receiver on a per area basis, the concentrator typically accounts for the largest amount of capital investment among all subsystems in a CSP project.[38] As such, concentrator systems present an attractive target for cost reduction.[39] Furthermore, reflector cost makes up approximately half of the concentrator cost, so low cost mirrors are an ongoing area of research.[40] Reflectors with lower cost, improved optical performance, higher durability, and lower maintenance/cleaning requirements are highly desirable and represent key areas of research. This section begins with a discussion of the important characteristics of concentrators and reflectors, then reviews the materials commonly used in reflectors, and finally discusses challenges with reflector degradation and methods for its prevention.

2.1.   Concentrator characteristics

A concentrator can be characterized by its concentration ratio and concentrator efficiency. The geometric concentration ratio refers to the ratio of the concentrator aperture area (the large mirror area intercepting sunlight) to the receiver aperture area (the small receiver area where the sunlight is redirected). Stated more intuitively, it is the maximum possible ratio that the concentrator is designed to concentrate sunlight to, so a concentrator with a geometric concentration ratio of 10× aims to provide a radiative flux ten times that of direct sunlight to the receiver. One-axis systems typically have concentration ratios less than 100× while two-axis systems typically have concentration ratios greater than 500×. It should be noted that by this definition, PTC concentration ratio is typically around 80-100×, however if the receiver surface area (given by PTC tube receiver circumference) is used rather than receiver aperture area (given by tube diameter) then the concentration ratio will be smaller by a factor of π, and some literature follows this

convention.[41] The concentrator efficiency refers to the ratio of sunlight that reaches the receiver divided by the sunlight incident on the concentrator. Concentrator efficiency drops below unity in real systems due to imperfect reflector materials and challenges associated with varying solar elevation (e.g., cosine losses from angled reflectors when the sun is low in the sky). The optical properties of the reflectors and the design of the concentrator (e.g., placement of heliostats relative to the central receiver[42,43]) are both important to achieving high concentrator efficiency, however this review only focuses on reflector properties.

Ideally all concentrators would be able to achieve extremely high concentration ratios, however in practice the concentration ratio is limited due to the finite divergence angle of sunlight on earth (as previously mentioned in section 1.2). The maximum achievable concentration ratio C_{max} is determined by the rim angle of the concentrator ψ_{rim} and given by conservation of etendue:[35]

$$C_{max,1ax} = \frac{\sin\psi_{rim}}{\sin\theta_{sun}} \tag{4}$$

$$C_{max,2ax} = \left(\frac{\sin\psi_{rim}}{\sin\theta_{sun}}\right)^2 \tag{5}$$

where $C_{max,1ax}$ and $C_{max,2ax}$ are the maximum concentration ratios for one-axis and two-axis systems respectively, and θ_{sun} is the divergence half angle of sunlight on earth (approximately 4.8 mrad or 0.275°).[44] The rim angle refers to the largest angle at which reflected sunlight from the concentrator strikes the receiver (see Figure 4(a)). For a flat receiver, the largest possible rim angle is $\pi/2$, which corresponds to sunlight incoming from the entire hemispherical solid angle the receiver is exposed to. For such a receiver, the maximum attainable concentration ratios are approximately 210× for a one-axis system and 43000× for a two-axis system. Real concentrators cannot achieve such high concentration ratios due to imperfect tracking and imperfections in reflector surfaces.
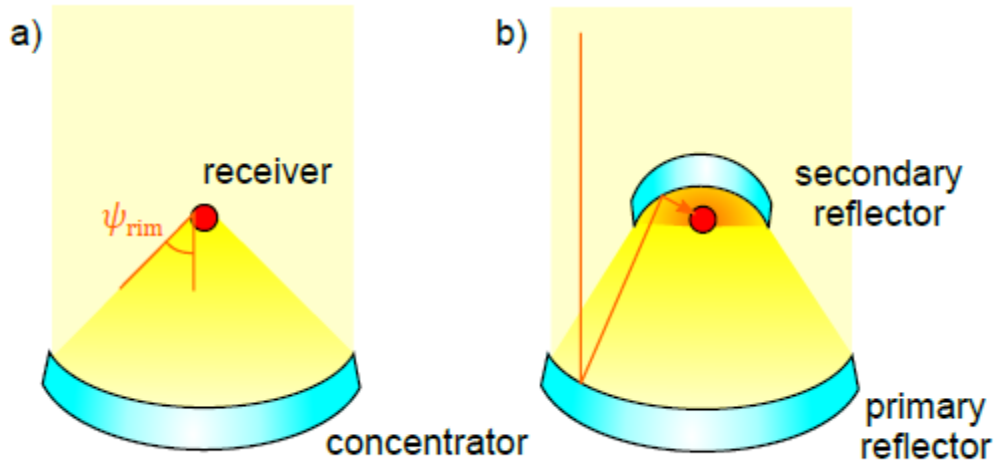
Figure 4 Diagram illustrating a) concentrator rim angle ψ_{rim} and b) secondary reflector concept. The rim angle is the largest angle that reflected sunlight from the concentrator strikes the receiver. A secondary reflector concentrates flux from the primary reflector further before directing it to the receiver

Reflector geometry can take a number of forms in the solar thermal system between line-focus and point-focus as well as continuous and faceted concentrators. For continuous surfaces, the reflectors need to be curved in order to concentrate sunlight, whereas faceted surfaces can use curved or flat reflectors. From the names of the continuous surfaces ("parabolic trough collector" and "parabolic dish") it is clear that a parabolic geometry is common for concentrators. Parabolic geometries are used because a parabola will reflect collimated rays to a point,[45] and therefore sunlight, which is close to collimated, can be focused to small area by a parabolic reflector. In practice, parabolic geometries are sometimes approximated by spherical surfaces, which can be easier to manufacture. Because sunlight is not perfectly collimated, better concentrator performance can be achieved by using principles of non-imaging optics. For example, the compound parabolic concentrator (CPC), which incorporates two different parabolic sections in the one-axis case, can reach maximum solar concentration in theory.[35] Faceted surfaces can focus sunlight with flat reflectors because the overall geometry still approximates a curved surface, however using curved surfaces will allow improved performance.[38,46] In addition to the primary reflectors described above, some systems utilize a secondary optical concentrator to further concentrate the sunlight before it reaches the receiver (see Figure 4(b)). While the potential for improved performance is promising,

18

secondary concentrators are exposed to additional stresses beyond those experienced by the primary mirror, including higher radiation fluxes and elevated temperatures.[37]

2.2. Optical properties and characterization

Low-cost and robust reflector materials are required in order to maintain high specular reflectance properties while exposed to harsh outdoor oxidizing/corrosive environmental conditions (such as heat, humidity, wind loading, salt spray, etc.) over the 10 – 30 year system lifetimes.[47] As summarized by Brogren *et al*., concentrating reflectors must fulfill a number of different, and often times competing, roles. These roles include aspects such as providing high reflectance of incident solar radiation onto the receiver/absorber; maintaining high reflectance values over the system lifetime; low cost; low operation and maintenance (O&M) costs; and high mechanical strength (suitable to handle wind/snow loading, etc.). Furthermore, mirrors should be lightweight, utilize environmentally benign fabrication techniques and construction methods (or at least low impact compared to competing technologies), and to some extent they should be aesthetically pleasing (depending on proximity to high population density areas).[48]

The primary optical property of importance for a reflector in a CSP concentrator is specular reflectance. In specular reflection, the reflected ray leaves the surface at the same angle which the incident ray struck the surface (with respect to the surface normal) and the incident, reflected and surface normal directions are coplanar (see Figure 5). Stated more simply, specular reflection is the reflective behavior one would expect of a mirror. This is in contrast to diffuse reflection, in which the reflected rays are scattered into all directions. Specular reflection is the only useful component of reflection for CSP concentrators because it allows incident direct sunlight to be redirected and concentrated, whereas diffuse reflection will almost entirely be lost to the surroundings. Furthermore, the only component of light that can be concentrated is

direct illumination, diffuse or scattered radiation (e.g., sunlight on a cloudy day when the sun is blocked)

is not concentrated.[49,50]
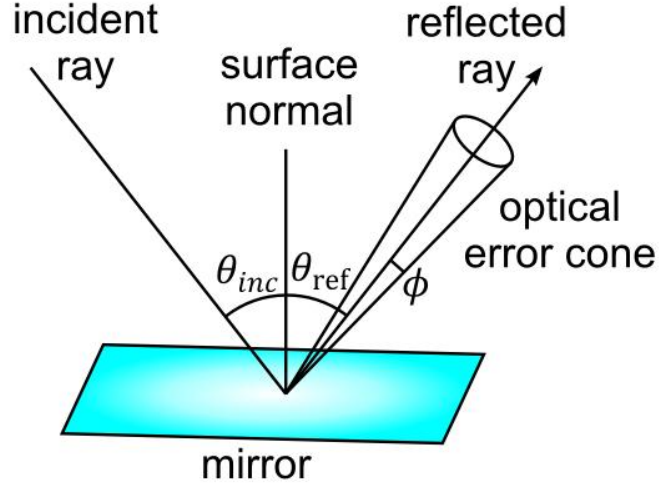
Figure 5 Illustration of specular reflectance and how it is measured. In specular reflection, the incidence angle θ_{inc} and reflection angle θ_{inc} of the reflected ray are equal with respect to the surface normal, and the incident ray, reflected ray and surface normal are coplanar. In measurements, reflected radiation is considered specular if it falls within the optical error cone of the reflected ray, defined by the divergence half angle ϕ

Three parameters that define the specular reflectance of a solar mirror are the wavelength of radiation (λ),

incidence angle (θ_{inc}), and optical error (ϕ).[51] The optical error refers to the divergence from the angle of

reflection that is acceptable to still be considered specular reflection (nominally a 4 mrad half cone angle

for two-axis systems and a 12.5 mrad half cone angle for one-axis systems, see Figure 5).[47] A smaller

optical error allows higher concentration ratios to be reached, but also requires more precise control of

reflector surface roughness. For a given wavelength, incidence angle, and optical error, specular

reflectance $\rho_{s,\theta,\lambda}$ is defined as the fractional proportion of an incident collimated beam reflected such that

the angle of reflectance is equal to the angle of incidence, within the optical error.[36] The solar weighted

specular reflectance ρ_s can be calculated by integrating over the solar spectrum (with incidence angle

typically taken as near normal to the mirror):[52]

$$\rho_s = \frac{1}{G\pi\phi^2} \int_0^\infty \int_{\Omega_s} \rho_{s,\theta,\lambda}(\theta_{inc}, \lambda) G_\lambda(\lambda) d\Omega d\lambda \qquad (6)$$

where G is the solar insolation and Ω_s is the solid angle of the reflected cone (reflected angle with error cone given by optical error ϕ). Specular reflectance can be affected by properties such as micro-roughness in the reflector surface, crazing of protective topcoats, and impurities in protective glass – all of which can reduce optical performance via reflectance of light outside of the target angle.[47]

Testing of optical properties and knowledge of reflector degradation over the system lifetime is essential to ensure adequate performance. Furthermore, thorough testing helps identify failure areas or weak points in material properties or fabrication techniques and enables targeting those specific areas for future research and development. NREL initiated an outdoor testing program in 1994, with the German Aerospace center (DLR) and Spanish research center (CIEMAT) joining in 1995 and 1996 respectively.[40] DLR, CIEMAT, and NREL developed a clear definition of the method and requirements needed of commercial instruments for reliable reflectance results.[53] For specular reflectance measurements, they recommend the use of a UV-Vis-NIR spectrophotometer. A round robin test performed between the three laboratories showed surprisingly large differences (given that these labs developed and followed the measurement standards) in hemispherical reflectance (ρ_h, ratio of sunlight reflected in any direction to incident sunlight) of up to 0.02 and specular reflectance (ρ_s) of up to 0.015 between the laboratories, indicating the importance of standardized testing procedures (for reference, the measured reflectance values were typically around 0.95 and the measurement uncertainty within a single lab was less than 0.005). Karim et al. pointed out that there is no mechanical durability standard related to the site exposure conditions, so they researched geologic and climate parameters to determine which ones most influenced surface wear rate of the solar mirrors.[54] They then defined an approach to determine these parameters on potential deployment sites, helping to evaluate potential mirror damage that would be expected at a particular site.

Due to the importance of concentrator performance in deployed systems, a number of methods have been developed to test the optical properties of reflectors installed in operating plants. These methods include

commercially available reflectometers which can be used to point check the specular reflectance of mirrors in the field, such as the 15R specular reflectometer from Devices and Services Instruments.[55] Sutter et al. developed a spatially resolved reflectometer to monitor corrosion of solar reflectors which is able to measure properties over a relatively large area (5 cm diameter spot) at a resolution of 37 pixels/mm.[51] Using a non-reflectometer approach, Valenzuela et al. presented a method to test optical performance of large scale parabolic-trough collectors which uses an energy balance on the heat transfer fluid to measure concentrator efficiency, and demonstrated this method on a PTC prototype at the Plataforma Solar de Almería (PSA) in Spain.[56]

2.3.   Reflector materials

A number of different methods are used to construct the reflector facets for CSP concentrators. These methods include the application of reflective coatings on the back of glass (back surface reflectors, see Figure 6(a) and (b)) and the application of reflective coatings on substrates (front surface reflectors, see Figure 6(c) and (d)). Silver and aluminum have the best reflectance (~97% and 92% respectively),[48] and as such are the most common coating materials used as the reflecting layers in CSP concentrators. While glass has been the traditional choice for use as a superstrate mirror material in CSP systems, other materials are presenting viable alternatives,[57] such as coated aluminum reflectors (Figure 6(c)) and polymeric film reflectors (Figure 6(d)).[58] Of the candidate materials, silver coated glass (Figure 6(a) and (b)) and silvered polymer films (Figure 6(d)) dominate.[47] Advantages to using glass generally include a higher level of performance than other options, as well as ability to maintain high performance levels for relatively long lifetimes.[57] Disadvantages to using glass (both thin and thick) can include fragility, weight, formability, and thermal expansion mismatch between glass and other layers.[57] Furthermore, the use of silver in reflectors requires careful protection from the environment,[59] which can be accomplished

through the incorporation of additional glass layers, metal coatings, or polymer stabilizers.[59] Conversely, silvered polymer reflectors address some of the issues inherent with glass, and introduce greater design flexibility, lighter weight, and potential for lower cost – albeit with several unsolved problems such as poor adhesion, lower performance and current costs higher than targets.[47] Table 3 summarizes the advantages and challenges associated with each major reflector type.

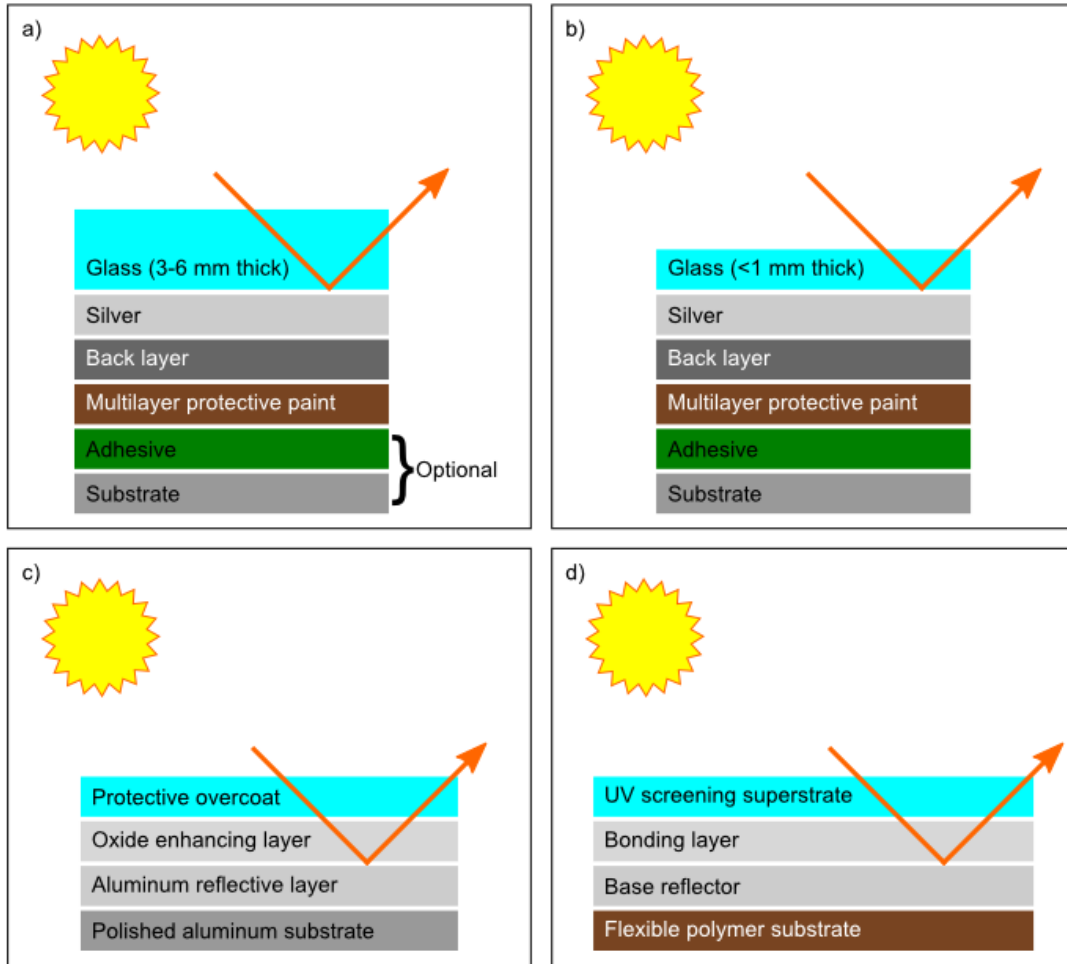**Figure 6 Examples of reflector construction:** a) **thick glass mirror, b) thin glass mirror,** c) **aluminum reflector, and d) polymer substrate reflector. Adapted with permission from reference** [47]. **Copyright 2005 American Society of Mechanical Engineers.**

Table 3 Advantages and challenges associated with the major reflector types

Reflector type	Primary advantage	Challenges

Thick glass mirror	High performance and good durability	Heavy
Thin glass mirror	Reduced weight	Fragility, reduced durability
Aluminum reflector	Reduced cost	Poor long term durability
Polymer substrate reflector	Reduced cost and weight	Durability and adhesion issues

Thick glass mirrors (Figure 6(a)), which refer to mirrors where the glass is thicker than 1 mm have demonstrated excellent durability, but at the cost of increased difficulties such as breakability, formability, brittleness, expansion, and weight.[48,57] Thick glass mirrors were deployed in the SEGS plants, which utilized Flabeg thick glass mirrors.[60,61] Mirrors produced after 2003 employ a low-lead paint system with the lead content reduced to the point where durability was anticipated to remain constant.[60] Construction of thick glass mirrors consists of the following layers: >1 mm thick low-iron glass with a reflective wet-silver layer, copper back layer, 2.5% lead paint layer, 1% lead intermediate paint, and finally an acrylic-based final coat.[47] The backing layers are used to protect the silver layer, which is susceptible to airborne pollutants and tarnishing, and use of the copper and protective layers has been found to significantly extend the lifetime of the reflectors.[47]

An alternative configuration, which uses a copper-less backing layer, also has lower lead content paint layers (<0.15%, originally developed for interior applications), followed by an adhesive layer and finally the substrate. Testing showed durability of these mirrors to be equivalent to the higher lead counterparts.[60] Accelerated testing indicated non-mirror back-protective paint applied after the mirrors were manufactured was not beneficial. While more environmentally friendly, the manufacturing process using the copper-free backing layer necessitates very strict quality control.[60] Additional types of thick glass

reflectors include Pilkington (UK, 4 mm) and Cristaleria Espanola S.A (Spain, 3 mm) with reflectances of 93.3% and 92.8% respectively.

In trying to address formability issues associated with glass mirrors (that is, difficulty in manufacturing the mirrors to be the desired shape), Angel et al. reported on a new method using radiative heating to shape the solar concentrator mirrors.[62] This high volume manufacturing method can be applicable to both point and line concentration. They successfully demonstrated their radiative heating approach using thick glass mirrors (4 mm).

Conversely, thin glass mirrors (Figure 6(b)) utilize <1 mm thick low-iron glass, a wet-silvered reflective layer, either copper or copper-free back layers, and lead-free paints.[60] For reflector materials, current state of the art systems use mechanically flexed thin (<1 mm) glass with a silver backing.[15] They typically have reflectances of 93% to 96%.[47] While lighter than thick glass mirrors, thin glass mirrors are more susceptible to chemical attack.[48] Naturally, this thinner structure is also more fragile, which increases handling difficulty and can negatively impact overall system costs.[47] As was noted by Kennedy and Terwilliger, a critical factor in performance degradation is the choice of adhesive and ensuring adequate edge protection – both of which can reduce the thin glass durability.[47]

Butel et al. investigated methods to increase the reflectance of silver back surface reflectors.[63] They found that a dielectric enhancing layer sandwiched between the silver and glass can improve performance at shorter wavelengths. At longer wavelengths, use of glass with low iron content further enhances reflectance.[63] Small amounts of iron impurities in the glass can cause it to absorb in the red and infrared, therefore the use of low iron content glasses is preferable. They reported an (absolute) increase in specular reflectance of 2.7% (CPV systems using triple junction cells) to 4.4% (full solar spectrum average), with a drawn crown glass and a silvered second-surface having 95.4% reflectance.[63]

While glass has been the traditional choice for use as a mirror material in CSP systems, other materials are presenting viable alternatives to achieve performance, cost, and reliability targets.[57] For example,

aluminum based reflectors (Figure 6(c)) use an aluminum substrate with an enhanced aluminum reflector layer topped by a protective coating (to prevent oxidation).[47] Reflectors using anodized or coated aluminum have good mechanical properties, are easily recyclable, offer initial reflectance values around 87-91%, are relatively low cost, and provide greater design flexibility.[48] However, they offer subpar durability long term, and unprotected surfaces will quickly degrade. To alleviate this issue, an anodizing layer (Al_2O_3) helps to protect the surface and increase reflector lifetime.[48]

Braendle reported that Alanod-Solar high efficiency metal mirrors (fabricated using a continuous air-to-air PVD process) achieve a reflectance of 95%.[57] This high value is achieved via the addition of a highly reflective layer to the aluminum substrate. Mirrors with an anodized aluminum substrate, a PVD aluminum reflective layer and a protective oxide topcoat to enhance reflectivity have inadequate durability.[60] While an additional polymeric overcoat improves the hemispherical durability, specularity is degraded. Recent NREL testing of aluminum mirrors (Alanod-Solar metal-based MIRO-SUN) over a three year period showed an average decrease of <1% in specular reflectance (measured on a 25 mrad half cone angle).[57] Brogren et al. proposed laminating a thin sheet of aluminum onto a steel substrate, therefore taking advantage of the high reflectance of aluminum and the rigidity of steel, and resulting in a cost reduction due to the more rigid structure.[48]

Fend et al. studied anodized/coated sheet aluminum and found they have solar weighted reflectances of 88–91%, good mechanical properties and are easy to recycle.[40] However, problems occur due to their limited corrosion resistance. In this study the optical properties were investigated for a number of different aluminized reflector materials after accelerated and outdoor exposure tests.[40] Materials tested included standard commercial anodized sheet aluminum with layers of different thicknesses and standard high specular aluminum with a metal-oxide layer system plus an anti-oxidation polymer coating.[40] Results show that optical degradation is strongly dependent on climatic conditions.

Recently, silvered polymer reflectors have been introduced (Figure 6(d)) which feature a polymer (PMMA) film with an evaporated silver reflective layer, a protective copper layer, and an adhesive layer (for attachment to a support structure).[47] Advantages to using acrylic reflectors include design flexibility, good weathering characteristics and good optical characteristics. Drawbacks include brittleness, and difficulty in adhesion between the polymer and the silver reflective layer resulting in delamination in rainy conditions.[47] ReflecTech, another polymer based reflector material, is fabricated from a flexible, polymer-based silver film, and supplied on a roll and co-developed with NREL.[64] This material has a specular reflectance of 94%.[64] Advantages to this material include low cost, light weight (3.6 kg/m^2), and flexibility.

2.4. Reflector degradation

Maintaining high concentrator efficiency is critical to a plant continuing to operate at high performance over the course of its lifetime, intended to exceed 30 years. For concentrator efficiency to remain high, the shape and specular reflectance of the reflectors must not degrade significantly over the long time scale of their operation. Specular reflectance is sensitive to the roughness of the mirror surface, and even small surface scratches and aberrations can diminish it, which is part of why reflector degradation is such a challenge. Reflectance can be reduced by delamination of the layered mirror structures and corrosion/oxidation of the reflecting metal layers, which is why so much of the construction is focused on protecting the reflective layer. Concentrator performance can also degrade from environmental factors: dust on the reflectors, mechanical deformation from wind loading, and weathering from environmental factors such as rain, humidity, temperature variations and UV radiation can all negatively impact performance. Reflectors are tested after aging has occurred in order to characterize their degradation with time. While ideally the aging conditions would match what is experienced in a deployed CSP plant, in order to obtain results in a timely manner accelerated aging is often used, where the reflectors are

subjected to controlled temperature, humidity and UV radiation cycling over a faster period than the diurnal cycling experienced in the field.[37,40,65]

Brogren et al. conducted accelerated aging research on optical properties of solar reflector materials.[65] They found that silvered glass fared very well in accelerated testing, with almost no change in optical properties after 2000 hours in the climatic test chamber. Anodized aluminum, thin film-coated aluminum, and lacquered rolled aluminum remained specularly reflecting after the tests, but had reduced performance (reflectance decreased by ~10%, ~5% and ~20%, respectively). Tests on laminated evaporated aluminum reflectors showed that reflectance, which was specular initially, became diffuse (<10% solar weighted specular reflectance).[65] These laminated and lacquered reflectors performed better in accelerated aging tests than unprotected thin film-coated and anodized aluminum – which show significant degradation.[65] Thus it was found that optical degradation depends both on the protective layer used and on environmental conditions. Brogren's work shows that discrepancies between results from outdoor and accelerated aging test demonstrate that a thorough understanding of corrosion processes is necessary in order to draw concrete conclusions regarding long-term performance.[65]

Fend et al. report on long-term durability tests of reflector materials in coordination with IEA–SolarPACES, NREL, USA, the Centro de Investigaciones Energeticas, Medioambientales y Tecnologicas (CIEMAT, Spain) and Deutsches Zentrum fur Luft- und Raumfahrt (DLR, Germany).[40] They conducted accelerated aging tests on a number of materials at various testing sites. They identified various silvered glass mirrors, a silvered polymer film, and an anodized sheet aluminum (featuring an additional protective polymer coating) as promising materials for long term durability (reflectances stayed within ~5% of the starting value after 48-84 months of testing).[40] Fend et al. determined that from more than 50 different reflector configurations, corrosion is the most severe factor limiting reflector lifetimes.[40]

Secondary concentrators are exposed to harsher conditions (higher incident flux, and therefore higher temperature) than primary reflectors, making degradation an even more important concern. Fernández-

García et al. published research about the durability of solar reflector materials used in secondary concentrators.[37] They simulated reflector degradation due to a combination of ambient environmental conditions and high concentrated irradiation. Their results showed that aluminum reflectors and thin silvered-glass reflectors glued to an aluminum structure showed minimum reflectance losses (<5%) and structural degradation (in a cooled secondary concentrating tower system). Furthermore, they identified three critical aspects to minimize degradation, including choice of adhesive material (for gluing silvered-glass reflectors), proper reflector edge protection, and a suitable cooling system and to avoid coupling high radiation fluxes with mechanical stress. Silvered-glass reflectors were shown to be suitable for uncooled 2D secondary concentrators in LFR systems.[37]

Dust accumulation can greatly affect performance of the reflectors used in CSP plants, as the dust will absorb or diffusely scatter incident sunlight (rather than the desired outcome of specular reflection), and dust is common in regions with high DNI sunlight that is desirable for CSP operation (e.g., deserts). Many studies have been published on the effects of dust accumulation on the performance of solar energy conversion systems, the interested reader is referred to a review by Sarver et al. for a thorough overview.[66] Currently, the most common method for dealing with dust accumulation is cleaning the reflector surfaces with water ("wet-cleaning"): as one example, Hegazy studied effects of dust accumulation on solar transmittance and recommended weekly cleaning of the glass surfaces.[67]

Wet-cleaning is not an ideal solution, as it is labor intensive and requires large amounts of water in areas where water is typically scarce (e.g., deserts).[66] Thus, an exciting area of current research is the investigation of so-called "self-cleaning" properties of glass surfaces which reduce the tendency of dust or pollutants to accumulate. A common approach is using the catalytic properties of TiO_2 nano-particle doped porous glass layers and semiconductor thin films on transparent glass substrates, whereby dirt is broken down photocatalytically which enables it to be washed away more easily (e.g., with rain).[59] Using another technique, Kim et al. demonstrated an inverted nanocone array in polyurethane acrylate (PUA) which had good optical and mechanical properties, as well as non-wetting and self-cleaning behavior.[68]

The same research group has also demonstrated improved transmission as well as superhydrophobicity in nanotextured glass surfaces.[69] Another technique is using an electrodynamic screen (EDS) to clean dust off reflectors. An EDS consists of thin parallel transparent conducting electrodes on a transparent dielectric surface, and can remove dust particles by charging them with high voltage pulses through the electrodes and subsequently propelling them away via electrostatic forces. Mazumder et al. reported an EDS which can restore a reflector to >95% of its original specular reflectance in less than two minutes using less than 1 Wh/m^2 of electrical energy per reflector area.[70] A commercially scalable self-cleaning surface which did not sacrifice optical performance or surface robustness could greatly improve the performance of CSP concentrators by reducing the detrimental effects of dust accumulation.

3. RECEIVER/ABSORBER

The receiver is the portion of a CSP system where the concentrated sunlight from the concentrator is focused. The receiver always has an absorber (where sunlight is converted to heat), often has piping which carries a heat transfer fluid to deliver the heat to storage or the heat engine, and can also include transmitting or reflecting optics. The purpose of the receiver is to efficiently convert sunlight to heat. This section will first review the principles behind achieving high receiver efficiency and then cover technologies used for absorbers and receivers in CSP systems.

3.1. Receiver efficiency

The usable heat Q_H is the heat absorbed by the receiver minus any heat losses, given by:

$$Q_H = \eta_{conc}CG\tau\alpha A - \epsilon\sigma A\left(T_H^4 - T_{amb}^4\right) - hA(T_H - T_{amb}) \qquad (7)$$

where η_{conc} is the concentrator efficiency, C is the concentration ratio, G is the solar insolation, τ is the receiver transmittance (if it has any transmitting optics, e.g., a glass aperture window), α is the absorptance of the absorber, A is the area of the absorber, ϵ is the emittance of the absorber, σ is the

Stefan-Boltzmann constant, h is the convection coefficient between the absorber and ambient, and T_H and T_{amb} are the absorber and ambient temperatures, respectively. Here losses are separated into radiative and convective losses, and all heat conducted out of the receiver is assumed to be delivered into the heat transfer fluid. In practice, receivers need to be designed such that conduction, convection, and radiation losses from non-absorbing portions of the receiver are all minimized.[71,72] Many studies have been performed to accurately measure these losses from receivers,[9,73,74] however, for investigating absorbers in this review only the simplified treatment above will be considered. In practice, aperture area can also play an important role in receiver efficiency: larger apertures (for a fixed concentrator) lead to higher thermal losses, but less spillage (incident sunlight from the concentrator missing the receiver aperture). The receiver efficiency can be found by dividing the usable heat by the solar energy incident upon it:

$$\eta_{rec} = \frac{Q_H}{\eta_{conc}CGA} = \tau\alpha - \frac{\epsilon\sigma(T_H^4 - T_{amb}^4) + h(T_H - T_{amb})}{\eta_{conc}CG} \tag{8}$$

The first term gives the portion of sunlight incident on the absorber which is absorbed and converted to heat. The second and third terms are the losses from the absorber (radiative and convective, respectively) normalized by the incident flux. A high efficiency receiver requires high transmittance, absorptance and concentration, and low emittance and convection. In practice, there is a tradeoff between many of these factors as well as with cost. Receiver efficiency decreases with increasing absorber temperature, however a high absorber temperature is desired because delivering the heat transfer fluid at higher temperatures leads to better heat to electricity conversion efficiency (see section 6 for further discussion).

Receiver designs and operating temperatures are very different for line-focus versus point-focus systems, since the achievable concentration ratios differ largely. This point is illustrated by Figure 7 which shows receiver efficiency as a function of concentration ratio for different receivers. The first is simply a blackbody absorber, which absorbs all light incident upon it, but has the maximum losses. Alternate receivers include an evacuated enclosure (suppressing convective losses but incurring transmission losses through the enclosure walls, typically glass) and a spectrally selective absorber, which has low IR

emittance but slightly lower solar absorptance than a blackbody absorber. At low concentration ratios (<500× in this particular case), the spectrally selective absorber and evacuated enclosure lead to the highest efficiency. While both lead to a slightly worse 1st term of Eq. (5), the reduction of the losses far outweighs the reduction in absorbed light. For high concentration ratios (>500×), the blackbody absorber is most efficient, since relative losses are naturally low due to the high concentration ratio.
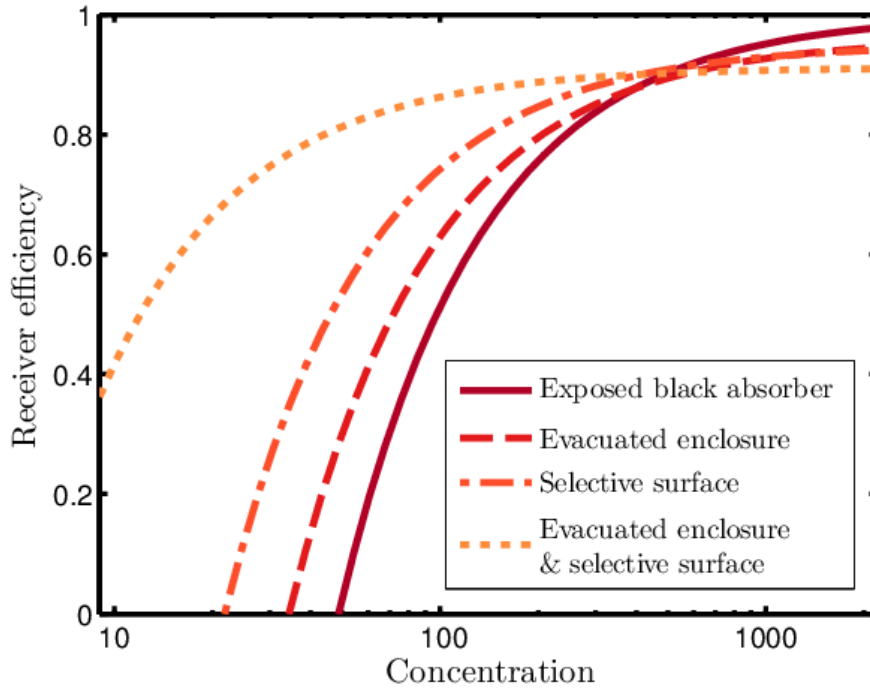

Figure 7 Receiver efficiency vs. concentration for various receivers at 500 °C. Product of insolation and concentrator efficiency $\eta_{conc}G$ is set to 600 W/m². In the base case of an exposed black receiver transmittance, absorptance and emittance are all set to unity and convective heat transfer coefficient h is set to 20 W/m²/K. The evacuated enclosure has a reduced transmittance of 0.96 and reduced h of 0 W/m²/K. The selective surface has a reduced absorptance of 0.95 and a reduced emittance of 0.15. In the concentration regime of line-focus systems the evacuated, spectrally-selective receiver performs best. In the concentration regime of point-focus systems, the exposed black absorber performs best. It should be noted that in practice lower concentration systems (<100×) would typically operate at lower temperatures than 500 °C, while higher concentration systems (>500×) would typically operate at higher temperatures

Therefore, for line-focus systems, with concentration ratios typically <100×, it is most common to use spectrally selective surfaces inside vacuum enclosures for the best performance. These systems are limited to around 500 °C for efficient operation (and in practice often lower due to HTF stability). With point focus systems, much higher concentration ratios can be achieved (~1,000×). This allows for higher operating temperatures, and the denominator in the 2nd term of the equation keeps losses low relative to

32

absorbed insolation. Thus for point-focus systems the primary concern is high absorptance, for maximizing the first term in Eq. (8). Additionally, at high temperatures and concentrations reliability is a much more difficult issue, and it is significantly easier to achieve good high temperature stability with a simple black receiver than other systems.

3.2.   Spectrally selective surfaces

The goal of an absorber is to effectively absorb sunlight with minimal thermal losses. The ideal absorber therefore has high solar absorptance but low emittance at its operating temperature. This goal is complicated by Kirchhoff's law of thermal radiation, which mandates that for a given surface in a specified direction and at a specific wavelength, absorptance and emittance must be equal. If this did not hold, the 2nd law of thermodynamics could be broken by allowing for radiative heat flow from a cold surface to a hotter surface. Even with Kirchhoff's law, high solar absorptance can be achieved with low emittance by leveraging spectral or directional selectivity. Total absorptance and emittance are given by integrating over directional and spectral properties:[52]

$$\alpha = \frac{2}{G \sin^2 \theta_{inc}} \int_0^\infty \int_0^{\theta_{inc}} \alpha_{\theta,\lambda}(\theta,\lambda) \cos\theta \sin\theta\, G_\lambda(\lambda) d\theta d\lambda \qquad (9)$$

$$\epsilon = \frac{2}{\sigma T^4} \int_0^\infty \int_0^{\pi/2} \epsilon_{\theta,\lambda}(\theta,\lambda) \cos\theta \sin\theta\, E_{b\lambda}(T,\lambda)\, d\theta\, d\lambda \qquad (10)$$

where θ is the incidence angle of radiation (a subscript of θ denotes angular properties), θ_{inc} is the maximum incidence angle of sunlight on the absorber, λ is the wavelength of radiation (a subscript of λ denotes spectral properties), $E_{b\lambda}$ is the blackbody emissive spectrum, and with $\alpha_{\theta,\lambda}(\theta,\lambda) = \epsilon_{\theta,\lambda}(\theta,\lambda)$ from Kirchhoff's law. For example, with spectral selectivity, one can take advantage of the relatively small overlap between the solar spectrum and the blackbody emittance spectrum at typical CSP absorber operating temperatures.
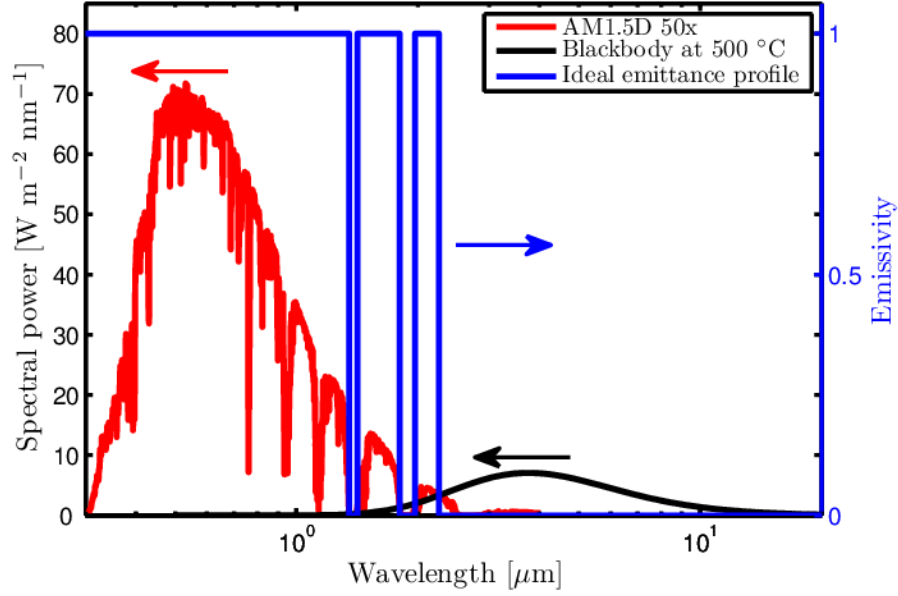
Figure 8 Spectral power of solar spectrum at 50× (red curve) compared to a blackbody at 500 °C (black curve). Ideal emittance spectrum for a solar absorber under these conditions is plotted as well, taking a value of unity when the solar spectral power is greater and a value of zero when the blackbody spectral power is greater (blue curve, right axis)

If the receiver efficiency is cast assuming only radiative losses it can be re-written:

$$\eta_{rec} = \tau\alpha - \frac{\epsilon\sigma T^4}{\eta_{coll}CG} \tag{11}$$

In addition, if only wavelength selectivity is considered (i.e., assuming no angular dependence) then total absorptance and emittance are given by:

$$\alpha = \frac{1}{G}\int_0^\infty \epsilon(\lambda)G_\lambda(\lambda)d\lambda \tag{12}$$

$$\epsilon = \frac{1}{\sigma T^4}\int_0^\infty \epsilon(\lambda)E_{b\lambda}(T,\lambda)d\lambda \tag{13}$$

Combining these into the receiver efficiency yields:[75]

$$\eta_{rec} = \frac{1}{\eta_{coll}CG}\int_0^\infty \epsilon(\lambda)[\tau\eta_{coll}CG_\lambda(\lambda) - E_{b\lambda}(T,\lambda)]\,d\lambda \tag{14}$$

34

To maximize receiver efficiency, the spectral emittance should be maximized when the term in the square brackets is positive and minimized when the term in the square bracket is negative. Intuitively, the term in the square bracket is the solar radiosity (modified by concentration, transmission and concentrator efficiency) minus the blackbody radiosity at the absorber operating temperature. Thus it makes sense that in the ideal case, for wavelengths where the bracketed term is positive, emittance should be 1 and for wavelengths where the bracketed term is negative, emittance should be 0. This ideal emittance spectrum is shown in the example case of Figure 8. For more practically achievable properties, there is typically a single transition from high to low emittance between 1 μm and 2.5 μm, with the exact ideal transition wavelength depending on concentration ratio and operating temperature.[76] Stated simply: spectrally selective surfaces should have high absorptance (and therefore emittance) in the solar spectrum and low emittance in the IR spectrum. Figure 9 shows some example emittance spectra of surfaces designed to be efficient solar absorbers.
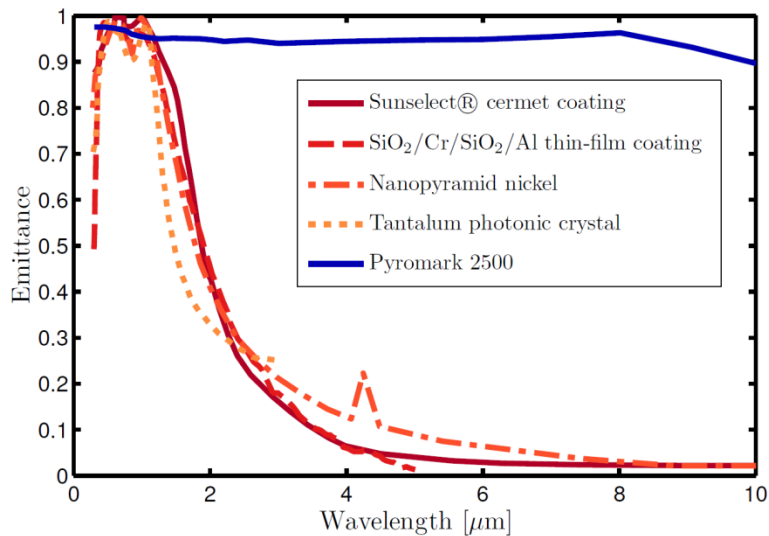
Figure 9 Sample emittance spectra of various spectrally selective absorbers. All follow the same trend of high emittance in the solar spectrum and low emittance in IR. Sunselect (solid curve) is a commercial cermet coating.[77] A number of coatings resulting from university research are also plotted: a SiO2/Cr/SiO2/Al thin-film coating (dashed curve),[78] a nickel nanopyramid structured surface (dash-dotted curve),[79] and a tantalum photonic crystal coating (dotted curve).[80] A commercial black paint, Pyromark 2500, is plotted along with the spectrally selective absorbers for comparison[81]

Spectrally selective absorbers are typically characterized by their solar absorptance and their emittance at their intended operating temperature. In practice, these properties are usually measured by taking the

spectral reflectance $\rho(\lambda)$ for the surface using UV-Vis and FTIR spectrometers and using $\epsilon = 1 - \rho$ to determine the spectral emissivity $\epsilon(\lambda)$. This can be used to calculate absorptance and emittance using Eqs. (12) and (13). This is not a perfectly accurate method, as measurements of $\epsilon(\lambda)$ are taken at room temperature and near normal incidence, whereas the true absorptance and emittance depend on properties at operating temperature and for varying angles. This method will still provide a reasonable estimate as long as the properties are not strongly dependent on temperature or incident angle. There are measurement techniques to determine total hemispherical radiative property values at high temperature,[82,83] however using spectrometers is more common due to their convenience.

To achieve spectral selectivity in practice, one can first consider metals. Metals have high IR reflectance and are capable of absorbing visible light (the imaginary part of the dielectric constant in metals is large). Reflection at interfaces depends on the refractive indices of the different materials, and metals are very reflective in the visible spectrum because their refractive index is much higher than that of air.[45] Reflectivity R can be calculated using the Fresnel equations, and in the case of normal incidence light it is given by:

$$ R = \left| \frac{n_1 - n_2}{n_1 + n_2} \right|^2 \tag{15} $$

where n_1 and n_2 are the refractive indices of the materials on the two sides of the interface. If this surface reflectivity was reduced for a metal in the solar spectrum, the metal would become an effective selective absorber. Reflectivity can be reduced through the use of an anti-reflection coating (ARC).[84] The simplest ARC introduces an intermediate refractive index layer between the air and the material to be coated. Despite the introduction of an additional interface, the overall reflectance is lower due to the smaller refractive index mismatches between the new interfaces. Multiple intermediate refractive index layers or a material with a graded index of refraction can further reduce reflectance. ARCs can also be formed by introducing a layer of quarter wavelength thickness (for the wavelength you want to transmit) of a

material which has a refractive index of $\sqrt{N}$, where N is the refractive index of the material to be coated.[85] This approach results in perfect transmission for the desired wavelength due to destructive interference in the reflected waves. However, for solar applications, this is more difficult to accomplish due to the breadth of the solar spectrum (wavelengths from 350 nm - 2500 nm correspond to 98% of the direct solar spectrum).[86]

These concepts of graded indices and interference effects, along with inherent properties of some materials (e.g., the band gap in semiconductors), provide a number of tools for designing spectrally selective surfaces. The methods for achieving spectral selectivity in practice are commonly grouped into six categories: intrinsic materials, ceramic-metal composites (known as cermets), semiconductor metal tandems, multi-layer thin-film structures, structured surfaces, and photonic crystals.[75] These six types of selective absorber are illustrated in Figure 10. Intrinsic materials are homogeneous materials which have some inherent spectral selectivity due to their dielectric dispersion varying with wavelength. Cermet absorbers consist of fine metal particles in a ceramic matrix (acting as a graded index ARC) deposited on metal substrates, and have been shown to achieve good spectral selectivity.[76] In semiconductor metal tandems, a semiconductor layer on top of a metal absorbs high energy photons (above the material band gap) while the metal substrate naturally has low IR emittance. In multilayer thin-film structures, alternating layers of metal and dielectric allow for interference effects and can lead to high solar absorptance and low IR emittance.[87] Structured surfaces can trap short wavelength photons within wavelength scale features, while reflecting IR photons with wavelengths much larger than the features.[88] Photonic crystals are metamaterials which have wavelength scale periodicity in the light propagation direction, allowing for tight control of radiative properties.[89] The distinction between multi-layer thin-film structures, structured surfaces and photonic crystals is not always clear, as thin-film structures resemble 1-dimensional photonic crystals and structured surfaces can resemble 2-dimensional photonic crystals. Here we consider a coating a photonic crystal if it has been explicitly designed to create forbidden energy bands using a substantial number of periods (e.g., at least order 10). Table 4 lists some materials which

have been investigated as spectrally selective absorbers and the achieved performance. Intrinsic materials, semiconductor metal tandems, multi-layer thin-film structures, and structured surfaces will only be covered briefly, as there is limited work in these areas. Cermet absorbers have seen the most commercial success while photonic crystals show promise for significant performance improvements in the future, so both of these classes of absorber will be covered in more depth. The interested reader is referred to the reviews by Bermel, et al. and Kennedy for a more comprehensive overview of spectrally selective absorbers for use with CSP.[75,87]
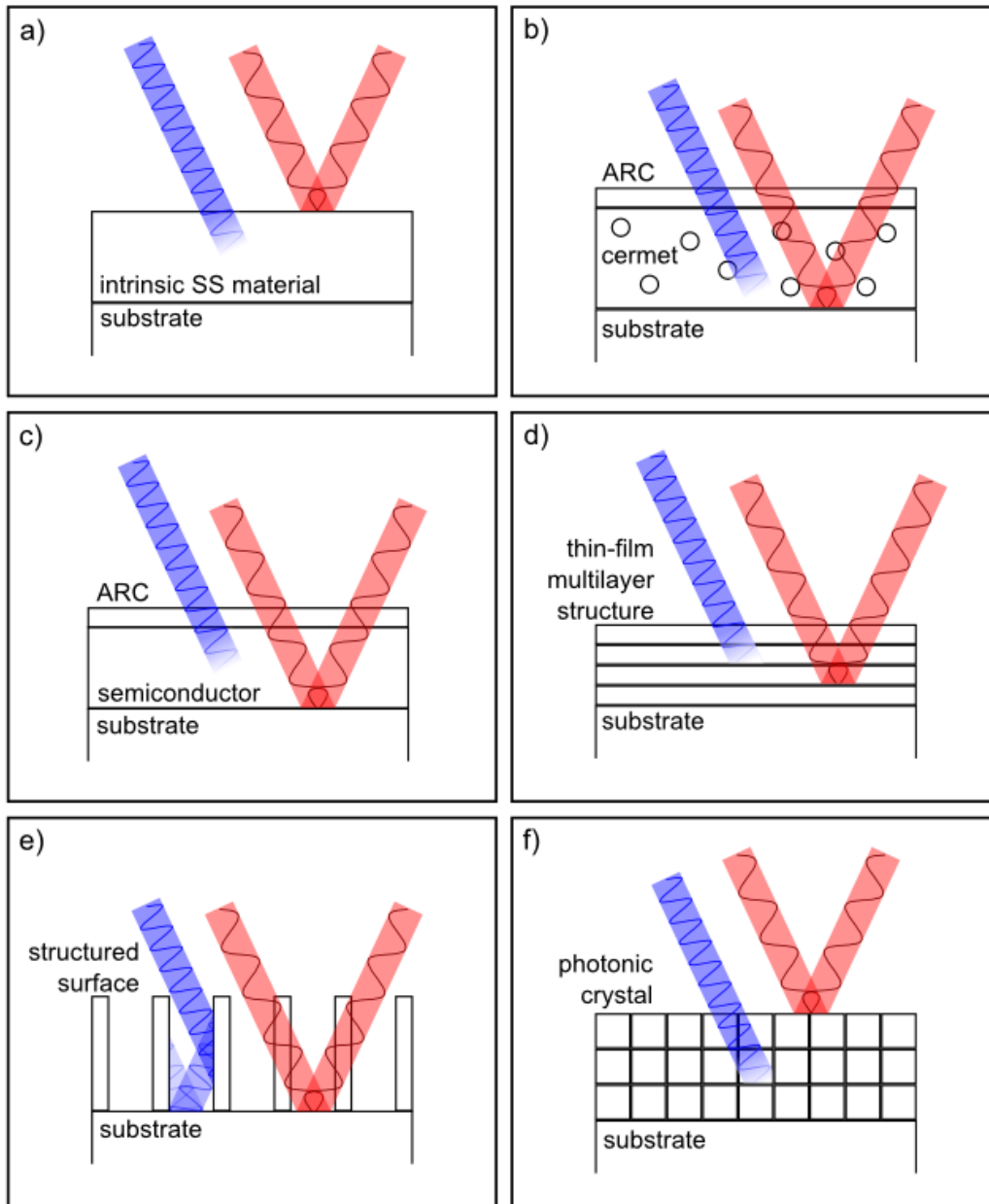
Figure 10 Illustrations of different types of spectrally selective absorbers: a) instrinsic, which relies on inherent optical properties of the absorbing material, b) cermet, which has metal particles dispersed in a ceramic matrix, c) semiconductor-metal tandem, which uses the electronic band gap of the semiconductor for selective absorption, d) thin-film multilayer, which takes advantage of interference effects in the thin-layers, e) structured, which uses nanostructures on the scale of solar wavelengths and f) photonic crystal, which uses wavelength scale periodicity to create forbidden photon energy bands

Table 4 Performance of various spectrally selective absorbers. Asterisk denotes simulation results, caret denotes value is calculated from figures in the cited reference (rather than reported directly). In all instances besides "industry state of the art" reported temperature stability refers to lab conditions. Pyromark 2500 is a commercial black paint (not spectrally selective) included for comparison.

Material	Class	Solar Absorptance	IR Emittance	Temperature stability	Reference
Pyromark 2500	Black paint	0.97	0.9 at 1000 °C	750 °C in air	[81]
ZrB_2	Intrinsic	0.93	0.09 at 102 °C	527 °C in air	[90]
$Cr:Cr_2O_3$	Cermet	0.868	0.088 at 121 °C		[91]
$Cr:Cr_2O_3$	Cermet	0.94	0.06 at 82 °C		[92]
$Ni:CrO_x$	Cermet	0.961	0.022 at 100 °C		[93]
$Ni:Al_2O_3$	Cermet	0.94	0.18 at 100 °C^	500 °C in air	[94]
$Mo:Al_2O_3$	Cermet	0.97	0.17 at 350 °C	650 °C in vacuum	[95]
$W-Ni:Al_2O_3$	Cermet	0.90	0.15 at 500 °C		[96]
$W:Al_2O_3$	Cermet	0.95	0.106 at 400 °C	400 °C in air, 580 °C in vacuum	[97]
$Zr:ZrO_2$	Cermet	0.96	0.05 at 80 °C		[98]
Ti:AlN	Cermet	0.95	0.07 at 82 °C	600 °C in air	[99]
Hf/Mo:HfMoN	Cermet	0.95	0.14 at 82 °C	475 °C in air, 650 °C in vacuum	[100]
$Mo:SiO_2$	Cermet	0.946	0.15 at 400 °C	600 °C in vacuum	[101]
Industry state of art	Cermet	0.95	0.05 at 100 °C	500 °C in	[77,102,103]

				vacuum	
a-Si	Semiconductor metal tandem	0.79-0.81	0.12-0.14 at 400 °C		[104]
PbS	Semiconductor metal tandem	0.95-0.97	0.21-0.27 at 102 °C		[105]
Ge	Semiconductor metal tandem	0.907*	0.016 at 127 °C*		[106]
Si	Semiconductor metal tandem	0.868*	0.073 at 727 °C*		[106]
W, TiO2, and MgF2	Multi-layer	>0.94*	< 0.07 at 447 °C*		[107]
Mo and MgO	Multi-layer	>0.85*	< 0.16 at 1477 °C*		[107]
Si3N4/NbAlON/NbAlN	Multi-layer	0.959	0.07 at 82 °C	450 °C in air	[108]
SiO_2/Cr/SiO_2/Al	Multi-layer	0.904^	0.04 at 300 °C^	600 °C in vacuum	[78]
SiO_2/Ti/SiO_2/Ti/SiO_2/Cu	Multi-layer	0.955	0.136 at 427 °C		[109]
Mo-Si_3N_4	Multi-layer	0.926	0.017 at 25°C, 0.109 at 600°C		[110]
MgO/Zr/MgO	Multi-layer	0.92	0.10 at 400°C		[111]
Nanopyramid W	Structured	0.965*^	0.198 at 700 °C*^		[112]
Multi-scale $Si_{0.8}Ge_{0.2}$	Structured	~0.9	~0.3 at 500 °C		[113]
Laser sintered W	Structured	0.87	0.33 at 300 °C^	650 °C in air	[114]
Nanopyramid Ni	Structured	0.9^	0.09 at 400 °C^	800 °C in vacuum	[79]

Tungsten	Photonic crystal	0.89*^	0.19 at 900 °C*^		[115]
Tungsten with dielectric filled cavities	Photonic crystal	0.78*^	0.32 at 1000 °C*^		[116]
Tantalum coated with HfO$_2$	Photonic crystal	0.86	0.26 at 727 °C		[80]
Molybdenum	Photonic crystal	0.919*	0.149* at 1000 °C		[117]
Nickel	Photonic crystal	0.84*	~0.3 at 700 °C*^		[118]

3.2.1. Intrinsic absorbers

Certain materials, such as transition materials and semiconductors, show intrinsic spectral selectivity, however their natural transition wavelength is typically far from the desired value for solar absorber applications.[75] Some examples of materials with intrinsic selectivity well suited for solar absorbers are Cu$_2$S, graphite and ZrB$_2$.[119,120] Randich and Allred demonstrated a chemically vapor-deposited (CVD) ZrB$_2$ absorber with a solar absorptance of 0.93 and an emittance of 0.09 at 102 °C, with thermal stability in air at 527 °C.[90] Performance can almost always be improved by combining intrinsically selective materials with more advanced techniques such as multi-layer thin-film structures, so in practice intrinsic materials are not typically pursued alone.

3.2.2. Cermet absorbers

A cermet (a portmanteau of "ceramic" and "metal") is a composite material in which metal particles are embedded in a ceramic matrix. Cermets have been shown to be good selective absorbers when combined with an ARC on top and a reflective metal substrate on bottom (or a cermet can simply be deposited on a

reflective substrate).[75] Performance can be further improved with more complicated structures, such as multi-layer or graded cermet coatings, where the metallic content is controlled through the depth of the cermet much like a multi-layer or graded index ARC, as well as structured cermet coatings.[92,97,121] Of the different types of spectrally selective coatings, cermets have seen the most commercial success (being used in essentially all commercial vacuum tube receivers) due to their compatibility with inexpensive manufacturing techniques and reliability at temperatures up to 500 °C.[102] In general, solar absorptance can be improved with smaller metallic particles and thicker cermet layers, whereas low IR emittance can be achieved with larger metallic particles and thinner cermet layers.[76,122] However, the exact performance is difficult to predict using modeling alone, as the optical properties of cermets (and even the structures in cermet coatings) are not completely understood.[93,123] A number of fabrication methods have been used to successfully create cermet selective solar absorbers, including sputtering, evaporation, chemical vapor deposition (CVD), electroplating, anodization, and solution based methods.[76] Sputtering, an inexpensive physical vapor deposition (PVD) technique, is used commercially to produce large absorber areas, while the other methods are more common for lab scale fabrication. Solution based methods offer the potential for even lower cost production, however the coating quality is more difficult to control than with PVD. There are also a number of different materials systems which have been investigated including Cr_2O_3, Al_2O_3, AlN and SiO_2 as the ceramic matrix and Cr, Ni, Mo, W, SS, Al and some noble metals as the metallic inclusions.[76,102] The choice of ceramic matrix and metallic inclusion is important for stability, as the metal must be stable in the ceramic matrix for high temperature operation. We will briefly highlight a cross section of some of the work that has been performed investigating cermet solar selective absorbers, the interested reader is referred to the review by Cao et al. which covers cermet absorbers in more depth.[76]

Chromium oxide based cermets, including black chrome ($Cr:Cr_2O_3$) comprises some of the earliest work in cermets as solar absorbers. As early as 1975, McDonald reported an electroplated black chrome spectrally selective absorber with a solar absorptance of 86.8% and an emittance of 8.8% at 121°C.[91] More recent work has shown improved performance from this early work. Nunes et al. demonstrated a

graded chromium based cermet coating with a solar absorptance of 94% and an emittance of 6% at 82°C.[92] Gaouyat et al. demonstrated a sputtered $Ni:CrO_x$ cermet solar selective absorber, with a solar absorptance of 96.1% and an emittance of 2.2% at 100°C, showing very competitive radiative properties.[93]

Another common ceramic matrix for cermet absorbers is aluminum oxide, and Al_2O_3 based cermets have shown some of the best high temperature stability for solar selective coatings, especially in air. Craighead and Buhrman demonstrated an evaporated $Ni:Al_2O_3$ cermet coating with a solar absorptance of 94% and an emittance of 18% at 100 °C, which was thermally stable up to 500 °C in air.[94] Lanxner and Elgat demonstrated a sputtered Mo:Al2O3 cermet coating with a solar absorptance of about 97% and an emittance of around 17% at 350 °C which was stable up to 650 °C in vacuum.[95] Cao et al. demonstrated a sputtered $W-Ni:Al_2O_3$ selective coating on stainless steel with a solar absorptance of 0.90 and a total hemispherical emittance of 0.15 at 500 °C, with this high temperature stability achieved by using tungsten as the infrared reflector.[96] Rebouta et al. demonstrated a sputtered, multi-layer $W:Al_2O_3$ cermet absorber, which achieved a solar absorptance of 95% and an emittance of 10.6% at 400 °C, with stability in air up to 400 °C and in vacuum up to 580 °C.[97]

Successful solar selective absorbers have been shown with other materials as well. Zhang et al. fabricated a sputtered $Zr:ZrO_2$ based cermet solar selective absorber with a solar absorptance of 96% and an emittance of 5% at 80 °C.[98] Barshilia et al. demonstrated a titanium and aluminum nitride based cermet absorber with a solar absorptance of 95% and an emittance of 7% at 82 °C which was thermally stable in air up to 600 °C.[99] The same group also fabricated a HfMoN based cermet absorber with a solar absorptance of 95% and an emittance of 14% at 82 °C, with thermal stability up to 650 °C in vacuum and 475 °C in air.[100] Zheng et al. demonstrated a sputtered $Mo:SiO_2$ cermet selective absorber with a solar absorptance of 94.6% and an emittance of 15% at 400 °C that was stable up to 600 °C in vacuum.[101] From this work it is clear that there are many promising ceramic matrices to explore beyond Cr_2O_3 and Al_2O_3.

In order to make a difference in the CSP industry, performance of cermet solar absorbers should be improved beyond the current industry state of the art. Commercial cermet coatings typically achieve solar absorptances of around 95% and emittances of around 5% at 100 °C.[102] Thermal stability up to 500 °C is also necessary, as surface temperatures routinely reach this high during operation of a vacuum tube receiver in a PTC. Higher absorptance and lower emittance naturally lead to better receiver efficiencies, and higher temperature stability would be required for new heat transfer fluids or high temperature heat engines, as well as for use in power tower receivers. Economic manufacturing processes at large scale also need to be kept in mind for making an impact in new CSP installations, as solution based methods which still achieve high performance could lead to lower coating costs. From a research perspective, a better understanding of the optical properties of cermet coatings would also allow for better optimization of different layered or structured cermet coatings.

3.2.3. Semiconductor absorbers

Semiconductors show intrinsic selectivity because they are usually transparent for photons with energy below their electronic band gap, but absorb effectively for energies above the band gap. If the semiconductor is layered on top of a reflective metal, long wavelength photons will be reflected away. This is the operating principle behind semiconductor-metal tandem absorbers.[124,125] Semiconductors typically have a high refractive index in the solar spectrum which leads to reflection of photons which should be absorbed, so it is common to use an ARC on top of the semiconductor. Achieving low emittance can be challenging for semiconductor absorbers, as electron-hole pair generation and free carrier emission at high temperatures can lead to large radiative losses. Semiconductors with band gaps suitable for solar absorbing applications include silicon, germanium and lead sulfide. Okuyama et al. experimentally demonstrated an amorphous silicon based absorber with a solar absorptance of $0.79 - 0.81$ and an emittance of 0.12-0.14 at 400 °C.[104] Chatterjee and Pal fabricated selective absorbers by thermal evaporation of galena (lead sulfide) demonstrating a solar absorptivity of $0.95 - 0.97$ and an emittance of $0.21 - 0.27$ at 102 °C.[105] Bermel et al. investigated the use of silicon and germanium absorbers via

numerical simulation.[106] For an optimized germanium absorber, they reported a solar absorptance of 0.907 and an emittance of 0.016 at 127 °C. For higher concentration, higher temperature applications, they designed an optimized silicon absorber with a solar absorptance of 0.868 and an emittance of 0.073 at 727 °C.

3.2.4. Thin-film multilayer absorbers

Using multi-layer thin-films can enhance the spectral selectivity of solar absorbers, typically with dielectric layers as absorbers and metal layers as reflectors. When a layer's thickness is a quarter of the wavelength of the relevant photons, destructive interference prevents reflection, leading to enhanced absorption. Adding more layers can widen the spectral band over which absorption is enhanced. While these very thin layers allow the exploration of interference effects, they decrease the length that atoms need to diffuse to move between layers, so high temperature stability becomes challenging. Sergeant et al. modeled thin-film absorbers and optimized structures for CSP and solar thermophotovoltaic applications. For CSP, a W, TiO_2, and MgF_2 structure was predicted to have solar absorptance >94% and emittance of <7% at 447 °C, while for STPV a Mo and MgO structure was predicted to have solar absorptance >85% with an emittance of <16% at 1477 °C.[107] Barshilia et al. demonstrated a sputtered $NbAlN/NbAlON/Si_3N_4$ coating with a solar absorptance of 95.6% and an emittance of 7% at 80 °C with stability in air up to 450 °C.[108] Zhou et al. designed a solar absorber with a $SiO_2/Cr/SiO_2/Al$ structure, and a sample fabricated with sputtering demonstrated high solar absorptance (>90%) and low IR emittance (4% at 327 °C), as well as vacuum stability up to 600 °C.[78] Liu et al. used an additional two layers in a $SiO_2/Ti/ SiO_2/Ti/ SiO_2/Cu$ configuration to achieve 95.5% solar absorptance and an emittance of 0.136 at 427 °C.[109] Céspedes et al. demonstrated a sputtered $Mo-Si_3N_4$ coating which achieved a solar absorptance of 92.6% and an emittance of 11% at 600 °C.[110] Nuru et al. demonstrated 92% solar absorptance and 10% emittance at 400 °C using a e-beam deposited MgO/Zr/MgO structure.[111] The current work has thus shown that the multi-layer thin-film approach to spectral selectivity can be very effective. Thin-film multilayer absorbers which are compatible with PVD and have good high temperature stability could compete with cermet

absorbers in commercial applications, if their absorptance and emittance properties can outperform current industry state of the art cermet absorbers.

3.2.5. Structured surface absorbers

Structuring a surface at scales near or smaller than the desired transition wavelength can enhance the performance of spectrally selective surfaces. Such structures can help trap short wavelength photons, either via multiple reflections inside the structures or by providing a more gradual gradient in refractive index,[124,126] without increasing the absorption for longer wavelengths. Rephaeli and Fan designed a tungsten nano-pyramid absorber and predict high absorptance in the solar spectrum (96.5%) with low absorptance in the IR spectrum (19.8% emittance at 727 °C).[112] In a similar approach, Ungaro et al. used computational electrodynamics simulations to investigate nanostructured tungsten cone absorbers, and reported a very high solar absorptance (~0.99) along with moderate IR reflectance.[127] Moon et al. fabricated a multi-scale structured silicon germanium absorber via a spark erosion process with a solar absorptance of ~0.9 and an emittance of ~0.3 in the IR spectrum (Moon et al. suggest that this emittance value is valid at 500 °C, however spectral emittance data from 1 - 3.5 µm is not reported).[113] Kim et al. found that a tandem structure combining copper oxide nanowires and cobalt oxide nanoparticles led to good spectrally selective performance.[128] Shah et al. developed a structured tungsten spectrally selective surface using laser sintering with a measured solar absorptance of about 87% and thermal stability in air up to 650 °C.[114] Li et al. developed a scalable method for fabricating nanopyramid structured surfaces using a silicon wafer inverted nanopyramid template. They demonstrated a nickel nanopyramid structured surface with a solar absorptance of 90% and an emittance of about 9% at 400 °C which was stable up to 800 °C in vacuum.[79] These demonstrations show that good spectral selectivity is possible using structured surfaces (although their IR emittance tends to be higher than that of cermet absorbers), and they offer a promising option if cost-effective, commercial-scale production lines can be developed.

3.2.6. Photonic crystal absorbers

Photonic crystals allow unprecedented control of radiative properties of a surface, with important applications in solar applications in addition to many other fields.[89,129] In a photonic crystal, periodicity on the scale of the wavelengths of light where control is desired leads to bands of allowed and forbidden photonic states. Photonic crystals with allowed states in the solar spectrum and forbidden states in the IR spectrum can be used as effective solar absorbers. Much of the application focus for high temperature photonic crystal has been as selective emitters for use with solar thermophotovoltaic (STPV, discussed in section 6.3.2) systems,[130–133] but they can be used as absorbing surfaces for conventional CSP systems as well. The main challenge in using photonic crystals as solar selective absorbers is creating structures which are robust at high temperature. Combining multiple materials in a photonic crystal creates many interfaces, which can lead to delamination and other thermal stability issues.[134] Thus, the most commonly investigated systems for photonic crystal absorbers are refractory metals, since they are naturally reflective in IR, can be structured to absorb in the solar spectrum, and have high thermal stability.[135]

Tungsten has been one of the most popular metals to work with for high temperature photonic crystals, as its high melting temperature leads to good stability. As early as 2000, Heinzel et al. fabricated two-dimensional (2D) tungsten photonic crystals, and successfully demonstrated selectivity enhancement over a plane tungsten surface.[136] These 2D photonic crystals can be fabricated by using lithography to provide a desired surface pattern, followed by etching to remove tungsten and form the crystal structure.[137] Wu et al. designed a 2D tungsten photonic crystal with a predicted solar absorptance of 89% and an emittance of 19% at 927 °C, and fabricated a gold sample which demonstrated lower absorptance (and would not have high temperature stability).[115] Despite the high melting temperature of tungsten, it is still challenging to fabricate tungsten nanostructures with high temperature stability over the extended periods which would be required in deployed CSP systems. Only single crystal tungsten has shown the requisite stability, while polycrystalline structures deform at high temperature and lose their intended optical properties.[138] One approach to improve the stability of these photonic crystals is to fill the cavities with a dielectric material. Lee et al. studied hafnia filled 2D photonic crystals and estimated a >30 year lifetime of hafnia filled

tungsten photonic crystals at 827 °C.[139] Chou et al. investigated the use of dielectric filled cavities in the 2D photonic crystal structure, and predicted absorptance of 78% and emittance of 32% at 1027 °C.[116] There are also many examples of fabricated tungsten photonic crystals intended for use as selective emitters, that have properties similar to those which would be desired for a selective absorber.[131–134]

Furthermore, there has been investigation into tantalum for use in high temperature photonic crystals,[140] as it has similar desirable properties as those of tungsten, but is machinable and weldable, and would thus be easier to integrate into systems in practice.[134] Tantalum photonic crystals can be fabricated in a similar process as is used for tungsten, via interference lithography and reactive ion etching.[141] Rinnerbauer et al. demonstrated a hafnium oxide coated tantalum photonic crystal with a solar absorptance of 86% and an emittance of 26% at 727 °C.[80] An additional anti-reflective coating could also improve this performance further.[142]

Other metals have also been suggested for use with high temperature photonic crystals, although for many of these materials experimental fabrication and characterization have yet to be performed. Wang et al. proposed a molybdenum photonic crystal, and using rigorous coupled wave analysis predicted a structure with a solar absorptance of 91.9% and an emittance of 14.9% at 1000 °C.[117] Lee et al. investigated a nickel photonic crystal and predicted a solar absorptance of 84%.[118] Chou et al. demonstrated high solar absorptance in a HfO_2 filled ruthenium photonic crystal.[143] The radiative property tuning afforded by photonic crystal design combined with the many material systems available thus indicate that very high performance is possible if the challenges of working with these new material systems can be overcome.

3.3.   Angularly selective surfaces

Angular selectivity can be leveraged for absorbers paired with concentrators that have a small rim angle, which refers to the largest incident angle at which concentrated sunlight hits the absorber (as described in section 2.1). Absorption at angles larger than the rim angle is not necessary, and therefore by Kirchhoff's

law emission at the larger angles is also unnecessary. As such, if emission at these large angles can be suppressed, the total hemispherical emittance can be significantly reduced (illustrated in Figure 11).[144,145] Angular selectivity is not currently implemented in any commercial CSP systems, as development is still at a research stage for many of the proposed techniques. The two primary means of achieving directional selectivity are photonic crystals and geometrical optics techniques. Recently, Shen et al. showed that by using stacked photonic crystals they could achieve transmission over a broad spectral range for a narrow angular window.[146] Angular selectivity can also be achieved with geometrical optics approaches. Perlmutter and Howell proposed angular selectivity with reflective V-grooves on a black absorber, such that normally incident rays are absorbed but incident rays at large angles are reflected.[147] Weinstein, et. al. demonstrated angular selectivity with a reflective hemisphere placed over a black absorber.[148] For photonic crystal angular selectivity, the challenges are similar to those faced when designing for spectral selectivity. For geometrical optics approaches, the challenges are similar to those faced in reflector technology, as most of the schemes are based on reflecting surfaces.
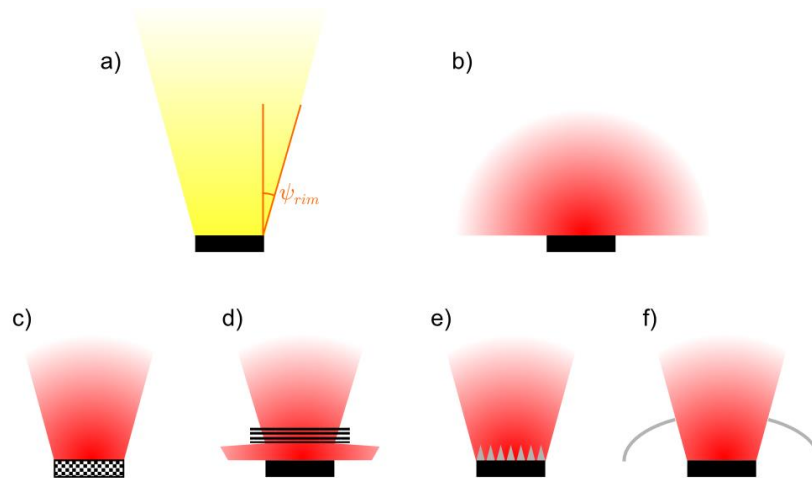
Figure 11 Diagram illustrating concept of angular selectivity. If a concentrator has a small rim angle ψ_{rim}, a) the absorber does not need to absorb at large incidence angles, however b) a regular black absorber will absorb and emit in all directions. Emission at large angles can be reduced through a number of methods, for example: c) photonic crystal absorbers, d) photonic crystal transmitters, e) grooved reflecting surfaces or f) reflective cavities

3.4.   Receiver technologies

3.4.1. Vacuum tubes

Vacuum tubes are the primary receiver technology associated with line-focus CSP systems; a typical vacuum tube receiver is illustrated in Figure 12. They consist of a pipe through which the HTF flows, which is coated with a spectrally selective surface. The pipe is inside a glass tube, and the space between the glass tube and the pipe is evacuated to suppress convection losses. Examples of commercial producers of vacuum tubes are Schott and Rioglass. As discussed in section 3.2, the spectrally selective pipe coating should be highly absorptive in the solar spectrum and reflecting in IR, with an ideal transition wavelength of 1.8 μm for the operating temperatures typical of vacuum tube receivers (~400 °C). Cermet absorbers are the most common for vacuum tube receivers due to their inexpensive sputtering deposition process and good high temperature stability in vacuum. Since these surfaces are used in an evacuated environment, air stability is not a primary concern. Bellows at the ends of the receiver tubes are designed to accommodate the thermal expansion that occurs during operation. The glass to metal seal must be durable in order to ensure vacuum is maintained, this is accomplished by using combinations of materials with matching coefficients of thermal expansion.[149]
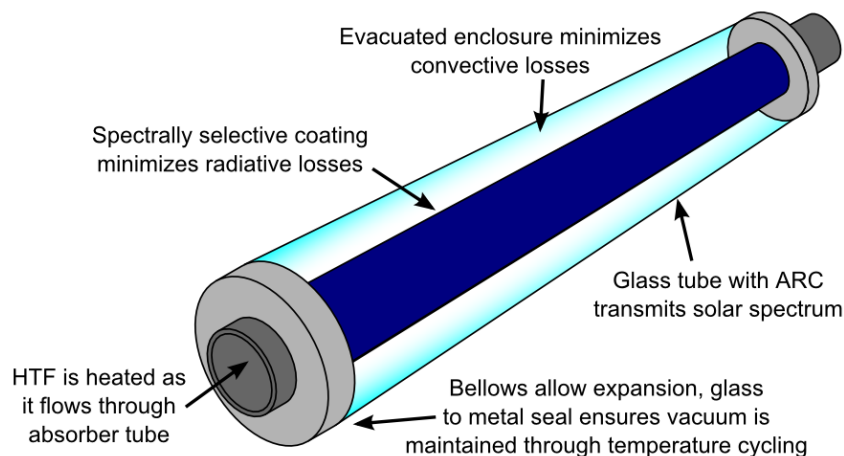
Figure 12 Diagram of a typical vacuum tube receiver. The receiver consists of a tube coated in a spectrally selective surface which the heat transfer fluid flows through. The tube is in an evacuated enclosure which is maintained by a glass tube with an anti-reflective coating. Metal bellows at the end of the tube accommodate expansion during daily temperature cycling and a glass to metal seal with matched coefficients of thermal expansion ensures the vacuum is maintained

The glass tubes in these receivers should ideally be very transparent in the solar spectrum. If regular crown glass is used, solar transmittance is about 92%. This transmittance can be enhanced by using

ARCs, as discussed earlier in this section. Glass has a relatively low refractive index of about 1.5 in the solar spectrum, and there are limited transparent materials with lower indexes of refraction. For this reason, ARCs on glass are often created by using sub-wavelength structures, such that the effective refractive index is of that between the base material and air. Hiller et al. demonstrated an effective ARC ($\tau \geq 0.98$) from 350 nm – 1400 nm using multi-layers of porous poly(allylamine hydrochloride)/poly(acrylic acid) (PAH/PAA) prepared with a simple aqueous coating process.[150] Kennedy and Brett demonstrated a broadband antireflection coating using glancing angle deposition to produce SiO_2 nanostructures for gradient index which had high transmittance ($\tau \geq 0.99$) from 400 nm to beyond 1000 nm.[151] Moghal et al. demonstrated high transmission ($\tau \geq 0.97$) from 400 nm – 2500 nm with a single-layer of silica nanoparticles using a spin coating process, which also showed robust mechanical properties.[152] Sood et al. demonstrated an ARC providing high transmittance ($\tau \geq 0.98$) from 400 nm – 2000 nm using oblique angle deposition of multiple layers of SiO_2 and TiO_2 nano-pillars for very gradual changes in refractive index.[153] Krause et al. have investigated taking glancing angle deposition techniques to roll to roll processes for potential commercialization of such techniques for ARC fabrication.[154] Current state of the art receiver tubes typically have solar transmittance values around 96% using SiO_2 nano-particles,[155] so robust, economically produced ARCs with higher transmittance could improve performance further.

An important concern in vacuum tubes is keeping the evacuated enclosure free of hydrogen, which can be released by HTF oils at high temperature. Hydrogen which permeates through the HTF pipes into the receiver tube annulus leads to convection losses, reducing receiver performance.[72,156] Since the hydrogen is released by decomposition of the HTF at high temperature, selection of more stable HTFs can reduce this issue (HTFs will be discussed in further detail in section 4). One method proposed to deal with hydrogen in the receiver is actively pumping to maintain vacuum.[157] In current systems however, these leaks are combated by putting hydrogen getters inside the tube to adsorb hydrogen. When hydrogen molecules strike the getter materials, the hydrogen can become adsorbed, removing it from the enclosure

and maintaining vacuum. Over time, these getters can become saturated, so for long term reliability it is beneficial to have more effective getters.[158] Hydrogen getter materials include ZrCo[159,160], 1,4-diphenylbutadiyne (DPB)[161] and 1,4 bis(phenylethynyl)benzene (DEB).[162–164] Stronger understanding of hydrogen uptake mechanisms could lead to improved hydrogen getter performance in new materials,[165] and therefore higher performance and reliability in vacuum tube receivers.

3.4.2. LFR receivers

While PTC systems almost always use vacuum tubes, LFRs are typically used with arrays of heat collection tubes in a flat or trapezoidal receiver (illustrated in Figure 13a).[16] These receivers operate in an air environment (not evacuated), since non-circular cross sectional geometries are not well suited for resisting the high pressure differences required to maintain vacuum.[166] Flat receivers have a smaller absorber area for losses to originate from (by a factor of π compared to a tube) but the lack of vacuum makes convective losses more substantial.[167,168] The lack of vacuum also limits options for spectrally selective surfaces (which have lower stability in air than vacuum) although some proposed designs use a glass cover with an inert gas purge so that spectrally selective absorbers may still be used.[169] Using aerogels, which are porous, low-density, low-thermal conductivity materials, have the potential to improve the performance of non-evacuated receivers.[170] Silica aerogels can be highly transparent in the solar spectrum, but still have extremely low thermal conductivity.[171,172] Thus, in a receiver which uses a silica aerogel layer as a selective transmitter, most sunlight would reach the absorber, but the exposed surface temperature of the aerogel would be greatly reduced, leading to much lower thermal losses.[173] This makes aerogel receivers a promising candidate for more efficient receivers in line-focus systems (illustrated in Figure 13b).[174] There is active research into making aerogels more transparent, and methods such as a two-step sol-gel process,[175] heat treatment,[176] and a "pin-hole" drying technique[177,178] have all shown improved solar transmittance compared to conventionally fabricated aerogels.
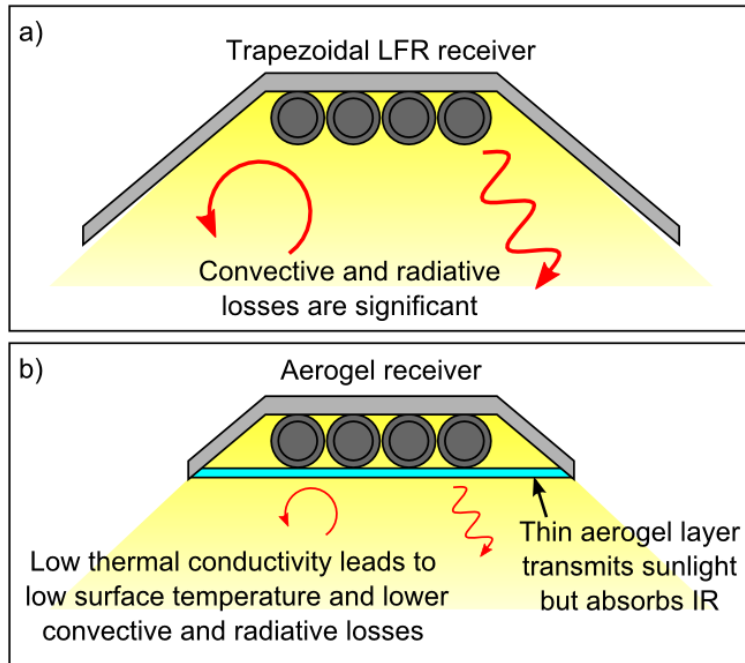
Figure 13 Diagram of a) trapezoidal LFR receiver and b) aerogel receiver. In a flat or trapezoidal configuration, the receiver cannot be evacuated, which leads to higher convective losses and limits options for selective surfaces due to temperature stability issues in air. A transparent aerogel layer can reduce convective and radiative losses at the cost of slightly lower transmittance

3.4.3. Central receivers

Central receivers are the technology associated with point-focus heliostat field CSP systems. These systems are often referred to as "power towers," since the receiver typically sits atop a large tower which the heliostats reflect sunlight to. Heliostat fields have large concentration ratios around 1000×, so high absorptance is the primary concern for good receiver efficiency in central receivers.[179] There are two primary designs for central receivers: external receivers and cavity receivers, both of which are shown in Figure 14.[180] In an external receiver the absorbing surface is on the outer surface of the receiver, which typically takes a cylindrical shape, and the heliostat field can completely surround the central receiver. In a cavity receiver, sunlight is focused on an aperture leading to an internal cavity where the sunlight is absorbed. In this case, the heliostat field is only on the side of the receiver which the aperture faces (e.g., in the northern hemisphere the aperture would face north and the heliostat field would only be on the

north side of the receiver). A less mature central receiver design is the "beam-down" concept, so called because the raised receiver is replaced by a reflecting optic that focuses sunlight from the heliostats to a receiver on the ground (see Figure 14).[181] The raised receiver can also be avoided by locating the heliostat field on a hill.[182] While a beam-down test plant is operational at the Masdar Institute in the United Arab Emirates,[183] it is not clear that the benefits (primarily that the heavy receiver can be located on the ground) outweigh the drawbacks (e.g., further reflective losses are introduced due to the additional optics and a secondary concentrator is required at the receiver to achieve comparable concentration ratios) compared to traditional designs.[184] Regardless, in principle any improvements to the absorbers for external or cavity receivers could be applied to beam-down receivers.

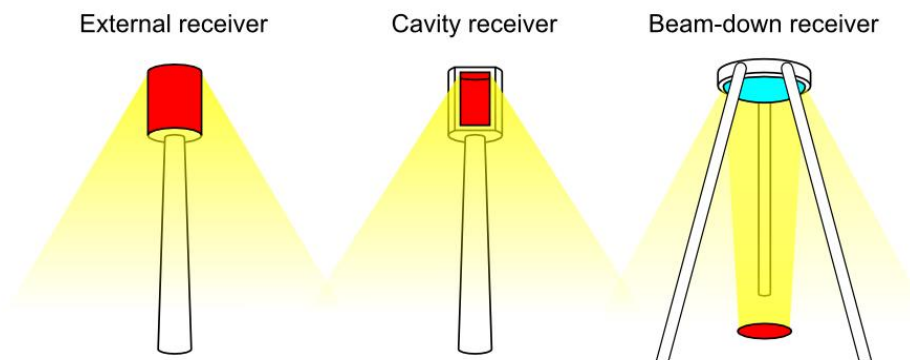**External receiver** **Cavity receiver** **Beam-down receiver**

Figure 14 Diagrams of different central receiver configurations, with red denoting the absorbing surface. In an external receiver (left) sunlight from all around the receiver can be absorbed. In a cavity receiver (center) sunlight can only be absorbed from the side of the receiver which the cavity is facing. In a beam-down receiver (right) the receiver is on the ground and sunlight is reflected down to it from a secondary reflecting optic

The most common absorber coating for external receivers is Pyromark 2500, which is a black silicone-based paint with high temperature stability.[81] It has a high solar absorptance of about 0.95 but also has a high emittance (>0.85) at elevated operating temperatures. While the high emittance indicates room for improvement in performance, due to the high temperatures, large heat fluxes, and large number of thermal cycles experienced by central receivers, the importance of reliability makes it a competitive option. Lower emittance spectrally selective coatings have been evaluated for use with central receivers, but their performance did not show significant improvement above Pyromark 2500.[185] While there are coatings

such as the cermet absorbers discussed in section 3.2.2 that would offer higher performance, the big challenge for compatibility with central receivers is high temperature stability in air. Vacuum or inert gas enclosures are undesirable because transmission losses become more significant with high concentration. One potential solution is using metallic photonic crystals, such as those discussed in section 3.2.6. There is room for performance enhancement if spectral selectivity can be achieved for a surface which is robust at high temperature in air. An alternative approach to improving receiver performance is through receiver design (e.g., novel geometries) which can improve effective absorptance and reduce losses compared to the same coating being used with a traditional external receiver.[186] In another approach, a directionally selective absorber (or a reflective cavity designed to provide directionally selective behavior) applied to a central receiver could reduce the required solar concentration ratio for efficiency high temperature operation, leading to a smaller heliostat field and significantly lower concentrator cost.[187]

For cavity receivers, the absorptance is naturally high due to the cavity geometry: light that enters through the aperture is much more likely to be absorbed at a point on the large interior cavity surface than be reflected back out of the aperture. As such, there is not a strong need for better absorber surfaces than Pyromark paint. One area of research is falling particle receivers, in which small particles absorb sunlight in the cavity and transfer heat to the air (or other working fluid) they fall through.[188] This allows for lower thermal resistance between the absorbing surface and the air, since the particles have a much higher surface area to volume ratio.[189,190] Falling particle receivers could also allow for higher receiver temperatures and a lower cost "HTF" and integrated TES system by using the particles for the transfer and storage of heat. Advances in particle absorptance and stability, as well as advances in system level issues such as receiver design, particle thermal storage and conveyance could lead to an improvement in state of the art for cavity receivers.[191]

While parabolic dish concentrators are similar to heliostat fields in that they have a point focus, their receivers are much smaller. The receivers typically have a cavity type configuration, so there is not a pressing need for more advanced absorber coatings for use with parabolic dish systems.

4. HEAT TRANSFER FLUID

In solar thermal systems, sunlight is focused on a receiver where it is absorbed and ultimately converted to thermal energy. The thermal energy is typically delivered to what is known as a heat transfer fluid (HTF) through convection, but this heat transfer could also be accomplished in less traditional ways (*e.g.* radiation,[192] conduction[193]). The multi-functional HTF needs to collect, transport, and exchange heat obtained from solar radiation and is therefore an extremely important part of a CSP system.

When absorbed photons originating from the sun thermalize in the receiver, the temperature will rise according to its heat capacity unless an equivalent amount of heat is removed from the receiver. At a steady-state operating temperature, the HTF removes the heat generated due to the absorption of photons as shown in **Figure 15**. This heat is then transported to a heat exchanger, connected to a power cycle for electricity generation or temporarily stored for subsequent use, as discussed in sections 5 and 6.

This section will highlight the essential features for a good heat transfer fluid, review and analyze existing fluids, and identify recent research trends and future directions.
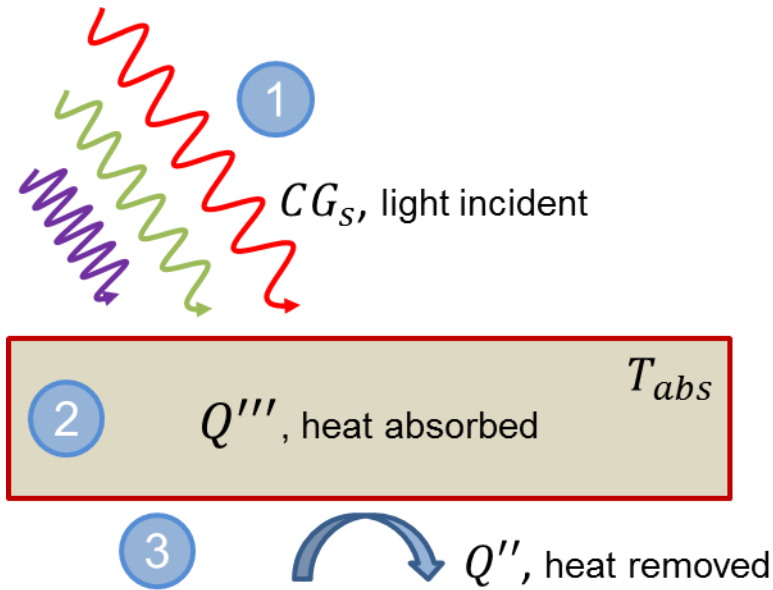
Figure 15: Simplified schematic of the energy conversion process showing the role of the HTF. 1) Incident concentrated sunlight impinges the solar absorber. 2) Heat is absorbed as the photon causes thermalization within the absorber lattice. 3) Heat must be removed *via* convection (most common), conduction (*e.g.* thermoelectrics), or radiation (*e.g.* thermophotovoltaics)

4.1. Desired characteristics and figures of merit

The heat transfer fluid is designed to carry heat from the receiver to the power block where it fuels the hot-side temperature of the cycle (*i.e.,* replaces the fuel input). Similar to its ability to gain heat from the receiver, it must also be able to efficiently reject heat to the thermodynamic power cycle. This heat transfer capability will be related to the convective heat transfer characteristics of the HTF which include a high thermal conductivity that enables efficient transfer of heat from the absorber and to the power block, a high density and specific heat capacity which enables high heat fluxes at reasonable mass flow rates, and low viscosity which minimizes the required pumping power.

Before reviewing different HTFs, it is important to introduce the different figures of merit that researchers have developed in order to help compare different HTFs for solar thermal applications. Comparison of a large number of HTFs was performed by Becker using individual physical and transport properties of the

fluids.[194] However, the study was inconclusive since it did not capture the physics of HTF performance, which should be determined through an appropriate combination of these properties.

Mouromtseff studied the problem for the cooling of vacuum tubes (while not exactly solar thermal fluids, the same physics are considered).[195] In this work, only the heat transfer in the radial direction was considered in detail. He proposed the Mouromteseff number (Mo) to compare the performance of heat transfer fluids based on the Dittus-Boelter correlation for internal turbulent flow:

$$\text{Mo} = \frac{\rho^{0.8} c_p^{0.33} k^{0.67}}{\mu^{0.47}} \tag{16}$$

where ρ is the density, c_p is the specific heat capacity, k is the thermal conductivity, and μ is the viscosity of the fluid.

Bonilla considered only axial heat flow to compare HTFs, ignoring the flow of heat from the wall.[196] He suggested the following figure of merit (FOM):

$$\text{FOM}_{Bonilla} = \frac{\rho^2 c_p^{2.8}}{\mu^{0.2}} \tag{17}$$

Lenert *et al*. performed a complete review of HTFs for solar thermal collection and storage.[197] Their analysis used Murakami's approach for optimizing multichannel heat sinks in electronic devices for the case of solar collectors.[198] The optimization was based on the minimization of pumping power given a certain temperature rise in the collector tube. The resulting FOM (shown below) was used to compare different HTFs.

$$\text{FOM}_{Lenert} = \frac{\rho^{2.0} c_p^{1.6} k^{1.8}}{\mu^{1.4}} \tag{18}$$
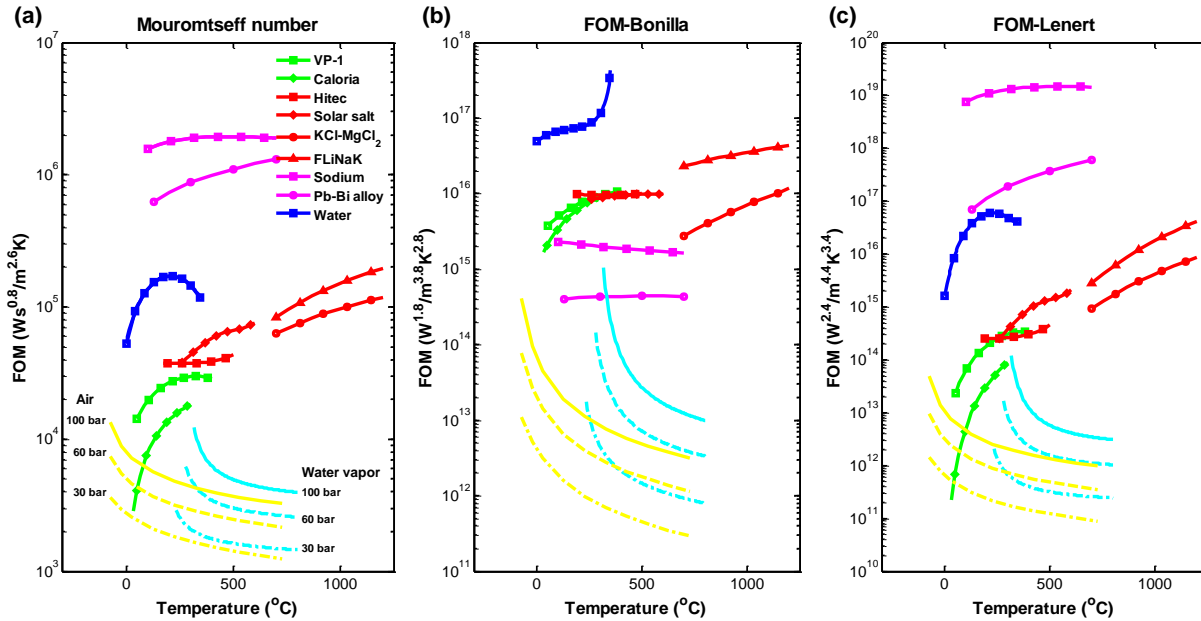
Figure 16: Temperature-dependent performance of heat transfer fluids compared using three figures of merit: (a) the Mouromtseff number, (b) FOM proposed by Bonilla,[196] and (c) FOM proposed by Lenert et al.[197] Liquid metals (purple) show a superior heat transfer performance in comparison to oils (green) and molten salts (red)

Figure 16 shows a comparison of the three figures of merit for several heat transfer fluids relevant for solar-thermal systems. The HTFs currently used fall into one of four categories: oils, molten salts, pressurized gases, and other liquids. The Mouromtseff's number and FOM$_{Lenert}$ show similar trends, whereas FOM$_{Bonilla}$ shows different results as it ignores heat transfer in the radial direction, which is important to HTF performance. The Mo and FOM$_{Lenert}$ of liquid metals is the highest, primarily because of their high thermal conductivity. Among the HTFs shown, saturated water has the highest FOM$_{Bonilla}$ and second highest Mo and FOM$_{Lenert}$ because of the high heat capacity which increases drastically at its critical point (374 °C). Despite having very low viscosity, pressurized air and water vapor have the lowest FOMs because of their low density, heat capacity and thermal conductivity. The FOMs of all liquid HTFs increase with increasing temperature due to significant reduction in their viscosity. However, the viscosity of water vapor and air increases with increase in temperature and hence their performance as HTF degrades with increasing temperature.

Since the outlet temperature of the solar collector is effectively the hot-side temperature of the power cycle, it has a large effect on the efficiency of the power cycle (this will be discussed in more detail in section 6). Higher efficiencies are possible at higher temperatures and therefore the HTF should remain stable at as high a temperature as possible. While the operating temperature of a solar thermal plant varies, it is commonly limited by the highest temperature that the HTF remains stable. The development of thermally stable HTFs which exceed the disassociation points of currently used HTFs is an active area of research.[199–201]

Another important aspect regarding the temperature stability of the HTF is its freezing point. The diurnal nature of the sun forces the HTF to operate between the CSP plant's peak operating temperature and the night-time temperature. The HTF must therefore freeze at or below the night-time conditions or safeguards must be built into the system to prevent the HTF from freezing in the plumbing, which can cause damage and accelerated wear.

Other factors that cannot be ignored for any practical application include the HTF's toxicity, environmental danger, stability, compatibility with materials including metals, effect of impurities, and cost. The long-term durability of different HTFs is another important concern that should be examined experimentally.[202] Additionally, some recent studies have investigated the optical transmittance of several HTFs, with the goal of using them as direct-absorption beam-splitting filters.[203]

4.2.   Types of heat transfer fluids

Considering the functionality of the HTF, there are a broad range of constraints, both practical and fundamental, which determine the performance of a HTF. Figure 17 shows the operating temperature range for different classes of HTFs. Synthetic and mineral oils have been the HTF of choice for a majority

of solar thermal plants due to their stability over a relatively large temperature range. On the other hand, molten salts promise higher efficiencies due to the possibility of higher operating temperatures, however these efficiency gains are coupled with challenges associated with melting the salts and higher pumping costs. Additionally, several new approaches using ionic liquids, fluids with nanoparticles and liquid metals are currently being explored to overcome the deficiencies of oils and molten salts.[199,204–206] Finally, some recent work in the literature has investigated using gas-based HTFs, *e.g.,* using pressurized air and steam, which can reduce the cost of electricity production.[201,207]
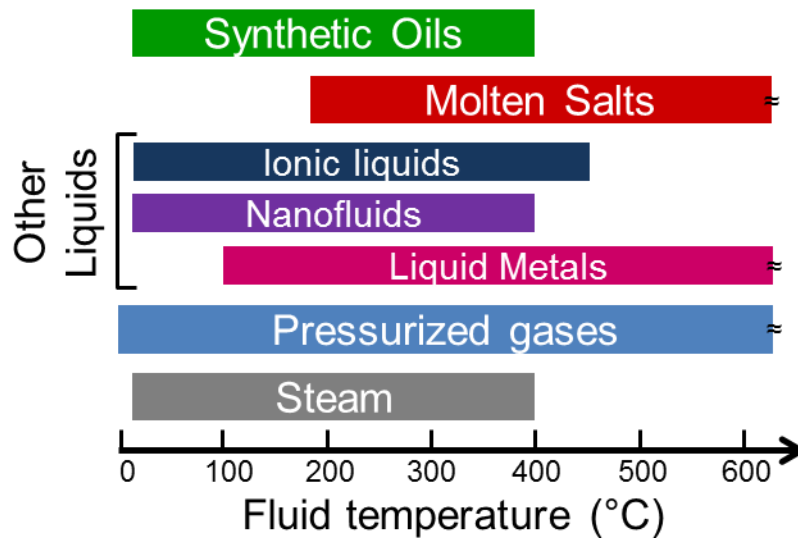
Figure 17: Operating range of different types of CSP heat transfer fluids. Adapted with permission from reference [208]. Copyright 2011 American Society of Mechanical Engineers. Traditional HTFs such as synthetic oils are stable only up to ~400 °C. Research efforts are targeted towards advanced HTFs, such as liquid metals and pressurized gases, which can operate at much higher temperatures leading to higher efficiency

4.2.1. Oils

The most common types of HTFs are oils. They may be either mineral or synthetic oils. Mineral oils generally include a mixture of higher alkanes obtained as petroleum distillate. Synthetic oils, on the other hand, are artificially manufactured from chemically modified petroleum components. Synthetic oils have

both a higher thermal conductivity and a lower viscosity which make them more attractive than mineral oils (*e.g.* Caloria HT 34). Furthermore, mineral oils can be quite flammable and were responsible for an accident at the first solar electricity generating station (SEGS 1) in 1999. In comparison, synthetic oils are less flammable and are generally preferred over mineral oils.

Oils are important HTFs for solar-thermal applications since they offer the best available combination of low freezing point and high upper temperature limit. **Table 5** shows the temperature range and thermophysical properties of some commercially available mineral and synthetic oil based heat transfer fluids. These HTFs are liquid at ambient conditions and do not require external temperature control to maintain a reasonably low viscosity. Synthetic oils (*e.g.* Therminol® VP-1, Solutia Inc.) are common in parabolic trough solar plants but are ultimately limited by their relatively low operating temperature of about 393 °C. While in principle the HTF performance improves with increasing temperature (due to the reduction in the liquid's viscosity and therefore required pumping power), solar engineers are typically faced with stability issues which ultimately sets the operating temperature and maximum attainable exergetic efficiency (see Section 5). Some recent studies suggest that biphenyl- and diphenyl- oxide based thermal fluids such as Therminol VP-1 and Dowtherm A undergo gradual thermal decomposition at temperatures close to 400 °C.[209] This gradual thermal breakdown results in hydrogen gas formation that permeates through steel tubes into the vacuum enclosure and increases the heat loss. A pressurization system and a nitrogen blanket is thus provided to prevent air from contacting the hot oil which could lead to performance degradation due to oxidation and increased flammability hazard. However, these preventive mechanisms increase the operation cost significantly.

Oils have lower densities and heat capacities compared to other HTFs such as molten salts and, consequently lower FOM (ref. **Figure 16**). Therefore larger fluid volumes are required that demand larger storage space and higher costs. Additionally, the flammability and environmental toxicity of some of these oil-based HTFs continue to be concerns and are active areas of development.

Table 5: Representative list of oil-based HTFs (at ambient temperature). Table adapted from Looser.[203]

Fluid name	Chemistry	Temperature range	Density (kg/m^3)	Specific heat (kJ/kgK)	Viscosity (mPa s)	Thermal conductivity (W/mK)
Mineral oils						
Therminol® XP – Solutia	White mineral oil: petroleum	-20 to 315 °C	875	1.85	22.7	0.124
Heat transfer oil S2 – Shell	Hydrocarbons	Max. 320 °C	863	10	25	0.134
Xceltherm® 445FP – Radco	Naphthenic oil	Max. 288 °C	862	36	36	0.132
Duratherm® 600 – Duratherm	Paraffinic hydrocarbons	Max. 315 °C	844	1.97	65.86	0.142
Synthetic oils						
Therminol® VP-1 – Solutia	Biphenyl and diphenyl oxide	12 to 400 °C	1060	1.57	3.57	0.136
Dowtherm A – Dow/IMCD	73% diphenyl oxide, 27% biphenyl blend	15 to 400 °C	1064	1.56	5	0.140
Royco 782 – Anderol Inc.	60-70% polyphaloefins, 30-40% esters	-40 to 205 °C	829	1.96	18	0.167
Syltherm XLT – Dow/IMCD	Dimethyl polysiloxane	-40 to 400 °C	814	1.86	0.80	0.102
Duartherm S –	Silicone based	-50 to 343 °C	957	1.69	49.24	0.130

Duratherm						
PSF-20cST Silicone HTF – Clearco	Polydimethylsiloxane	-50 to 220 °C	950	1.60	20	0.142
Duratherm G – Duratherm	Polyalkylene glycol	-40 to 260 °C	914	1.97	82.08	0.164

4.2.2. Molten salts

One promising class of HTFs is molten salts, as they can operate at much higher temperatures than oils. The higher operating temperature is enabled by a lower vapor pressure of the molten salts compared to synthetic oils. While the highest operating temperature of molten salts (>1000 °C) is not yet reachable due to receiver material limitations (as discussed in section 3), the higher operating temperatures that are achieved today (as high as 550 °C) result in a higher exergetic efficiency and lower LCOE. Additionally, molten salts can be directly used for thermal storage which increases the hours of electricity production and further reduces the LCOE (discussed further in section 0).[210]

Molten salts are typically binary and ternary compounds of inorganic ions and are divided in three main classes – nitrates, chlorides and fluorides. From a thermophysical perspective, molten salts have much higher volumetric heat capacity, thermal conductivity, and comparable viscosity (at their respective operating temperature) than oil-based HTFs. **Table 6** shows a representative list of a variety of molten salts and their thermophysical properties (adapted from Sohal *et al.*).[211] A more complete list of physical properties of molten salts including density, viscosity, vapor pressure, surface tension and refractive index is provided by Janz.[212]

While salt-based HTFs are extremely promising, there is still room for significant improvement through further research and development. One of the most important areas of research is the problem associated with the solidification of molten salts when the sun is not shining. For example, commercially available

Hitec Solar Salt has a freezing point of above 140 °C which makes anti-freezing strategies a very important consideration due to the diurnal nature of solar radiation. Studies investigating the practicality of using molten salts in parabolic trough solar collectors also identified solidification of the salt as one of the largest issues facing this technology.[213] The solidification of salt ultimately increases the cost through freeze prevention mechanisms. Conventionally, these issues are solved through continuous circulation of the fluid overnight (added pumping cost), auxiliary heaters to maintain a minimum temperature (added fuel cost), or electrical heaters along the pipeline (added electricity cost).[210] It is then of great importance for researchers to investigate the lowering of the freezing point of these HTFs without compromising their thermal-fluidic performance.

The working principle of reduced melting points is related to the entropy of mixing of pure components.[214,215] Recent work by Raade created a molten salt HTF with a novel mixture of inorganic salts.[208] While many different unique mixtures exist, nitrate salts mixed with lithium, sodium, potassium, cesium, and calcium cations were investigated by the authors. This work demonstrated a low melting point around 65 °C by exploiting eutectic behavior. In addition, the thermal stability of the mixtures was demonstrated to about 500 °C.

The chemical stability of molten salts was studied by Bradshaw and Siegel and key degradation mechanisms were identified.[216] The process of creating nitrite from the nitrate species in the HTF will occur in the presence of oxygen and depends on its partial pressure in the surrounding environment. This work identified the nitrate-nitrate reaction as the characteristic process of degradation regardless of other existing components. In addition, nitrate salts react with carbon dioxide and moisture in the ambient air to form carbonates and oxides which degrade the salt mixture characteristics. Molten fluoride salts may release harmful acids such as HF with exposure to atmosphere and significantly increase metal corrosion rates. Therefore, it is important to carefully control the operating environment of some molten salts.

Corrosion of metal alloys by molten salts is another issue that needs to be addressed. While several common nitrate-based salts, like *Hitec*, showed negligible corrosion of seamless stainless steel, other copper and nickel-based alloys have reported corrosion rates of 1-10 μm per year at 570 °C. The corrosion rates can be >100 μm per year for halogen-based salts for high temperature operation.[199] Pipes and containers made from Inconel and Hastealloys were recommended for use with chloride and fluoride salts. More experimental studies are required to ascertain material compatibility of molten salts at different temperature and in the presence of air and impurities.

Table 6: List of some molten salts and their thermophysical properties. Adapted from Sohal,[211] and Vignarooban *et al*.[199]

Fluid	Chemistry	Temperature range	Density (kg/m^3)	Specific heat (kJ/kgK)	Viscosity (mPa s)	Thermal conductivity (W/mK)
Nitrates						
Hitec®	$NaNO_3$-$NaNO_2$-KNO_3	142 to 535 °C	875	1.85	22.7	0.124
Solar Salt	$NaNO_3$-KNO_3	220 to 600 °C	863	10	25	0.134
Chlorides						
K-Mg chlorides	KCl-$MgCl_2$	435 to 800 °C	1060	1.57	3.57	0.136
Halotechnics SS-700	-	257 to 700 °C	2310	0.79	4	0.35-0.4
Fluorides and *Carbonates*						
FLiNaK	LiF-NaF-KF	454 to >900 °C	2020	1.88	2.9	0.92
Li-Na-K fluorides/ carbonates	LiF-Na_2CO_3-K_2CO_3	~400 to 920 °C	2100	1.9	-	1.18

Li-Na-K carbonates	Li$_2$CO$_3$-Na$_2$CO$_3$-K$_2$CO$_3$	~400 to 850 °C	2143	1.45	4.3	1.25

4.2.3. Other liquids

Several other liquids have been proposed as possible heat transfer fluids for solar-thermal applications. Most of these HTFs are currently in the research and development phase. These include ionic liquids and nanofluids which are actively being studied in the community. In addition, liquid metals have received significant attention as high performance heat transfer fluids. The main thrust of research for the liquid metals is to develop corrosion resistance and safe handling processes, while improving the heat transfer performance is the main focus for ionic liquids and nanofluids.

Ionic liquids are similar in nature to molten salts but, by definition, have freezing points below that of water.[204] As discussed previously, molten salts are usually binary and tertiary compounds of inorganic ions (*e.g.* nitrates, chlorides, and fluorides). Significant suppression of the melting point, below room temperature, is achieved in ionic liquids by replacing the inorganic cations with large unsymmetrical organic cations, in addition to choosing eutectic compositions of binary and ternary systems as is done for molten salts.[217] These large organic cations result in strong ion-ion interactions that reduce the melting point drastically.

Table 7 shows a list of ionic liquids with the imidazolium cation ([im]) investigated for solar thermal applications and their thermophysical properties. Ionic liquids with other cations have also been studied, but the large and asymmetrical nature of [im] enables melting point depression below room temperature which is quite attractive for CSP applications. Fredlake *et al.*[205] report thermophysical properties of several [im]-based ionic liquids as well as how they change with chemistry. For instance, better thermal stability was associated with a large anion size, and the heat capacity was found to increase with

increasing number of atoms in the ionic liquid. Overall, the density, heat capacity and thermal conductivity are comparable to synthetic oils, however the viscosity is an order of magnitude higher.

The low vapor pressure, stability over a large temperature range, as well as large heat capacity of ionic liquids suggests their suitability as HTFs for solar-thermal applications. However, issues such as higher pumping cost due to large viscosity and chemical compatibility with certain metals need to be addressed. Contamination by other species such as water, metal cations and chloride can alter the properties of the ionic liquids and deteriorate heat transfer performance.[204] The high cost and limited availability of ionic liquids are additional issues that need to be addressed.

Other heat transfer fluids that have been widely studied in the past two decades consist of suspensions of sub-micrometer sized particles in a base fluid.[218–220] The motivation behind nanofluids, as they are commonly known, is to enhance the heat transfer performance by adding high thermal conductivity nanoparticles to the base fluid. However the degree of performance improvement is not easy to predict in practice since it depends upon several competing factors such as the nanoparticle concentration, base fluid, and particle size and morphology.[218]

Nanofluids achieve higher thermal conductivities under proper conditions,[221] however that does not necessarily lead to a higher efficiency.[219,220] In addition, high nanoparticle concentrations increase the viscosity (pumping power) and may lead to sedimentation issues. Optimal nanoparticle size and cluster structure for nanofluids is also unclear. In contrast to thermophysical properties which may not change drastically with the addition of nanoparticles, significant variation in the optical properties are possible. This allows the use of nanofluids for direct solar absorption in the collector.[222,223] The solar absorption is enhanced by the addition of nanometer-sized particles, comparable in size to the wavelength of incident radiation, to the base fluid. The extent of absorption is dependent on the particle size, particle shape, and the optical properties of the particle and base fluid.[224] In general, greater absorption is achieved for fluids with non-metallic particles whereas metallic particles are desirable for a higher thermal conductivity.

However, despite these advances, no study has shown evidence of nanofluid-based collectors outperforming commercial vacuum tubes receivers.[219]

Several challenges need to be addressed for nanoparticle suspensions to be seriously considered for solar thermal applications. Agglomeration in nanofluids due to particle-particle interaction can lead to significant changes in the effective thermal conductivity as well as viscosity. This can lead to fluctuations in the convective heat transport as well as pumping. More studies are necessary to understand the effect of agglomeration and instabilities on the thermophysical properties and heat transfer performance. Additionally, the high viscosity of the nanofluids results in large pressure drop and high pumping power demand. The long-term stability of nanofluids also needs to be investigated since nanoparticles may lead to erosion of metal surfaces. In addition, the cost of production remains prohibitively high.

Liquid metals, with their superior heat transport properties and high operating temperature, are a promising candidate for heat transfer fluids in CSP systems. Liquid metals have low vapor pressure, high thermal conductivity and relatively low viscosity. As a consequence, FOMs of liquid metals are roughly one order of magnitude higher than molten salts and several orders of magnitude higher than pressurized air, allowing operation at higher heat flux densities. In addition, efficiency is improved by operating at fluid outlet temperatures in the 700-1000 °C range, compared with <650 °C used currently.[200]

Pacio et al.[206,225] have analyzed the performance of liquid metals as HTFs and compared three promising candidates: liquid sodium, lead-bismuth eutectic (LBE) and molten tin (**Table 7** shows the thermophysical property values). Among the three, liquid sodium has the most favorable properties – highest heat capacity, lowest density and lowest melting point. Furthermore, its cost is comparatively low and is compatible with common structural materials such as steel. Liquid sodium and, to a lesser-extent, LBE have been investigated for operation in the nuclear sector. The high reactivity of alkali metals, like sodium, with both air and water make it a potential safety hazard. LBE is comparatively safer as it oxidizes slowly in the presence of air and water, but corrodes steels much faster than sodium at high

temperatures. Material compatibility studies of LBE with alternate structural materials such as tungsten, molybdenum, and aluminum-coated steels have shown promise and are currently under investigation.[226] Molten tin also has good thermophysical properties but its high melting point and incompatibility with steel at operating temperatures are issues that need to be addressed.

More recently, a multi-university team led by UCLA, as part of DOE's SunShot Initiative, is working on identifying new liquid metal HTFs using combinatorial material synthesis and thermochemical modeling.[227] Another SunShot CSP project, led by Asegun Henry of Georgia Institute of Technology, is developing high temperature (>1000 °C) thermochemical reactors using liquid metal HTFs to split water and generate hydrogen fuel.[228] The main goals of the project are to lower the melting temperature and increase the upper limit of stable operation to above 800 °C. Other technical targets include parameters such as melting point (≤ 100 °C), thermal conductivity (> 10 W/m-K), heat capacity (> 2 MJ/m^{3}K) and viscosity (≤ 2 mPa-s) of the fluid.[227] Additionally, the project has specific materials compatibility requirements as well as an aggressive cost goal of $\leq \$1/kg$ – the approximate price of popular molten salts. Other challenges include solidification, toxicity, corrosion and reactivity with materials used for storage.[228] Realizing these challenging targets would almost certainly lead to commercialization of liquid metal HTFs in solar-thermal systems.

Table 7: Thermophysical properties of some ionic liquids and liquid metals used as heat transfer fluids.[204,206]

Fluid	Chemistry	Temperature range	Density (kg/m^3)	Specific heat (kJ/kgK)	Viscosity (mPa s)	Thermal conductivity (W/mK)
Ionic liquids						
[emim][BF$_4$]	1-methyl-3-ethylimidazolium	14 to 446 °C	1253	1.28	36	0.20

	tetrafluoroborate					
[bmim][BF₄]	1-methyl-3-butylimidazolium tetrafluoroborate	-87 to 424 °C	1175	1.66	120	0.19
[dmpi]Im	1,2-dimethyl-3-porpylimidazolium bis(trifluorosulfonyl) imide	11 to 457 °C	1421	1.20	90	0.13
Liquid Metals						
Sodium	Na	98 to 883 °C	808	1.25	0.21	46.0
Lead-Bismuth eutectic alloy	44.5-55.5%wt Pb-Bi	125 to 1533 °C	9660	0.15	1.08	12.8
Molten tin	Sn	232 to 2687 °C	6330	0.24	1.01	33.8

4.2.4. Pressurized gases

Pressurized gases offer several advantages over conventional HTFs in solar-thermal systems. Gases can reduce some of the complexities associated with the handling of heat transfer fluids such as chemical stability, material compatibility issues, sealing and safety. In addition they are capable of operating at higher receiver temperatures which leads to higher energy conversion efficiency and lower operating costs. One of the promising prospects is direct expansion, *i.e.,* using the same fluid in the receiver as well as in the turbine, eliminating the need for a heat exchanger and thereby reducing cost and complexity. However, one of the biggest drawbacks is the poor thermal capacity of gases which may be overcome by using high pressures and large mass flow rates, but it makes the handling difficult and increases the cost. In this section we present some of the pros and cons of using pressurized gases such as CO_2, N_2 and air.

CO_2 has been widely studied as an HTF since its critical point (31 °C) is close to atmospheric temperature. Operation close to the critical point results in a significant enhancement of the cycle efficiency as a sharp increase is observed in the fluid heat capacity.[229] Several studies have looked at enhancing the performance of linear (parabolic trough and Fresnel) solar-thermal systems by using close-to-critical CO_2 cycles, multi-stage expansion/compression and regeneration, and optimizing the receiver design.[201,229,230] However, one of the drawbacks of using CO_2 is that the cycle must be closed, *i.e.,* the fluid must be recirculated from the collector to the turbine, to the condenser, and back to the collector. This requires thicker pipes and measures to prevent leaks. Nonetheless, the promise of high efficiency and compact size achieved by combining directly with supercritical CO_2 (s-CO_2) cycle has made CO_2 an appealing HTF.[231–233] More details of the s-CO_2 heat engines are provided in section **Error! Reference ource not found.**.

The use of air as an HTF, unlike CO_2, is simpler since operating pressure can be close to ambient and perfect sealing is not a concern. A comparison between air and CO_2 as HTFs showed no significant difference between the two as far as the receiver performance was concerned.[201] However, using air provides other advantages, including compatibility with packed-bed thermal storage and no fluid cost. For these reasons, and because the large surface area of cavity receivers offsets the low heat transfer capacity of gas-based HTFs, air is often used in central receiver systems.[234,235] Investigations with other gas-phase HTFs, such as N_2, have shown performance comparable to synthetic oils, however commercial development is unlikely due to the high capital cost.[236]

Table 8: List of pressurized gas-based heat transfer fluids.[237]

Fluid	Chemistry	Temperature range	Density (kg/m^3)	Specific heat (kJ/kgK)	Viscosity (mPa s)	Thermal conductivity (W/mK)

Air (30 – 100 bar)	>-215 °C	1.20	1.01	0.019	0.024
CO_2	-73 to 1000 °C	1.84	0.844	0.015	0.015
N_2	>-196 °C	1.165	1.04	0.018	0.024
Water vapor (30 – 100 bar)	>234 °C	0.80	1.97	0.012	0.016

4.2.5. Steam

The HTF in a traditional solar thermal power plant transports heat to the power cycle which is most commonly a water-steam cycle such as steam-Rankine. To avoid excessive costs associated with the HTF or the large heat exchanger equipment which thermally couples the HTF to the power cycle, engineers have tested the idea of direct steam generation (DSG). Water collects the heat directly and it becomes superheated steam which is *directly* fed into the power cycle. The high temperature water-steam mixture (>400 °C) has a higher heat capacity than other gases which increases the efficiency of the receiver as well as the power cycle. The feasibility of DSG was initially proven under real conditions at the Direct Solar Steam (DISS) facility at Plataforma Solar de Almeria (PSA) in 1997-98.[238] The success of DISS and other studies led to the development of pre-commercial DSG facilities including a 5-MW INDITEP plant, and commercial power plants including 11 MW PS10 and 20 MW PS 20 power plants in Andalusia, Spain.[239,240] The results from these projects point towards a 8-14% reduction in LCOE compared to SEGS-like plants using synthetic oils as the HTF.[241]

Despite the promise of direct steam generation, several engineering challenges, arising due to the two-phase flow, need be addressed. These include the higher operating cost due to high pressure required to pump the two-phase mixture.[207] The non-uniform heat transfer from pipe walls result in large temperature gradients which can damage the pipes. At a system-level, the stability of the temperature and pressure at the outlet is another big concern. Hence current research efforts are focused on the optimization of the

collector loop and power cycle design, the regulation of outlet temperature and pressure, and the reduction of collector piping costs.[197]

5. Thermal Energy Storage

To generate electricity on demand despite solar transients (such as clouds passing overhead or the sun setting) storage should be used. Storage is very valuable for renewable energy technologies, as storage makes them more reliable, more amendable to integration in the grid, and in the case of solar power allows electricity production to be shifted to meet peak demand.[242,243] The most appropriate storage mechanism for use with CSP is thermal energy storage (TES) due to the intermediate heat step already present in CSP systems.[244,245] Plants with solar multiples greater than unity, defined as the ratio of insolation to the receiver at the design point to the nominal heat input of the heat engine, can use the extra solar energy collected during peak sunlight hours to charge a TES system, and discharge the TES later to produce electricity when the sun is no longer shining.

Thermal energy storage is one of the main advantages of CSP, because TES is significantly cheaper than other energy storage technologies (e.g., batteries) and is not compatible with other intermittent renewable energy technologies such as photovoltaic cells and wind turbines. There are some grid-level energy storage technologies that are economically competitive with TES, such as pumped hydro and compressed air, however these exceptions are geographically limited.[246] For intermittent renewable sources, the value of their generated electricity decreases at high grid penetration.[247] If storage is included, e.g., CSP with TES, then the generated electricity maintains a high value even in the high renewable penetration scenario. Jorgenson et. al. found that in certain deployment scenarios, electricity from CSP with storage could be more than twice as valuable as electricity from PV to the utility provider.[32]

There are two primary characteristics of a TES system: capacity and power. Capacity is a measure of how much thermal energy a TES system can store, while power is a measure of how much heat the system can deliver while discharging. Ideally a TES system can have both high capacity and power at low cost, and for commercial TES systems a primary concern is achieving low specific cost (cost per unit capacity, e.g., $/kWh). System capacity and power are related to the thermal properties of the materials being used for the TES (e.g., specific heat for capacity or thermal conductivity for power) as well as the system design (e.g., volume of material for capacity or heat exchanger area for power). The system also typically has a specific range of operating temperatures which need to be compatible with the concentrator, receiver and heat engine. The TES system also has a characteristic storage time, i.e., how long the system can provide power for, which can be found simply by dividing system capacity by power. There are different applications for different storage times,[246] and TES is most appropriate for response on the order of hours. In this several hour range of response, TES can address weather transients and load shifting to the evening.[244] At the long end of this range, base load (i.e., continuous) power generation has also been considered by using TES systems with ≥ 15 hour storage time.[248]

An important metric for TES systems is exergetic efficiency. In electrical storage systems (e.g., batteries) an important metric is the round trip efficiency, which refers to how much electrical energy you can recover from the charged system divided by the electrical input required to charge the system. Round trip efficiency would be the relevant metric for TES in the case where electrical heaters were being used to charge the system. In TES used with CSP, the relevant metric is exergetic efficiency, which refers to how much exergy can be recovered from the charged system divided by the exergy input required to charge the system.[245,249] Exergy is the maximum work available in heat of a given temperature, assuming a certain cold reservoir temperature. Exergy B can be calculated by multiplying the thermal energy Q by the Carnot efficiency:

$$B = Q \left(1 - \frac{T_C}{T_H} \right) \tag{19}$$

where T_H is the temperature the heat is delivered at and T_C is the cold reservoir temperature. The exergetic efficiency η_B of the TES system can be calculated by:

$$\eta_B = \frac{Q_{out}\left(1 - \frac{T_C}{T_{H,out}}\right)}{Q_{in}\left(1 - \frac{T_C}{T_{H,in}}\right)} \tag{20}$$

where Q_{out} and Q_{in} refer to the heat recovered from and supplied to the TES system, respectively, and $T_{H,out}$ and $T_{H,in}$ refer to the temperature at which heat is recovered from and supplied to the TES system, respectively. Exergetic efficiency will be reduced below unity due to a few factors. The first factor is heat losses from the storage media while it is being stored in its charged state (e.g., due to storing thermal energy materials at high temperature) which can be minimized with insulation and good container design. The second factor is the temperature drop required to charge or discharge the TES, and is influenced by the material thermal conductivity as well as system design. For example, to heat a storage medium to 400 °C, the charging process might need to be driven with an HTF at 410 °C, and in discharging that storage medium the HTF might be recovered at 390 °C. It can be challenging to minimize this exergy loss because the thermal conductivity of many TES materials is inherently low and because high performance heat exchangers for efficiently charging and discharging the TES can lead to large system costs. It is important to consider exergetic efficiency, not just energy efficiency, in TES system design.[250]

Material properties and system design are both important to the TES system performance.[245] This review will focus primarily on the choice of storage materials, however some system design concepts will be covered briefly. One distinction in system designs is one-tank vs. two-tank systems. In a one-tank design, all the storage media is kept in the same container, but separated spatially (e.g. hot fluid at the top of the tank and cold fluid at the bottom in a thermocline design).[251,252] In a two-tank design, the charged (e.g., hot) and discharged (e.g., cold) storage media are kept in separate tanks. One-tank systems have the

potential to be cheaper, while two-tank systems allow decoupling of capacity from power.[244,253–255] Another distinction in system types is direct versus indirect systems. In direct systems the HTF is also used as the storage medium while in indirect systems, the HTF transfers heat to another medium for storage. While indirect systems suffer from lower exergetic efficiency than direct methods, they are often used due to cost and storage density reasons.[256] Another big part of system design is overcoming the low thermal conductivity of many TES materials. This is typically accomplished by using extended heat transfer surfaces of materials with high thermal conductivity (e.g., metals) or heat pipes within the space where the TES is stored to quickly deliver or recover heat.[257,258]

Selecting an appropriate storage material is critical to a high performance TES system. For all types of TES, there are certain desirable material characteristics:[244]

1. Large gravimetric and volumetric storage capacity (high heat capacity/latent heat/heat of reaction as well as high density) – (to achieve high storage capacity)
2. High thermal conductivity/diffusivity/effusivity – (to achieve high thermal power and exergetic efficiency)
3. High cycling and thermal stability – (for long system lifetime)
4. Non-toxic, non-flammable, non-corrosive and can be handled/contained easily – (for ease of system implementation)
5. Small coefficient of thermal expansion – (to minimize thermal stresses in system)
6. Inexpensive and earth abundant materials – (for low system cost)

The first two characteristics relate directly to the system performance for achieving high storage capacity, high power, and high exergetic efficiency. The rest do not relate directly to these performance metrics but are critical to the implementation of actual systems and their feasibility as utility-scale, commercial solutions.

There are three classes of TES material: sensible, latent and thermochemical. In sensible TES, heat is stored by raising the temperature of the storage material. In latent TES, heat is stored by subjecting the storage material to a phase change, thus latent TES materials are also referred to as phase change materials (PCM). In thermochemical TES, heat is stored by subjecting the storage material to a reversible chemical reaction, i.e., an endothermic reaction is facilitated by input heat, and heat can be recovered later

78

by the reverse exothermic reaction. Sensible TES is the most commercially developed type of TES but has the lowest storage density, while thermochemical TES is the least developed but offers the highest potential for storage density (see Figure 18).[244] As TES technologies mature, more CSP plants will be able to move from sensible storage to latent and then thermochemical storage to take advantage of the higher storage densities. The rest of this section will cover these three classes of TES, primarily addressing materials that have been investigated for use in TES systems.
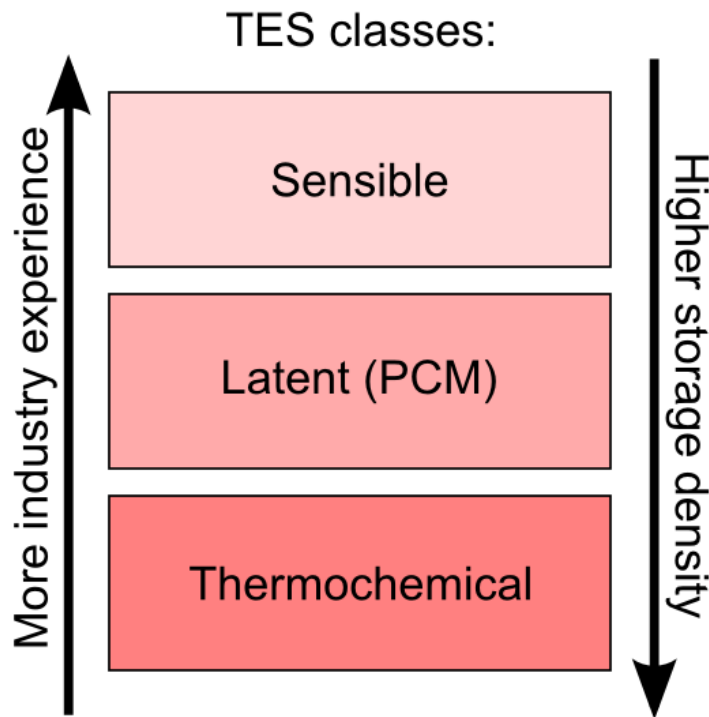
Figure 18 The different classes of thermal energy storage: sensible, latent (or phase change material), and thermochecmical. Sensible TES is the most commercially mature but has the lowest energy density, while thermochemical TES is the least commercially mature but has the potential for the highest energy density

5.1.   Sensible storage

Sensible TES can be broadly divided into two categories: solid and liquid (gas is not used due to its low density). In principle there are also systems that combine solid and liquid, for example a fluid flowing over a packed bed of solid particles.[244] This distinction is not overly important, as both solid and liquid

sensible TES operate on the same principle: heat is stored by heating up a material. In both cases, the heat stored $Q_{sensible}$ depends on the temperature change ΔT and the specific heat c_p of the material:

$$Q_{sensible} = V\rho c_p (T_2 - T_1) = m c_p \Delta T \tag{21}$$

where V is the volume of the storage material used, ρ is the density of the material, m is the mass of storage material used, and T_2 and T_1 are the charged and discharged material temperatures, respectively. Specific heat values of solids can be estimated by the Dulong-Petit law:

$$q_{mol} \cong 3R\Delta T \tag{22}$$

$$c_p \cong \frac{3R}{M} \tag{23}$$

where q_{mol} is the heat stored per mole, R is the universal gas constant, and M is the molar mass of the material. It was found that a mole of a material almost always has the same heat stored for an identical ΔT, which is approximately 25 J/K/mol. This can equivalently be understood as a heat capacity of $3k_b T$ for each atom from the equipartition theorem (6 degrees of freedom, 2 vibration modes in each direction, multiplied by $\frac{1}{2} k_b T$ for each degree of freedom), where k_b is the Boltzmann constant and T is the absolute temperature of the material. Since interatomic spacing does not vary significantly among solids, the relative volume of atoms in the lattice (i.e., the packing fraction) does not change much between materials which leads to similar volumetric energy densities ρc_p. Because most non-porous materials have similar ρc_p values (i.e., less than an order of magnitude variation among them), as shown in Figure 19, the energy storage in sensible TES technologies is strongly driven by the volume of the system. The total capacity of the system (i.e., in kWh$_t$/m^3 rather than kWh$_t$/m^3/K) can be calculated by integrating the volumetric heat capacity over the operating temperature range. Larger operating temperature ranges will give higher capacities, but the system must be compatible with receiving heat over widely varying temperatures. Table 9 lists some materials which have been considered for sensible TES, as well as their relevant properties. Sensible storage technologies are relatively mature, and deployed sensible TES

systems have achieved efficiencies higher than 90%.[259] The remainder of this section will discuss sensible

TES materials in more detail.
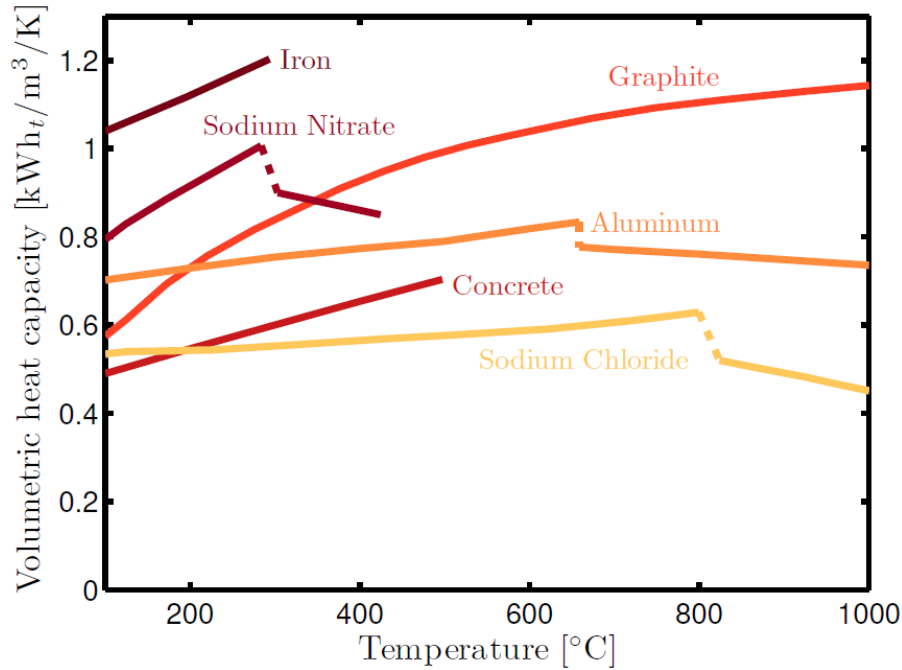
Figure 19 Volumetric heat capacity vs. temperature for various materials. Discontinuities in curves correspond to phase changes. Adapted with permission from reference [244]. Copyright 2012 Begell House, Inc.

Table 9 Selected materials which have been considered for sensible TES. Material properties are representative values from within operating temperature range. Values are from Geyer (Ref. [260]) unless noted otherwise

	Material	Operating temperature range (°C)	Thermal conductivity (W/m/K)	Density (kg/m^3)	Specific heat capacity (kJ/kg/K)	Volumetric heat capacity (kWh$_{th}$/m^3/K)
Liquids	Water	200-300	0.7	800	4.9	1.09
	Mineral oil	200-300	0.12	770	2.6	0.56
	Synthetic oil	250-350	0.11	900	2.3	0.57
	Silicone oil	300-400	0.10	900	2.1	0.52
	Liquid sodium	270-530	71	850	1.3	0.31

	Nitrite salts	250-450	0.57	1825	1.5	0.76
	Nitrate salts	265-565	0.52	1870	1.6	0.83
	Carbonate salts	450-850	2	2100	1.8	1.05
	Hitec[261]	220-600	0.46	1900	1.5	0.79
	HitecXL[262]	120-500	0.52	1990	1.4	0.77
Solids	Cast iron	200-400	37	7200	0.56	1.12
	Cast steel	200-700	40	7800	0.60	1.30
	Sand/rocks/gravel	200-300	1	1700	1.30	0.61
	Concrete	200-400	1.5	2200	0.85	0.52
	Castable ceramic[263]	200-390	1.35	3500	0.87	0.84
	Advanced concrete[263]	200-390	1.0	2750	0.92	0.70
	NaCl	200-500	7	2160	0.85	0.51
	Silica fire brick	200-700	1.5	1820	1.00	0.51
	Magnesia fire brick	200-1200	5	3000	1.15	0.96
	Graphite[264]	200-2000	40	1900	1.75	0.92

One well established method for storing thermal energy is using a steam accumulator, which uses water as the TES material.[265,266] In a steam accumulator pressurized, saturated water stores the thermal energy. To extract the thermal energy, steam is produced by lowering the pressure of the saturated water. While there is a phase change process occurring, thermal energy is stored in raising the temperature of the water, not in boiling it and converting it to steam. Since the thermal energy is extracted from the steam accumulator via the evaporated steam, the discharge rate is not limited by the thermal conductivity of water. Such a system can be charged with saturated water directly or can be fed with cool water and heated with a different HTF through a heat exchanger. Operating temperature and pressure in these systems are limited by the critical point of saturated water (374 °C, 221 bar). For its operational

temperature range, a steam accumulator is a very cheap and energy dense option for TES. A deployed example of a steam accumulator used with CSP is at the Planta Solar towers in Sevilla, Spain, where such a system provides approximately 1 hour of thermal storage, operating at temperatures from 250 – 300 °C.[34,267]

Oils are another liquid that have been considered for use as sensible TES materials. Mineral oil could be used as an effective thermal storage material with low cost, however its flammability leads to safety concerns.[259] Mineral oil also has a limited operating temperature range without going to expensive pressure vessels. While in principle synthetic oils or silicone oils could be used as a thermal storage material, they are too expensive to achieve a reasonable storage capacity at acceptable system costs.

For higher temperature storage than can be achieved with a steam accumulator, molten salts are the best option. Salts have reasonably high storage densities and are inexpensive, making them an economical storage material.[253] For molten salts, the operating temperature range is limited on the low end by the freezing temperature and on the high end by corrosion. Freezing is a major concern for these systems, as frozen salts can damage piping and pumps, so they are often equipped with protection measures such as auxiliary heaters.[253] Nitrite, nitrate and carbonate salts all have reasonable properties as TES materials, however improved properties (in terms of both cost and performance, especially lowering melting temperature) can be achieved by mixing salts. One commercially used salt mixture is $NaNO_3$-$NaNO_2$-KNO_3 (0.07-0.40-0.53 by mass) which is known as Hitec.[261] A slightly different mixture of $Ca(NO_3)_2$-$NaNO_3$-KNO_3 (0.48-0.07-0.45) is known as HitecXL and has a lower melting point. Research effort continues to attempt to develop better molten salts for thermal energy storage. Peng et al. designed a quaternary mixed molten salt for TES composed of K, $NaNO_2$, Cl and NO_3 with a melting point as low as 172 °C for certain eutectic mixtures.[268] Zhao and Wu demonstrated a mixed salt of KNO_3, $LiNO_3$ and $Ca(NO_3)_2$ with a very low melting temperature of 80 °C. Ionic liquids (salts with organic cations and low melting temperatures discussed previously in section 4) have also been considered for use as TES materials.[269,270] Their low melting temperatures makes freezing less of a concern than for molten salts.

While their other properties (volumetric storage capacity and thermal conductivity) are similar to molten salts, ionic liquids are more expensive than molten salts, which has limited their adoption in commercial TES systems.

Solids also offer promising, inexpensive sensible TES solutions.[271,272] With a solid material as the TES, it is common to use a packed bed of solids with HTF running through to charge and discharge the system. If the HTF is a gas (e.g., air) its sole purpose is to transfer heat, however if the HTF is a fluid, the fluid heat capacity will commonly be comparable to the solid and it thus can act as a supplementary storage material.

At first glance, metals seem like they could provide a competitive TES material. Metals offer high thermal conductivity and heat capacity, which would lead to high system capacity and power, but they are significantly more expensive than other options.[273] Due to their high cost, metals are used for enhancing the thermal conductivity of a TES system (e.g., through the integration of metal fins), but are not typically considered for use as the bulk storage material in TES systems.

A very inexpensive approach is to use sand, gravel or concrete as the solid sensible TES material. With sand or gravel, a packed bed configuration is typically used, however flowing sand configurations have also been proposed.[274,275] Concrete can be formed into bricks and arranged in a packed bed configuration or HTF pipes can be set to run through large concrete blocks.[260,276] Work has been performed to develop concretes with better thermal properties, and which are compatible with finned HTF heat exchanger designs.[271] Concretes and castable ceramics have been developed with volumetric heat capacities greater than 0.7 $kWh_{th}/m^3/K$.[263] For higher temperature applications, silica, alumina and magnesia bricks have been suggested with molten salt as an HTF.[272] Another proposed thermal energy storage material using sensible heat is graphite, due to its good high temperature stability and high specific heat at elevated temperatures. The company Graphite Energy has a demonstration project integrating graphite TES into a 3MW demonstration power tower plant in Lake Cargelligo, Australia.[277]

5.2.   Latent storage

In latent TES, thermal energy is stored by subjecting the storage material to a phase change process, thus latent TES systems are commonly referred to as phase change materials (PCM). Typically the phase change process used is melting a solid into a liquid, but occasionally solid-solid phase changes are used (e.g. between two different crystalline phases). Liquid-gas phase changes are not used due to the large expansion undergone in boiling, which leads to either high storage volumes or strict pressure vessel requirements. In latent TES, the energy stored Q_{latent} depends on the latent heat (or enthalpy) of melting for the material Δh_m:

$$Q_{latent} = V\rho\Delta h_m = m\Delta h_m \tag{24}$$

where V is the volume of the storage material used, ρ is the density of the material and m is the mass of storage material used. Latent heat of melting roughly scales linearly with melting temperature for different classes of materials, e.g., metals tend to have a molar latent heat value of 1 - 1.5 times the melting temperature times the universal gas constant (8.3 J/mol/K).[278] Thus higher energy densities can typically be achieved for PCMs with higher melting temperatures, as shown in Figure 20, however the intended application will limit the usable melting temperature range. PCM storage can also take advantage of sensible temperature change if the operating temperature range extends significantly beyond the melting temperature.
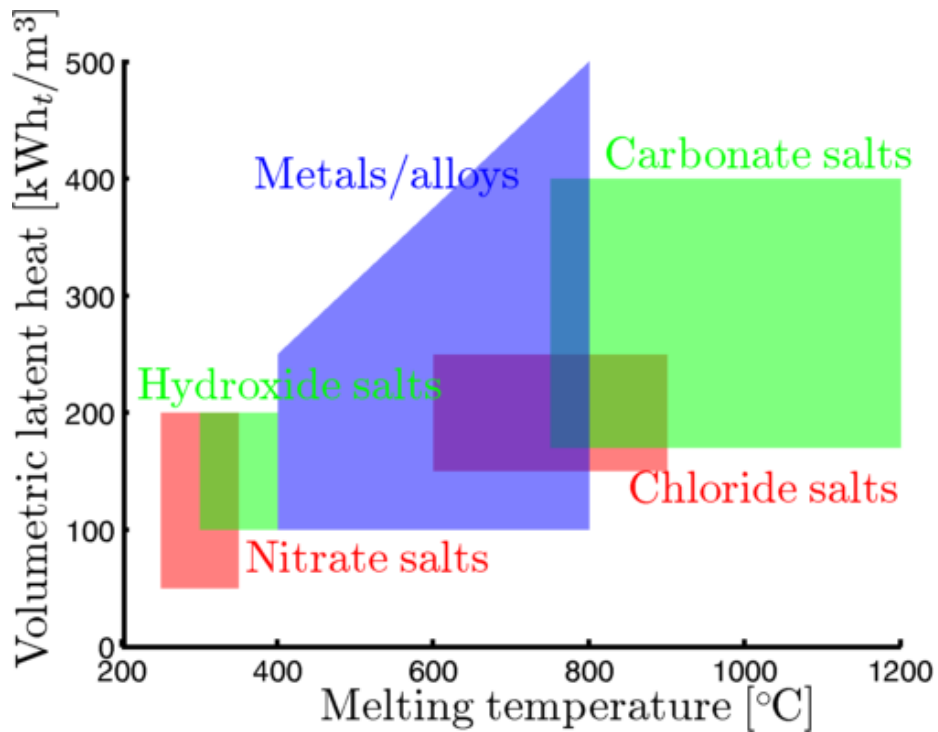
Figure 20 Typical ranges of melting temperatures and volumetric latent heats for different categories of materials considered for PCM TES. There are metals and metal alloys with melting temperatures higher than 800 °C, however there are limited examples with competitive latent heats at the time of writing

Latent TES offers a few advantages compared to sensible TES. First, the energy density is typically much higher, since $\Delta h_m \gg c_p \Delta T$ for most systems. Second, the charging and discharging processes usually occur at a constant temperature, which can be advantageous from a system standpoint for targeting a specific heat engine operating temperature. For non-eutectic alloys there is a melting range rather than a specific melting temperature. For latent TES materials, a high enthalpy of melting is desired to achieve good energy density. Many different materials systems have been investigated in search of high latent heats.[279,280] High thermal conductivity is also desirable to allow quick (and efficient) charging and discharging of the PCM. Some materials used or proposed for use in latent TES systems are listed in Table 10.

Table 10 Selected PCM TES materials. Not all thermal conductivity values are available, however salts tend to have low values (<1 W/m/K) while metals tend to have high values (>50 W/m/K).

Material	Phase	Thermal	Density	Specific	Volumetric	Ref.

		change temperature (°C)	conductivity (W/m/K)	(kg/m³)	latent heat (kJ/kg)	latent heat (kWh_th/m³)	
Metals	Zn	419	50	6760	112	210	[244]
	Al	660	91	2380	397	262	[244]
Alloys	Mg-Zn (46-54)	340	n.a.	4600	185	236	[257]
	Mg-Cu-Zn (60-25-15)	452	n.a.	2800	254	198	[257]
	Al-Si (88-12)	557	n.a.	2540	498	351	[257]
	Al-Si (12-88)	576	160	2700	471	353	[257]
	Zn-Cu-Mg (49-45-6)	703	n.a.	8670	176	424	[257]
Salts	$LiNO_3$	254	0.6	1780	360	178	[244]
	$NaNO_2$	270	0.6	1810	180	91	[244]
	$NaNO_3$	306	0.51	1910	175	93	[244]
	NaOH	322	0.8	2130	210	124	[244]
	KNO_3	337	0.45	1880	100	52	[244]
	KOH	380	0.5	2044	150	85	[258]
	$MgCl_2$	714	n.a.	2140	452	269	[258]

	NaCl	800	7	2160	480	288	[257]
Salt mixtures/ composites	KNO$_3$-KCl (95.5-4.5)	320	0.5	2100	74	43	[257]
	NaCl-Li$_2$CO$_3$-Na$_2$CO$_3$ (24.5-20.5-55)	393	1.0	1800	240	120	[244]
	K$_2$CO$_3$-Li$_2$CO$_3$-Na$_2$CO$_3$ (35-32-33)	397	n.a.	1900	275	145	[244]
	MgCl$_2$-NaCl (52-48)	450	0.95	2230	430	266	[257]
	K$_2$CO$_3$-Li$_2$CO$_3$ (65-35)	505	n.a.	2000	345	192	[244]
	BaCl$_2$-KCl-CaCl$_2$ (47-24-29)	551	0.95	2930	219	178	[257]

	LiNaCO$_3$-C (90-10)	510	4.3	2500	530	368	[281]

Metals and metal alloys have been proposed as PCM TES materials, as they have properties which are desirable for PCMs: they have high thermal conductivity and large latent heat. While from a performance point of view metals are a promising option for PCM TES, they are expensive. The cost drawback can be addressed in part by alloying metals with cheaper materials. For example, aluminum silicon alloys have been shown to have good thermal properties, and silicon is inexpensive and earth abundant.[282]

Salts offer a more economical option than metals for a PCM TES. There is a wide range of melting temperatures for different single and mixed salts.[280] While some salts have sufficient latent heat, they typically have very low thermal conductivity (<1 W/m/K) which limits the thermal power that can be achieved in salt-based TES systems. As such, significant effort has been made to develop system designs which can achieve reasonable thermal powers despite the low intrinsic thermal conductivity of salts. PCM systems can be augmented with fins of higher thermal conductivity (e.g., metal) to increase the effective thermal conductivity of the material.[257] Another system design encapsulates PCMs and stores the capsules in packed beds to enable faster charging and discharging, since the relevant length scale for heat penetration becomes the capsule diameter rather than the tank diameter.[283] Graphite has also been used as a matrix to increase the effective thermal conductivity of PCMs.[284,285] Similarly, an enhancement of thermal conductivity has been demonstrated by integrating carbon structures (e.g., graphite or carbon nanotubes) into the PCM at a microscopic level, with Ge et al. achieving a thermal conductivity of >5 W/m/K in LiNaCO$_3$ based PCM composites.[281]

In order for PCM TES to become more widely adopted, it is important to find inexpensive PCM candidates with improved properties compared to what has already been proposed and demonstrated. In addition to new latent storage materials, it is also critical to find affordable materials to make containers,

heat exchangers and capsules which are compatible with the PCMs and allow for fast and efficient charging and discharging. High performing PCMs, appropriate materials to contain the PCMs and good system design are all necessary for latent storage to be utilized in real applications.

5.3. Thermochemical storage

In thermochemical TES, thermal energy is stored in a reversible chemical reaction. An endothermic reaction is driven by heat input, and energy is stored in chemical bonds of the chemical product.[286] The product of this reaction can be stored until the thermal energy needs to be recovered. To recover the thermal energy, the reverse exothermic reaction is performed, releasing the thermal energy for use with the heat engine to produce electricity. Such a chemical reaction can be written:

$$AB \overset{\Delta H_r}{\Longleftrightarrow} A + B \tag{25}$$

where AB is the reactant (the discharged state), A and B are the products (the charged state), and ΔH_r is the molar heat of reaction. Thermochemical energy stored $Q_{thermochemical}$ is given by:

$$Q_{thermochemical} = n_A \Delta H_r \tag{26}$$

where n_A is the number of moles of one of the products. Advantages of thermochemical storage include higher energy density than sensible or PCM storage, and no thermal losses, as typically the chemicals can be stored at room temperature in their charged state.[287] Some chemical systems can also supply heat at different temperatures than the heat is absorbed at (called heat transformers when heat is supplied at a higher temperature and chemical heat pumps when heat is supplied at a lower temperature).[244] Some chemical processes can be driven by sunlight directly rather than heat (these are known as "solar fuels"),[288] however such reactions will not be covered in this review.

One distinction between different types of thermochemical TES systems is open versus closed systems.[244] In an open system, the reaction is performed at ambient pressure and exchanges gas with the atmosphere, whereas in a closed system the reaction occurs in a sealed container. Open systems are less expensive to implement, however open processes are less controlled and can be contaminated by particulates from the

environment. Another important distinction is the phases of the chemicals involved in the reaction. Some well-studied reactions involve only liquids and gasses. For example, NaOH-water systems have been demonstrated, however the operating temperatures are not high enough for CSP applications.[289] Another reaction that has been demonstrated with parabolic dishes is disassociation of ammonia into nitrogen and hydrogen gases.[290] A similar NH_3SO_4 system with higher storage density has been proposed but has yet to be demonstrated.[287] Cyclohexane (C_6H_{12}) dehydrogenation (reacting to form benzene and hydrogen) is another potential reaction which has been proposed for use as thermochemical TES with reasonable energy density. Work has explored other organic systems as well, such as methane reforming, however they have significantly lower energy densities. Challenges with these organic systems include the need for good catalysts and poor reaction reversibility.[287] Much more effort has been focused on solid-gas reactions, such as dehydration of metal hydroxides or metal hydrides, decarboxylation (removing carbon dioxide) of metal carbonates, and redox reactions of metal oxides. An example for each of these types of reactions is listed in Table 11 and will be covered briefly below.

Table 11 Selected thermochemical TES materials.[287]

Material	Chemical reaction	Operating temperature [°C]	Reaction enthalpy [kJ/mol]	Energy density [kWh/m³]
Ammonia	$NH_3 \Leftrightarrow \frac{1}{2}N_2 + \frac{3}{2}H_2$	400-500	67	745
Cyclohexane	$C_6H_{12} \Leftrightarrow C_6H_6 + 3H_2$	300-400	207	530
Calcium hydroxide	$Ca(OH)_2 \Leftrightarrow CaO + H_2O$	400-600	104	437
Magnesium hydride	$MgH_2 \Leftrightarrow Mg + H_2$	350-500	75	580
Calcium	$CaCO_3 \Leftrightarrow CaO + CO_2$	900	178	692

carbonate				
Cobalt oxide	$2Co_3O_4 \Leftrightarrow 6CoO + O_2$	900	205	295

In dehydration of metal hydroxides, energy is stored by removing water from a metal hydroxide. One potential system is calcium hydroxide: the dehydration reaction is performed by removing a water molecule from calcium hydroxide ($Ca(OH)_2$) to form calcium oxide (CaO). Repeated cycling of the calcium hydroxide dehydration reaction has been successfully demonstrated in fixed bed reactor configurations.[291,292] One of the recurring challenges in metal hydroxide systems is the low material thermal conductivity which limits the reaction rate.[293]

In dehydration of metal hydrides, energy is stored by removing hydrogen from a metal hydride. One example is magnesium hydride (MgH_2), which is reacted to form magnesium and hydrogen. There have been successful experimental demonstrations of reversible reactions in excess of 1000 cycles.[294] These dehydration reactions face challenges in poor heat transfer and slow reaction kinetics, however doping (e.g., with iron or nickel) has been used to improve reaction rates in the case of magnesium hydride.

In decarboxylation of metal carbonates, energy is stored by removing carbon dioxide from a metal carbonate. These decarboxylation reactions usually occur at very high temperatures (>450 °C, typically around 900 °C),[287] which are not common in CSP plants now but may be appropriate for future, higher-efficiency, higher-temperature plants. As one example, calcium carbonate ($CaCO_3$) can be reacted to form calcium oxide (CaO) and carbon dioxide at around 900 °C. A number of studies have been performed exploring this reaction for use as thermal energy storage.[295,296] The poor reactivity of the reactant leads to conversion efficiencies around 20% when the bulk of the calcium carbonate had been decarboxylated, which would need to be improved considerably for use in CSP applications.

In redox reactions of metal oxides, energy is stored by reducing a metal oxide to form oxygen. An example metal oxide is cobalt(II,III) oxide (Co_3O_4), which can be reacted to form cobalt(II) oxide (CoO)

and oxygen. Redox reactions of metal oxides for thermal energy storage are relatively unstudied, but theoretically offer high energy density for high temperature systems.[287]

While these thermochemical storage materials show great potential with high energy densities and an absence of thermal losses (which allows for the prospect of TES with unlimited storage time), much work remains to be done before thermochemical TES technology can be commercially adopted. From the chemical perspective, high reversibility of reactions must be demonstrated, along with reasonable reaction rates and conversion efficiencies. Affordable system designs are also necessary for commercial feasibility. If these obstacles can be overcome, it would improve the current suite of options for CSP storage, and allow CSP to play a more significant role in the global renewable energy portfolio.

6. HEAT ENGINE

The heat engine is the system in a CSP plant which converts the collected heat to electricity. This is traditionally achieved via a thermodynamic cycle converting the heat to mechanical energy, which is used to drive a generator and produce electricity (some alternatives exist at the research stage and will be discussed in 6.3). The thermodynamic cycle typically has four steps:

- A working fluid is compressed to high pressure
- The fluid is heated using the solar energy input
- The fluid is expanded to low pressure through a turbine (which produces mechanical work)
- The fluid is cooled back to its initial temperature

The net power output of the heat engine is given by the power produced by the expansion step minus the power input required for the compression step. Current CSP plants typically use Rankine cycles with

water/steam as the working fluid, with water being evaporated during the heating portion of the cycle.[21] The other commonly used cycle is a Brayton cycle, which uses a single phase working fluid. Heat engines used in CSP plants share many parts with traditional (e.g., fossil fuel fired) power plants. Due to the long history of research into engines for use with fossil fuels, a great portion of the potential cost reduction in steam-Rankine and air-Brayton heat engines for use with CSP simply comes from scaling up the plant rather than technology improvements (scaling up these plants also leads to higher heat engine efficiency).[297] However, there are some newer engines and working fluids being developed which could lead to cost reduction in CSP plants.[298]

6.1. Heat engine efficiency

While the heat engine should be reliable and ideally require low capital investment, the main performance metric of the heat engine is how efficiently it coverts heat to electricity. Increase in efficiency is mostly driven by operating at higher temperatures. The highest achievable efficiency is the well known Carnot efficiency η_C, given by $\eta_C = 1 - T_C/T_H$, where T_C is the temperature of the sink where the heat is being rejected to in the cooling step (i.e., cold side temperature) and T_H is the temperature the heat is being supplied at in the heating step (i.e., plant operating temperature). It is clear that increasing the operating temperature will increase the maximum achievable efficiency if the cold side temperature can be held constant. Cold side temperature should be kept as low as possible, which is limited in practice by the ambient temperature the plant operates in as well as the heat transfer to the ambient environment.[298,299]

The Carnot efficiency represents the maximum performance limit, and cannot be achieved by real heat engines. A lower efficiency, called the Chambadal-Novikov efficiency, can be derived for a heat engine with irreversible heat transfer processes operating at maximum power output.[300] The Chambadal-Novikov efficiency η_{CN} is given by

$$\eta_{CN} = 1 - \sqrt{\frac{T_C}{T_H}} \tag{27}$$

The Chambadal-Novikov efficiency follows the same trend as the Carnot efficiency of increasing with operating temperature. The efficiency of real heat engines matches the Chambadal-Novikov efficiency much more closely than the Carnot efficiency, and as such the Chambadal-Novikov is generally a reasonable estimate to use for calculating heat engine performance in system level analysis.[9] A common (and reasonably accurate) estimate of Chambadal-Novikov efficiency in the temperature range typical of CSP systems is to simply take 2/3 of the Carnot efficiency. The Carnot and Chambadal-Novikov efficiencies are shown in Figure 21 for operating temperatures typical of current systems (350 °C - 600 °C) up to temperatures that could be achieved with high concentration ratio concentrators and advanced receivers. Table 12 lists typical operating temperatures and efficiencies for heat engines which are or could be used with CSP.

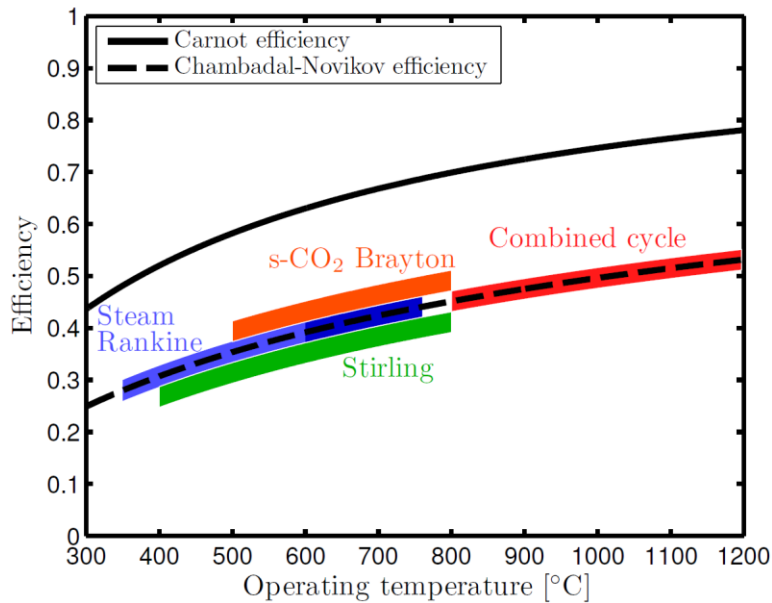**Figure 21 Carnot and Chambadal-Novikov efficiencies for typical CSP operating temperatures as well as approximate efficiencies of real cycles**

Table 12 Typical operating temperatures and efficiencies for heat engines compatible with CSP.

Cycle	Operating temperature range	Typical efficiency (at max temperature)	Reference
Steam-Rankine	350 - 600 °C	40%	[9]

Stirling	400 - 800 °C	45%	9
Supercritical Steam-Rankine	600 - 760 °C	45%	301
Supercritical CO$_2$ Brayton	500 - 800 °C	50%	302
Combined cycle	> 800 °C	60%	303

6.2. Novel cycles

While current CSP plants use steam Rankine cycles, since they are efficient in the appropriate operating temperature range, work is being done to investigate new engines and working fluids which operate at higher temperatures, in preparation for when deployed concentrator/receiver configurations can operate efficiently at higher operating temperatures (and heat transfer fluids are developed which are stable at those temperatures). The exception for current plants using Rankine cycles is parabolic dish receivers as they are typically paired with Stirling engines, since the engine is mounted to the dish which limits its size, and Stirling engines are more suitable at the kW scale. Stirling engines have been developed which could be paired with CSP systems that can achieve reasonable efficiencies (slightly below Chambadal-Novikov) for operating temperatures in the range of 400 – 800 °C.[9,304]

6.2.1. Supercritical steam

Typical steam Rankine cycles are limited in operation temperature to about 600 °C. Higher efficiency can be achieved in supercritical steam Rankine cycles, using higher pressures and temperatures up to 760 °C.[301] Supercritical fluids show compressibility and heat transfer characteristics similar to liquids (reducing compressor work and enhancing regenerative heat exchange), but can still reach high temperatures which typically lead to vaporization. Systems are limited to sub-critical operating

temperatures due to materials issues with the standard steels used for the boilers where the steam is heated. Reliable operation at higher temperatures will require different alloys, such as high nickel content steels.[298,305]

6.2.2. Supercritical CO_2

A promising option for a heat engine operating at temperatures from 500-800 °C is supercritical CO_2 used as the working fluid in a Brayton cycle.[306] Supercritical CO_2 (or s-CO_2) engines have been considered for nuclear plants as well as CSP,[231–233] although only small scale generators have been demonstrated at this point.[307] The primary advantages of the s-CO_2 engine are high efficiency (potentially > 50%) and small turbine size due to the relatively low fluid flow rate required.[302] Advances in the design of sub-components and finding materials which are reliable and resistant to the corrosive nature of supercritical CO_2 are needed before significant commercial adoption of s-CO_2 engines will be possible.[306,308]

6.2.3. Combined cycles

Another option for a heat engine to use with CSP is a combined cycle, which combines a high-temperature "topping" cycle and a lower temperature "bottoming" cycle. Typically a Brayton cycle is used as the topping cycle and a Rankine cycle is used as the bottoming cycle. Combined cycles are very efficient heat engines, with the potential to surpass 60% heat to electricity conversion efficiency.[303] Using a combined cycle is challenging for solar systems due to the high operating temperatures required ($\geq$ 800 °C). As such, most efforts to use combined cycles with CSP consider integration with fossil-fuel fired plants,[309,310] such as the 75 MW Martin Next Generation Solar Energy Center in Florida, even if the heat engine could be completely fueled by solar input in the design condition.[311]

If well-established cycles are used (e.g., air-Brayton for topping and steam-Rankine for bottoming), the challenges in further development of combined cycles with solar input largely lie in the receiver/concentrator end and efficient operation at high operating temperatures. There are however novel cycles that have been proposed for use as the bottoming cycles, such as organic Rankine cycles (ORC),[312]

mixed water-ammonia cycles,[313] and organic flash cycles (OFC).[314] These cycles offer the potential for higher efficiency with further development.

6.3. Direct heat-to-electricity conversion

While deployed solar thermal systems use traditional heat engines to convert heat to electricity via a two step process (heat to mechanical energy and mechanical energy to electricity), an active area of research is in developing direct heat-to-electricity conversion technologies which do not require an intermediate conversion to mechanical energy. An efficient and cost effective direct conversion technology would allow for scalable solar thermal systems (e.g., residential installations in addition to utility-scale), allowing investment in smaller plants that do not require the large amounts of capital necessary for 100 MW+ generators. Direct conversion technologies could also potentially offer better reliability and lower maintenance than current options due to the lack of moving parts in most direct heat-to-electricity technologies.[315] The most active areas of research for direct heat-to-electricity conversion of solar energy are solar thermoelectric generators (STEGs) and solar thermophotovoltaics (STPV), both of which will be briefly reviewed below.

6.3.1. Solar Thermoelectric Generators (STEG):

In a solar thermoelectric generator, heat is converted to electricity using a thermoelectric generator. Thermoelectric materials develop a voltage gradient when subjected to a temperature gradient due to the Seebeck effect, which arises due to majority carriers (electrons for n-type materials and holes for p-type materials) diffusing from the hot end to the cold end of the material.[316] If the thermoelectric material is then put in series with an electrical load, a current will flow and electrical power is generated. TEGs are commonly associated with waste heat recovery applications,[317] however when coupled to a solar absorber, thermoelectrics can produce electricity from renewable solar energy. A schematic of a typical STEG configuration is shown in Figure 22.
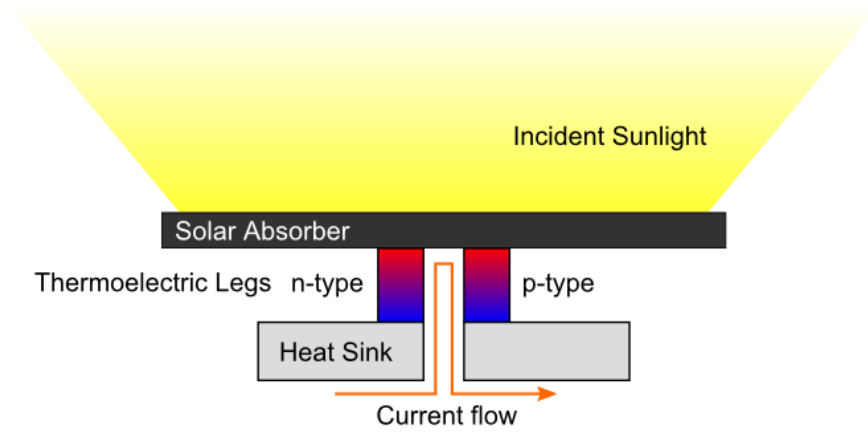
Figure 22 Diagram of a solar thermoelectric generator (STEG). A temperature gradient arises when a pair of thermoelectric legs is sandwiched between an illuminated solar absorber (hot side) and a heat sink (cold side). The TE legs are electrically in series, which allows for current to flow if the TEG is connected to an electrical load

STEG efficiency is the product of receiver efficiency (sunlight to heat efficiency) and TEG efficiency (heat to electricity efficiency). High performance STEGs typically use spectrally selective absorbers, so improvement to receiver efficiency can be driven by the same techniques discussed in section 3. TEG efficiency is a function of the dimensionless thermoelectric figure of merit ZT, defined by:

$$ZT = \frac{S^2 \sigma}{k} \tag{28}$$

where S is the material Seebeck coefficient, σ is the electrical conductivity and k is the thermal conductivity. This figure of merit is significant because the maximum efficiency achievable by a TEG with an average figure of merit $\overline{ZT}$ over its operating temperature range is given by:[318]

$$\eta_{TEG} = \left(1 - \frac{T_C}{T_H}\right)\left(\frac{\sqrt{1+\overline{ZT}}-1}{\sqrt{1+\overline{ZT}}+T_C/T_H}\right) \tag{29}$$

where T_C and T_H are the TEG cold and hot side temperatures, respectively. The first bracketed term is Carnot efficiency, while the second term is a value less than one, which increases with increasing $\overline{ZT}$. Thus, as $\overline{ZT}$ approaches infinity, the TEG efficiency approaches the Carnot limit. Early materials which achieved high ZT values (typically around 0.5-1) included bismuth telluride, lead telluride, and silicon germanium alloys.[319] More recently, higher ZT values have been reported in these same materials in

nanostructured forms,[320–322] as well as new materials such as skutterudites and lead antimony silver tellurium.[323–325] While the focus in thermoelectric materials development is often on increasing peak ZT, average $\overline{ZT}$ over the operational temperature range is more important for the performance of real devices, and should be the development driver for demonstrating high device efficiencies.[326] In addition to the development of TE materials themselves, good contact materials with high thermal and electrical conductivity and complementary Seebeck coefficients to their TE material are also very important to demonstrating high performance in a device.[327,328] There is significant room to improve ZT values and contact materials through investigating new materials systems and fabrication processes, and as such TEG efficiencies should continue to improve in the following decades.

The first experimental demonstration of a STEG was reported by Telkes in 1954, for which an efficiency of 0.63% was achieved without concentration and 3.35% was achieved with concentration.[329] Little experimental progress was made which outperformed this work until a demonstration of 4.6% solar to electric efficiency by Kraemer et al. in 2011, which was achieved under one sun insolation at an operating temperature around 200 °C.[193] This is a rare example of a solar thermal conversion process producing electricity without optical concentration, and was accomplished using an evacuated enclosure, a spectrally selective absorber, and thermal concentration (the absorber area is much larger than the cross sectional area of the thermoelectric legs). Other simulation work has predicted that with optical concentration and higher temperature thermoelectric materials, STEGs surpassing 10% efficiency should be achievable for line-focus systems and STEGs surpassing 15% efficiency should be achievable for point-focus systems.[330–332] Most existing work on STEGs with concentration still use low operating temperatures (~200 °C), thus achieving similar efficiencies to the non-concentrated work.[333] Recent work by Kraemer, et al. has demonstrated 9.6% efficiency (not considering concentrator efficiency) at high concentration in a segmented STEG.[334] If STEGs with efficiencies comparable to existing CSP technologies can be demonstrated, they could lead to more economic, scalable CSP systems.

6.3.2. Solar Thermophotovoltaics (STPV):

In a solar thermophotovoltaic (STPV) generator, heat is generated from the absorption of sunlight and is converted into thermal radiation. This thermal radiation is directed towards a single-junction thermophotovoltaic (TPV) cell where it is ultimately converted into electricity. The benefits of such a strategy are that the frequency dependent TPV converter is ideally illuminated by a photon spectrum that is much more efficiently converted than incident sunlight is on a PV converter. The challenge of STPV conversion is that an intermediate absorption/re-emission process is necessarily introduced into the system, and this must be done efficiently enough such that the spectral enhancement outweighs its effect.
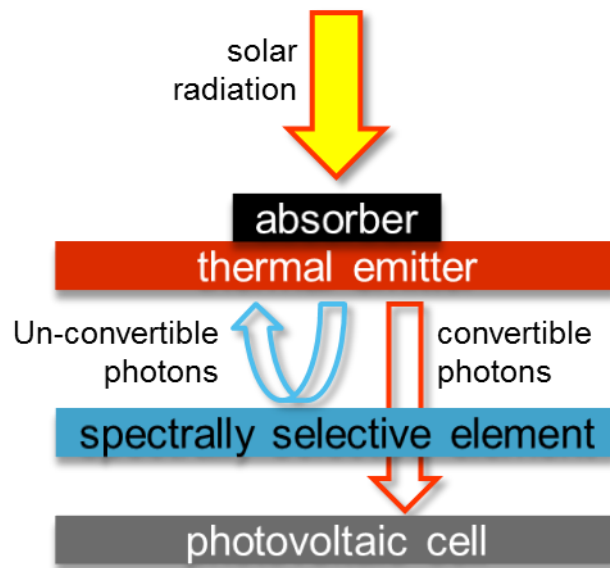
Figure 23: Schematic of a STPV device. Incident concentrated solar radiation is thermalized at the hot absorber element. The heat conducts to a thermal emitter which radiates photons to a photovoltaic cell. The photon spectrum is tailored either by spectrally selective emission or long wavelength reflection

The main reason why the absorption/re-emission process has proven to be so inhibiting is due to the necessary high temperature of operation. Because STPV relies on the conversion of thermal radiation into electricity, even the lowest bandgap semiconductor materials (~0.5 eV) require a blackbody spectrum of temperatures above 1000 °C in order to be efficient. While 1000 °C is certainly below the melting point of many materials, it is still an incredible engineering challenge to put together a reliable system that is capable of efficient STPV conversion.

The generation of heat from incident sunlight in an STPV converter has the same principles discussed in section 3. Once the absorber/re-emitter reaches its extraordinary equilibrium temperature, it will emit thermal radiation towards a single-junction TPV cell. An important characteristic of this TPV generator is spectral control. There must be a systematic way of suppressing the illumination of the TPV cell by sub-bandgap photons. Historically, this has been accomplished on the "cold-side" of the device, *e.g.,* with a back surface reflector or an optical filter attached to the TPV cell. However, recent research has focused on the development of refractory materials that provide spectrally selective emission.[75]

A selective emitter is a material that when heated to incandescence is able to discriminate emission based on the frequency of the photon. In this way, and because of Kirchhoff's law of thermal radiation, a selective emitter is quite similar to the selective absorber. Instead of the transition from high to low emission separating the solar spectrum and the blackbody thermal emission spectrum, however, in a selective emitter the transition separates supra-bandgap photon emission from sub-bandgap photon emission.

Chan, *et al.* developed and integrated a one-dimensional photon crystal made of alternating thin films of Si/SiO_2 in order to create both constructive and destructive wave interference.[335] Rinnerbauer *et al.* developed two-dimensional photonic crystal by fabricating a large array of nano-scale cavities in a tantalum slab in order to take advantage of cavity modes for enhanced emission above the bandgap, with a tunable transition frequency.[141] The emitter relies on the intrinsic low emission of the underlying metal at longer wavelengths. Li, *et al.* used interesting optical properties of titanium nitride to develop high temperature spectrally selective emitters.[336] Arpin, *et al.* developed a self-assembled three dimensional photonic crystal using a tungsten coated inverse opal structure.[132]

Recently, there have been a few successful demonstrations of solar powered thermophotovoltaic converters. Datas, *et al.* built a prototype which achieved about 1% solar to electric conversion efficiency. The low efficiency was largely due to over-heating of the TPV cells and reliance on natural selectivity of

high temperature emitters. [337] Lenert, *et al.* integrated nanophotonic surfaces including vertically-aligned carbon nanotubes to demonstrate a 3.2% STPV conversion efficiency.[192] Rinnerbauer, *et al.* used a monolithic two-dimensional photonic crystal absorber and emitter on a single chip to demonstrate 3.5% STPV conversion efficiency.[80] Shimizu, *et al.* also used a selective absorber/emitter to estimate up to 8% conversion efficiency, although this was not directly demonstrated.[338] STPV efficiency is predicted to reach 20% for systems scaled up to larger absorber/emitter areas (which reduces the effect of edge losses) and which use higher quality PV cells and sub-bandgap filtering.[192] A demonstration of an STPV device with efficiencies comparable to existing CSP plants would suggest the potential for economical STPV systems and smaller scale CSP technology.

7. CONCLUDING REMARKS

There is a wide spectrum of maturity for CSP technologies, ranging from PTC plants which are a well-established commercial technology, to parabolic dish concentrators, which have yet to be demonstrated at scales much greater than 1 MW. For the less mature technologies of power tower, LFR and parabolic dish, there are still many system level lessons to be learned as more of these systems become deployed. In addition to the plant level challenges, there are compelling research questions which can be explored at each stage of a CSP plant: the concentrator, the receiver, the heat transfer fluid, the thermal storage and the heat engine all have room for improvement to push overall plant performance higher. With the added requirements on reliability and cost for actual deployment, challenges in increasing performance are made even greater. While daunting, the pragmatic challenges associated with use in commercial plants are still interesting from a technical perspective as their solutions will involve innovative use of manufacturing methods and materials. With continued development moving into the future, CSP will maintain its role as an integral part of the renewable energy landscape.

8. AUTHOR INFORMATION

8.1. Corresponding Author

*Email: gchen2@mit.edu

8.2. Notes

The authors declare no competing financial interests

8.3. Biographies

Lee Weinstein is a Ph.D. candidate in the Department of Mechanical Engineering at the Massachusetts Institute of Technology, advised by Professor Gang Chen. He received a B.S. in Mechanical Engineering from the University of California, Berkeley in 2011 and received an M.S. in Mechanical Engineering from the Massachusetts Institute of Technology in 2013. His Ph.D. research has spanned multiple topics within CSP, including solar thermoelectric generators, directional selectivity, and transparent aerogels.

Dr. James Loomis received his PhD in Mechanical Engineering from the University of Louisville (UofL) in 2013. His PhD work focused on characterization and applications of photomechanical actuation in nanocarbon/elastomer composites. Additionally, while working in the UofL Micro/Nanotechnology Center, he developed software that enabled fabrication of complex 3D microstructures in photoresist. After receiving his PhD, James moved to Boston and joined the NanoEngineering Group at MIT as a Postdoc under Professor Gang Chen. There he worked on continuous fabrication techniques for large-area polymer films with tunable thermal conductivity; and design of a utility-scale high efficiency concentrating solar power receiver. In 2015, James joined the faculty at the University of Auckland as a Senior Lecturer.

Dr. Bikram Bhatia is a Postdoctoral Research Associate at the Device Research Lab at Massachusetts Institute of Technology (MIT) under Professor Evelyn Wang. Bikram received his Ph.D. from the Department of Mechanical Science and Engineering at the University of Illinois at Urbana-Champaign in

2014. His doctoral research investigated waste heat harvesting using nanometer-thick pyroelectric films. He received the B.Tech. degree in Mechanical Engineering from the Indian Institute of Technology (IIT) Guwahati in 2008 and his M.S. from the University of Illinois at Urbana-Champaign in 2010. He is currently working on solar thermal energy conversion systems.

David Bierman is a Ph.D. candidate in the Department of Mechanical Engineering at the Massachusetts Institute of Technology, advised by Professor Evelyn Wang. He received a B.S. in Mechanical Engineering from the University of Wisconsin -- Madison in 2012 and an M.S. in Mechanical Engineering from the Massachusetts Institute of Technology in 2014. His Ph.D. research is focused on solid state solar thermal energy conversion, including solar thermophotovoltaic converters and high temperature material stability, as well as other fundamental problems in thermal radiation.

Dr. Evelyn Wang is the Gail E. Kendall Associate Professor of Mechanical Engineering at the Massachusetts Institute of Technology. She is the Associate Director of the Solid State Solar Thermal Energy Conversion (S3TEC) Center, an Energy Frontier Research Center funded by the US Department of Energy. She received her B.S. in Mechanical Engineering at the Massachusetts Institute of Technology in 2000, her M.S. and Ph.D. from Stanford University in 2001 and 2006, respectively, each in Mechanical Engineering. She has received numerous awards including the DARPA Young Faculty Award in 2008, the AFOSR Young Investigator Award in 2011, the ONR Young Investigator Award in 2012. Her research interests include micro-/nano-scale heat and mass transport, two-phase transport, phase-change, nanoengineered surfaces, thermal management for high performance systems, bio-inspired micro-/nano-systems, energy efficient systems, solar thermal energy conversion, and water desalination.

Dr. Gang Chen is currently the Carl Richard Soderberg Professor of Power Engineering and Head of the Department of Mechanical Engineering at Massachusetts Institute of Technology. He obtained his Ph.D. degree from UC Berkeley in 1993. He was a faculty member at Duke University (1993-1997), and University of California at Los Angeles (1997-2001), before joining MIT in 2001. He is a recipient of the

NSF Young Investigator Award, the ASME Heat Transfer Memorial Award, the R&D100 Award, and the MIT McDonald Award for Excellence in Mentoring and Advising. He is a member of the US National Academy of Engineering, a Guggenheim Fellow, an AAAS Fellow, an APS Fellow, and an ASME Fellow. He has published extensively in the area of nanoscale energy transport and conversion and nanoscale heat transfer. He is the director of Solid-State Solar-Thermal Energy Conversion Center funded by the US DOE's Energy Frontier Research Centers program.

9. ACKNOWLEDGEMENTS

10. REFERENCES

(1)   Crabtree, G. W.; Lewis, N. S. Solar Energy Conversion. *Phys. Today* **2007**, *60* (3), 37–42.

(2)   Müller-Steinhagen, H.; Trieb, F. Concentrating Solar Power A Review of the Technology. *Ingenia Inf. QR Acad Eng* **2004**, *18*, 43–50.

(3)   REN21. *Renewables 2014 Global Status Report*; Paris, 2014.

(4)   Pitz-Paal, R. Concentrating Solar Power. In *Future Energy: Improved, Sustainable and Clean Options for our Planet*; Letcher, T. M., Ed.; 2008; pp 171–192.

(5)   Energy, U. D. of. *2014: The Year of Concentrating Solar Power*; 2014.

(6)   Baharoon, D. A.; Rahman, H. A.; Omar, W. Z. W.; Fadhl, S. O. Historical Development of Concentrating Solar Power Technologies to Generate Clean Electricity Efficiently − A Review. *Renew. Sustain. Energy Rev.* **2015**, *41*, 996–1027.

(7)   Thirugnanasambandam, M.; Iniyan, S.; Goic, R. A Review of Solar Thermal Technologies☆. *Renew. Sustain. Energy Rev.* **2010**, *14* (1), 312–322.

(8)   Administration, U. S. E. I. *Annual Energy Outlook 2014*; Washington, DC, 2014.

(9)   Karni, J. Solar-Thermal Power Generation. *Annu. Rev. Heat Transf.* **2012**, 37–92.

(10)   Energy, U. D. of. *CONCENTRATING SOLAR POWER: ADVANCED PROJECTS OFFERING LOW LCOE OPPORTUNITIES DE-FOA-0001186*; 2015.

(11)   Branker, K.; Pathak, M. J. M.; Pearce, J. M. A Review of Solar Photovoltaic Levelized Cost of Electricity. *Renew. Sustain. Energy Rev.* **2011**, *15* (9), 4470–4482.

(12)   Pitz-Paal, R.; Dersch, J.; Milow, B.; Téllez, F.; Ferriere, A.; Langnickel, U.; Steinfeld, A.; Karni, J.; Zarza, E.; Popel, O. Development Steps for Parabolic Trough Solar Power Technologies With Maximum Impact on Cost Reduction. *J. Sol. Energy Eng.* **2007**, *129* (4), 371–377.

(13)   IRENA. *Renewable Energy Cost Analysis - Concentrating Solar Power*; 2012.

(14)   IRENA. *Renewable Power Generation Costs in 2014*; 2014.

(15)   Mills, D. R.; Morrison, G. L. Compact Linear Fresnel Reflector Solar Thermal Powerplants. *Sol. Energy* **2000**, *68* (3), 263–283.

(16)   Zhu, G.; Wendelin, T.; Wagner, M. J.; Kutscher, C. History, Current State, and Future of Linear Fresnel Concentrating Solar Collectors. *Sol. Energy* **2014**, *103*, 639–652.

(17)   Mancini, T.; Heller, P.; Butler, B.; Osborn, B.; Schiel, W.; Goldberg, V.; Buck, R.; Diver, R.; Andraka, C.; Moreno, J. Dish-Stirling Systems: An Overview of Development and Status. *J. Sol. Energy Eng.* **2003**, *125* (2), 135–151.

(18)   Kalogirou, S. A. A Detailed Thermal Model of a Parabolic Trough Collector Receiver. *Energy* **2012**, *48* (1), 298–306.

(19)   Xie, W. T.; Dai, Y. J.; Wang, R. Z.; Sumathy, K. Concentrated Solar Energy Applications Using Fresnel Lenses: A Review. *Renew. Sustain. Energy Rev.* **2011**, *15* (6), 2588–2606.

(20) Prior, B. Concentrating Solar: Ready for Takeoff - or Stalled on the Launchpad? In *American Solar Energy Society*; Raleigh, NC, 2011.

(21) SunShot U.S. Department of Energy. *SunShot Vision Study*; 2012.

(22) Andraka, C. E. *Dish Stirling High Performance Thermal Storage.*; 2013.

(23) Ayre, J. New Solar Stirling Dish Efficiency Record Of 32% Set. *Clean Technica*. 2013.

(24) Siva Reddy, V.; Kaushik, S. C.; Ranjan, K. R.; Tyagi, S. K. State-of-the-Art of Solar Thermal Power plants—A Review. *Renew. Sustain. Energy Rev.* **2013**, *27*, 258–273.

(25) Pavlović, T. M.; Radonjić, I. S.; Milosavljević, D. D.; Pantić, L. S. A Review of Concentrating Solar Power Plants in the World and Their Potential Use in Serbia. *Renew. Sustain. Energy Rev.* **2012**, *16* (6), 3891–3902.

(26) Kaygusuz, K. Prospect of Concentrating Solar Power in Turkey: The Sustainable Future. *Renew. Sustain. Energy Rev.* **2011**, *15* (1), 808–814.

(27) Timilsina, G. R.; Kurdgelashvili, L.; Narbel, P. A. Solar Energy: Markets, Economics and Policies. *Renew. Sustain. Energy Rev.* **2012**, *16* (1), 449–465.

(28) Turchi, C. S.; Langle, N.; Bedilion, R.; Libby, C. *Solar-Augment Potential of U.S. Fossil-Fired Power Plants*; Golden, CO, 2011.

(29) Jamel, M. S.; Abd Rahman, A.; Shamsuddin, A. H. Advances in the Integration of Solar Thermal Energy with Conventional and Non-Conventional Power Plants. *Renew. Sustain. Energy Rev.* **2013**, *20*, 71–81.

(30) Denholm, P.; Mehos, M. *Enabling Greater Penetration of Solar Power via the Use of CSP with Thermal Energy Storage*; 2011.

(31) Wagner, S. J.; Rubin, E. S. Economic Implications of Thermal Energy Storage for Concentrated Solar Thermal Power. *Renew. Energy* **2014**, *61*, 81–95.

(32) Jorgenson, J.; Denholm, P.; Mehos, M. *Estimating the Value of Utility-Scale Solar Technologies in California Under a 40% Renewable Portfolio Standard*; Golden, CO (United States), 2014.

(33) Peters, M.; Schmidt, T. S.; Wiederkehr, D.; Schneider, M. Shedding Light on Solar technologies—A Techno-Economic Assessment and Its Policy Implications. *Energy Policy* **2011**, *39* (10), 6422–6439.

(34) SolarPACES. Concentrating Solar Power Projects http://www.nrel.gov/csp/solarpaces/ (accessed Apr 15, 2015).

(35) Winston, R.; Minano, J. C.; Benitez, P. G.; Shatz, N.; Bortz, J. C. *Nonimaging Optics*; Elsevier Academic Press: Burlington, MA, 2005.

(36)   John A. Duffie, W. A. B. *Solar Engineering of Thermal Processes*; 2013.

(37)   Fernández-García, A.; Cantos-Soto, M. E.; Röger, M.; Wieckert, C.; Hutter, C.; Martínez-Arcos, L. Durability of Solar Reflector Materials for Secondary Concentrators Used in CSP Systems. *Sol. Energy Mater. Sol. Cells* **2014**, *130*, 51–63.

(38)   Barlev, D.; Vidu, R.; Stroeve, P. Innovation in Concentrated Solar Power. *Sol. Energy Mater. Sol. Cells* **2011**, *95* (10), 2703–2725.

(39)   French, R. H.; Murray, M. P.; Lin, W.-C.; Shell, K. a.; Brown, S. a.; Schuetz, M. a.; Davis, R. J. Solar Radiation Durability of Materials Components and Systems for Low Concentration Photovoltaic Systems. *IEEE 2011 EnergyTech* **2011**, 1–5.

(40)   Fend, T.; Hoffschmidt, B.; Jorgensen, G.; Küster, H.; Krüger, D.; Pitz-Paal, R.; Rietbrock, P.; Riffelmann, K. J. Comparative Assessment of Solar Concentrator Materials. *Sol. Energy* **2003**, *74*, 149–155.

(41)   Fernández-García, A.; Zarza, E.; Valenzuela, L.; Pérez, M. Parabolic-Trough Solar Collectors and Their Applications. *Renew. Sustain. Energy Rev.* **2010**, *14* (7), 1695–1721.

(42)   Pitz-Paal, R.; Botero, N. B.; Steinfeld, A. Heliostat Field Layout Optimization for High-Temperature Solar Thermochemical Processing. *Sol. Energy* **2011**, *85* (2), 334–343.

(43)   Noone, C. J.; Torrilhon, M.; Mitsos, A. Heliostat Field Optimization: A New Computationally Efficient Model and Biomimetic Layout. *Sol. Energy* **2012**, *86* (2), 792–803.

(44)   Rabl, A.; Bendt, P. Effect of Circumsolar Radiation on Performance of Focusing Collectors. *J. Sol. Energy Eng.* **1982**, *104* (3), 237–250.

(45)   Pedrotti, F. L.; Pedrotti, L. M. S.; Pedrotti, L. M. S. *Introduction to Optics*, 3rd Editio.; Addison-Wesley: Boston, 2006.

(46)   Abbas, R.; Muñoz-Antón, J.; Valdés, M.; Martínez-Val, J. M. High Concentration Linear Fresnel Reflectors. *Energy Convers. Manag.* **2013**, *72*, 60–68.

(47)   Kennedy, C. E.; Terwilliger, K. Optical Durability of Candidate Solar Reflectors. *J. Sol. Energy Eng.* **2005**, *127* (March), 262–269.

(48)   Brogren, M.; Helgesson, A.; Karlsson, B.; Nilsson, J.; Roos, A. Optical Properties, Durability, and System Aspects of a New Aluminium-Polymer-Laminated Steel Reflector for Solar Concentrators. *Sol. Energy Mater. Sol. Cells* **2004**, *82*, 387–412.

(49)   Adolf Goetzberger, V. U. H. *Photovoltaic Solar Energy Generation*; 2005.

(50)   K Lovegrove, W. S. *Concentrating Solar Power Technology: Principles, Developments and Applications*; 2012.

(51) Sutter, F.; Meyen, S.; Heller, P.; Pitz-Paal, R. Development of a Spatially Resolved Reflectometer to Monitor Corrosion of Solar Reflectors. *Opt. Mater. (Amst).* **2013**, *35* (8), 1600–1608.

(52) Modest, M. F. *Radiative Heat Transfer*, Third.; Academic Press, 2013.

(53) Meyen, S.; Lüpfert, E.; Fernández-García, A.; Kennedy, C. Standardization of Solar Mirror Reflectance Measurements – Round Robin Test. In *SolarPACES 2010*; 2010.

(54) Karim, M.; Naamane, S.; El-Amrani El-Hassani, I.; Delord, C.; Belcadi, S.; Tochon, P.; Bennouna, A. Towards the Prediction of CSP Mirrors Wear: Methodology of Analysis of Influencing Parameters on the Mirrors Surface Degradation: Application in Two Different Sites in Morocco. *Sol. Energy* **2014**, *108*, 41–50.

(55) Crawford, J.; Stewart, J.; Pérez-Ullivarri, J. A Comparison of Three Portable Reflectometers for Use in Operations and Maintenance of CSP Plants. *Proc. SolarPaces Symp. …* **2012**.

(56) Valenzuela, L.; Lopez-Martin, R.; Zarza, E. Optical and Thermal Performance of Large-Size Parabolic-Trough Solar Collectors from Outdoor Experiments: A Test Method and a Case Study. *Energy* **2014**, *70*, 456–464.

(57) Braendle, S. Benefits of Metal Reflective Surfaces for Concentrating Solar Applications. In *SolarPaces Conference*; Greene, L. E., Sherif, R. A., Eds.; 2010; p 77690F – 77690F – 6.

(58) Margolis, R.; Coggeshall, C.; Zuboy, J. Sunshot Vision Study. *US Dept. Energy* **2012**, No. February.

(59) Deubener, J.; Helsch, G.; Moiseev, a.; Bornhöft, H. Glasses for Solar Energy Conversion Systems. *J. Eur. Ceram. Soc.* **2009**, *29*, 1203–1210.

(60) Kennedy, C.; Terwilliger, K.; Warrick, A. Optical Durability of Candidate Solar Reflector Materials. *National Renewable Energy …*. 2007.

(61) Riffelmann, K.-J.; Graf, D.; Nava, P. Ultimate Trough: The New Parabolic Trough Collector Generation for Large Scale Solar Thermal Power Plants. In *ASME 2011 5th International Conference on Energy Sustainability, Parts A, B, and C*; ASME, 2011; pp 789–794.

(62) Angel, R.; Stalcup, T.; Wheelwright, B.; Warner, S.; Hammer, K.; Frenkel, M. Shaping Solar Concentrator Mirrors by Radiative Heating; Plesniak, A. P., Pfefferkorn, C., Eds.; 2014; Vol. 9175, p 91750B – 6.

(63) Butel, G. P.; Coughenour, B. M.; Macleod, H. A.; Kennedy, C. E.; Olbert, B. H.; Angel, J. R. P. Second-Surface Silvered Glass Solar Mirrors of Very High Reflectance. In *Proceedings of the SPIE - The International Society for Optical Engineering*; VanSant, K., Sherif, R. A., Eds.; 2011; Vol. 8108, p 81080L – 81080L – 9.

(64) Digrazia, M.; Jorgensen, G. ReflecTech Mirror Film: Design Flexibility and Durability in Reflecting Solar Applications BT - 39th ASES National Solar Conference 2010, SOLAR 2010, May 17, 2010 - May 22, 2010; 39th ASES National Solar Conference 2010, SOLAR 2010; American Solar Energy

Society: ReflecTech, Inc., 18200 West Highway 72, Arvada, CO 80007, United StatesNational Renewable Energy Laboratory, 1617 Cole Blvd., Golden, CO 80401, United States, 2010; Vol. 1, pp 630–664.

(65)   Brogren, M.; Karlsson, B.; Roos, A.; Werner, A. Analysis of the Effects of Outdoor and Accelerated Ageing on the Optical Properties of Reflector Materials for Solar Energy Applications. *Sol. Energy Mater. Sol. Cells* **2004**, *82* (4), 491–515.

(66)   Sarver, T.; Al-Qaraghuli, A.; Kazmerski, L. L. A Comprehensive Review of the Impact of Dust on the Use of Solar Energy: History, Investigations, Results, Literature, and Mitigation Approaches. *Renew. Sustain. Energy Rev.* **2013**, *22*, 698–733.

(67)   Hegazy, A. A. Effect of Dust Accumulation on Solar Transmittance through Glass Covers of Plate-Type Collectors. *Renew. Energy* **2001**, *22* (4), 525–540.

(68)   Kim, J.-G.; Choi, H. J.; Park, K.-C.; Cohen, R. E.; McKinley, G. H.; Barbastathis, G. Multifunctional Inverted Nanocone Arrays for Non-Wetting, Self-Cleaning Transparent Surface with High Mechanical Robustness. *Small* **2014**, *10* (12), 2487–2494.

(69)   Park, K.-C.; Choi, H. J.; Chang, C.-H.; Cohen, R. E.; McKinley, G. H.; Barbastathis, G. Nanotextured Silica Surfaces with Robust Superhydrophobicity and Omnidirectional Broadband Supertransmissivity. *ACS Nano* **2012**, *6* (5), 3789–3799.

(70)   Mazumder, M. Optical and Adhesive Properties of Dust Deposits on Solar Mirrors and Their Effects on Specular Reflectivity and Electrodynamic Cleaning for Mitigating Energy-Yield Loss. *SPIE Sol. …* **2014**.

(71)   Padilla, R. V.; Demirkaya, G.; Goswami, D. Y.; Stefanakos, E.; Rahman, M. M. Heat Transfer Analysis of Parabolic Trough Solar Receiver. *Appl. Energy* **2011**, *88* (12), 5097–5110.

(72)   Gong, G.; Huang, X.; Wang, J.; Hao, M. An Optimized Model and Test of the China's First High Temperature Parabolic Trough Solar Receiver. *Sol. Energy* **2010**, *84* (12), 2230–2245.

(73)   Lüpfert, E.; Riffelmann, K.-J.; Price, H.; Burkholder, F.; Moss, T. Experimental Analysis of Overall Thermal Properties of Parabolic Trough Receivers. *J. Sol. Energy Eng.* **2008**, *130* (2), 021007–021012.

(74)   Cheng, Z. D.; He, Y. L.; Xiao, J.; Tao, Y. B.; Xu, R. J. Three-Dimensional Numerical Study of Heat Transfer Characteristics in the Receiver Tube of Parabolic Trough Solar Collector. *Int. Commun. Heat Mass Transf.* **2010**, *37* (7), 782–787.

(75)   Bermel, P.; Lee, J.; Joannopoulos, J. D.; Celanovic, I.; Soljačić, M. Selective Solar Absorbers. In *Annual Review of Heat Transfer Vol. 15*; Begell House, 2012; pp 231–254.

(76)   Cao, F.; McEnaney, K.; Chen, G.; Ren, Z. A Review of Cermet-Based Spectrally Selective Solar Absorbers. *Energy Environ. Sci.* **2014**, *7* (5), 1615–1627.

(77)   Alanod-Solar. *Alanod-Solar Product Brochure*; 2015.

(78)   Zhou, W.-X.; Shen, Y.; Hu, E.-T.; Zhao, Y.; Sheng, M.-Y.; Zheng, Y.-X.; Wang, S.-Y.; Lee, Y.-P.; Wang, C.-Z.; Lynch, D. W.; et al. Nano-Cr-Film-Based Solar Selective Absorber with High Photo-Thermal Conversion Efficiency and Good Thermal Stability. *Opt. Express* **2012**, *20* (27), 28953–28962.

(79)   Li, P.; Liu, B.; Ni, Y.; Liew, K. K.; Sze, J.; Chen, S.; Shen, S. Large-Scale Nanophotonic Solar Selective Absorbers for High-Efficiency Solar Thermal Energy Conversion. *Adv. Mater.* **2015**, *27* (31), 4585–4591.

(80)   Veronika Rinnerbauer, Andrej Lenert, David Bierman, Yi Xiang Yeng, Walker R. Chan, Robert D. Geil, Jay J. Senkevich, John D. Joannopoulos, Evelyn N. Wang, Marin Soljačić, and I. C.; Rinnerbauer, V.; Lenert, A.; Bierman, D. M.; Yeng, Y. X.; Chan, W. R.; Geil, R. D.; Senkevich, J. J.; Joannopoulos, J. D.; Wang, E. N.; et al. Metallic Photonic Crystal Absorber-Emitter for Efficient Spectral Control in High-Temperature Solar Thermophotovoltaics. *Adv. Energy Mater.* **2014**, *4* (12), 1400334.

(81)   Ho, C. K.; Mahoney, A. R.; Ambrosini, A.; Bencomo, M.; Hall, A.; Lambert, T. N. Characterization of Pyromark 2500 Paint for High-Temperature Solar Receivers. *J. Sol. Energy Eng.* **2013**, *136* (1), 014502–014505.

(82)   Kraemer, D.; McEnaney, K.; Cao, F.; Ren, Z.; Chen, G. Accurate Determination of the Total Hemispherical Emittance and Solar Absorptance of Opaque Surfaces at Elevated Temperatures. *Sol. Energy Mater. Sol. Cells* **2015**, *132*, 640–649.

(83)   Echániz, T.; Setién-Fernández, I.; Pérez-Sáez, R. B.; Prieto, C.; Galindo, R. E.; Tello, M. J. Importance of the Spectral Emissivity Measurements at Working Temperature to Determine the Efficiency of a Solar Selective Coating. *Sol. Energy Mater. Sol. Cells* **2015**, *140*, 249–252.

(84)   Raut, H. K.; Ganesh, V. A.; Nair, A. S.; Ramakrishna, S. Anti-Reflective Coatings: A Critical, in-Depth Review. *Energy Environ. Sci.* **2011**, *4* (10), 3779–3804.

(85)   Macleod, H. A. *Thin-Film Optical Filters, Third Edition*; CRC Press, 2001.

(86)   Standard, A. G173, Standard Tables for Reference Solar Spectral Irradiances: Direct Normal and Hemispherical on 37 Tilted Surface. *Annu. B. ASTM Stand.* **2008**.

(87)   Kennedy, C. E. Review of Mid- to High- Temperature Solar Selective Absorber Materials Review of Mid- to High- Temperature Solar Selective Absorber Materials. **2002**, No. July.

(88)   Atkinson, C.; Sansom, C. L.; Almond, H. J.; Shaw, C. P. Coatings for Concentrating Solar Systems – A Review. *Renew. Sustain. Energy Rev.* **2015**, *45*, 113–122.

(89)   Joannopoulos, J. D.; Johnson, S. G.; Winn, J. N.; Meade, R. D. *Photonic Crystals: Molding the Flow of Light (Second Edition)*; Princeton University Press, 2011.

(90) Randich, E.; Allred, D. D. Chemically Vapor-Deposited ZrB2 as a Selective Solar Absorber. *Thin Solid Films* **1981**, *83* (4), 393–398.

(91) McDonald, G. E. Spectral Reflectance Properties of Black Chrome for Use as a Solar Selective Coating. *Sol. Energy* **1975**, *17* (2), 119–122.

(92) Nunes, C.; Teixeira, V.; Prates, M. L.; Barradas, N. P.; Sequeira, A. D. Graded Selective Coatings Based on Chromium and Titanium Oxynitride. *Thin Solid Films* **2003**, *442* (1-2), 173–178.

(93) Gaouyat, L.; He, Z.; Colomer, J.-F.; Lambin, P.; Mirabella, F.; Schryvers, D.; Deparis, O. Revealing the Innermost Nanostructure of Sputtered NiCrOx Solar Absorber Cermets. *Sol. Energy Mater. Sol. Cells* **2014**, *122*, 303–308.

(94) Craighead, H. G.; Buhrman, R. A. Optical Properties of Selectively Absorbing Ni/Al2O3 Composite Films. *Appl. Phys. Lett.* **1977**, *31* (7), 423–425.

(95) Lanxner, M.; Elgat, Z. Solar Selective Absorber Coating for High Service Temperatures, Produced by Plasma Sputtering. In *The Hague '90, 12-16 April*; Granqvist, C.-G., Lampert, C. M., Eds.; International Society for Optics and Photonics, 1990; pp 240–249.

(96) Cao, F.; Kraemer, D.; Sun, T.; Lan, Y.; Chen, G.; Ren, Z. Enhanced Thermal Stability of W-Ni-Al 2 O 3 Cermet-Based Spectrally Selective Solar Absorbers with Tungsten Infrared Reflectors. *Adv. Energy Mater.* **2015**, *5* (2), 1401042.

(97) Rebouta, L.; Sousa, A.; Capela, P.; Andritschky, M.; Santilli, P.; Matilainen, A.; Pischow, K.; Barradas, N. P.; Alves, E. Solar Selective Absorbers Based on Al2O3:W Cermets and AlSiN/AlSiON Layers. *Sol. Energy Mater. Sol. Cells* **2015**, *137*, 93–100.

(98) Zhang, Q.-C.; Hadavi, M. S.; Lee, K.-D.; Shen, Y. G. Zr ZrO 2 Cermet Solar Coatings Designed by Modelling Calculations and Deposited by Dc Magnetron Sputtering. *J. Phys. D. Appl. Phys.* **2003**, *36* (6), 723–729.

(99) Barshilia, H. C.; Selvakumar, N.; Rajam, K. S.; Sridhara Rao, D. V.; Muraleedharan, K.; Biswas, A. TiAlN∕TiAlON∕Si3N4 Tandem Absorber for High Temperature Solar Selective Applications. *Appl. Phys. Lett.* **2006**, *89* (19), 191909–3.

(100) Selvakumar, N.; Manikandanath, N. T.; Biswas, A.; Barshilia, H. C. Design and Fabrication of Highly Thermally Stable HfMoN/HfON/Al2O3 Tandem Absorber for Solar Thermal Power Generation Applications. *Sol. Energy Mater. Sol. Cells* **2012**, *102*, 86–92.

(101) Zheng, L.; Zhou, F.; Zhou, Z.; Song, X.; Dong, G.; Wang, M.; Diao, X. Angular Solar Absorptance and Thermal Stability of Mo–SiO2 Double Cermet Solar Selective Absorber Coating. *Sol. Energy* **2015**, *115*, 341–346.

(102) Selvakumar, N.; Barshilia, H. C. Review of Physical Vapor Deposited (PVD) Spectrally Selective Coatings for Mid- and High-Temperature Solar Thermal Applications. *Sol. Energy Mater. Sol. Cells* **2012**, *98*, 1–23.

(103)   Almeco-TiNOX. *Almeco-TiNOX Product Brochure*; 2014.

(104)   Okuyama, M.; Saji, K.; Adachi, T.; Okamoto, H.; Hamakawa, Y. Selective Absorber Using Glow-Discharge Amorphous Silicon for Solar Photothermal Conversion. *Sol. Energy Mater.* **1980**, *3* (3), 405–413.

(105)   Chatterjee, S. Low-Cost Solar Selective Absorbers from Indian Galena. *Opt. Eng.* **1993**, *32* (11), 2923–2929.

(106)   Bermel, P.; Ghebrebrhan, M.; Chan, W.; Yeng, Y. X.; Araghchini, M.; Hamam, R.; Marton, C. H.; Jensen, K. F.; Soljačić, M.; Joannopoulos, J. D.; et al. Design and Global Optimization of High-Efficiency Thermophotovoltaic Systems. *Opt. Express* **2010**, *18 Suppl 3* (103), A314–A334.

(107)   Sergeant, N. P.; Pincon, O.; Agrawal, M.; Peumans, P. Design of Wide-Angle Solar-Selective Absorbers Using Aperiodic Metal-Dielectric Stacks. *Opt. Express* **2009**, *17* (25), 22800–22812.

(108)   Barshilia, H. C.; Selvakumar, N.; Rajam, K. S.; Biswas, A. Spectrally Selective NbAlN/NbAlON/Si3N4 Tandem Absorber for High-Temperature Solar Applications. *Sol. Energy Mater. Sol. Cells* **2008**, *92* (4), 495–504.

(109)   Liu, M.-H.; Hu, E.-T.; Yao, Y.; Zang, K.-Y.; He, N.; Li, J.; Zheng, Y.-X.; Wang, S.-Y.; Yoshie, O.; Lee, Y.; et al. High Efficiency of Photon-to-Heat Conversion with a 6-Layered Metal/dielectric Film Structure in the 250-1200 Nm Wavelength Region. *Opt. Express* **2014**, *22 Suppl 7* (107), A1843–A1852.

(110)   Céspedes, E.; Wirz, M.; Sánchez-García, J. A.; Alvarez-Fraga, L.; Escobar-Galindo, R.; Prieto, C. Novel Mo–Si3N4 Based Selective Coating for High Temperature Concentrating Solar Power Applications. *Sol. Energy Mater. Sol. Cells* **2014**, *122*, 217–225.

(111)   Nuru, Z. Y.; Msimanga, M.; Muller, T. F. G.; Arendse, C. J.; Mtshali, C.; Maaza, M. Microstructural, Optical Properties and Thermal Stability of MgO/Zr/MgO Multilayered Selective Solar Absorber Coatings. *Sol. Energy* **2015**, *111*, 357–363.

(112)   Rephaeli, E.; Fan, S. Absorber and Emitter for Solar Thermo-Photovoltaic Systems to Achieve Efficiency Exceeding the Shockley-Queisser Limit. *Opt. Express* **2009**, *17* (17), 15145–15159.

(113)   Moon, J.; Lu, D.; VanSaders, B.; Kim, T. K.; Kong, S. D.; Jin, S.; Chen, R.; Liu, Z. High Performance Multi-Scaled Nanostructured Spectrally Selective Coating for Concentrating Solar Power. *Nano Energy* **2014**, *8*, 238–246.

(114)   Shah, A. A.; Ungaro, C.; Gupta, M. C. High Temperature Spectral Selective Coatings for Solar Thermal Systems by Laser Sintering. *Sol. Energy Mater. Sol. Cells* **2015**, *134*, 209–214.

(115)   Wu, C.; Neuner III, B.; John, J.; Milder, A.; Zollars, B.; Savoy, S.; Shvets, G. Metamaterial-Based Integrated Plasmonic Absorber/emitter for Solar Thermo-Photovoltaic Systems. *J. Opt.* **2012**, *14* (2), 024005–024007.

(116) Chou, J. B.; Yeng, Y. X.; Lenert, A.; Rinnerbauer, V.; Celanovic, I.; Soljačić, M.; Wang, E. N.; Kim, S.-G. Design of Wide-Angle Selective Absorbers/emitters with Dielectric Filled Metallic Photonic Crystals for Energy Applications. *Opt. Express* **2014**, *22 Suppl 1* (101), A144–A154.

(117) Wang, J.; Chen, Z.; Li, D. Simulation of Two-Dimensional Mo Photonic Crystal Surface for High-Temperature Solar-Selective Absorber. *Phys. status solidi* **2010**, *207* (8), 1988–1992.

(118) Jae Lee, B.; Chen, Y.-B.; Han, S.; Chiu, F.-C.; Jin Lee, H. Wavelength-Selective Solar Thermal Absorber With Two-Dimensional Nickel Gratings. *J. Heat Transfer* **2014**, *136* (7), 072702–072707.

(119) Mattox, D. M. High Absorptivity Solar Absorbing Coatings. *J. Vac. Sci. Technol.* **1974**, *11* (4), 793–796.

(120) McKenzie, D. R. Effect of Substrate on Graphite and Other Solar Selective Surfaces. *Appl. Opt.* **1978**, *17* (12), 1884–1888.

(121) Mayer, A.; Gaouyat, L.; Nicolay, D.; Carletti, T.; Deparis, O. Multi-Objective Genetic Algorithm for the Optimization of a Flat-Plate Solar Thermal Collector. *Opt. Express* **2014**, *22 Suppl 6* (106), A1641–A1649.

(122) Arancibia-Bulnes, C. A.; Estrada, C. A.; Ruiz-Suárez, J. C. Solar Absorptance and Thermal Emittance of Cermets with Large Particles. *J. Phys. D. Appl. Phys.* **2000**, *33* (19), 2489–2496.

(123) Zhao, S. Spectrally Selective Solar Absorbing Coatings Prepared by Dc Magnetron Sputtering, Acta Universitatis Upsaliensis, 2007.

(124) Lampert, C. M. Coatings for Enhanced Photothermal Energy Collection I. Selective Absorbers. *Sol. Energy Mater.* **1979**, *1* (5-6), 319–341.

(125) McMahon, T. J.; Jasperson, S. N. PbS-Al Selective Solar Absorbers. *Appl. Opt.* **1974**, *13* (12), 2750–2751.

(126) Gittleman, J. I.; Sichel, E. K.; Lehmann, H. W.; Widmer, R. Textured Silicon: A Selective Absorber for Solar Thermal Conversion. *Appl. Phys. Lett.* **1979**, *35* (10), 742–744.

(127) Ungaro, C.; Gray, S. K.; Gupta, M. C. Black Tungsten for Solar Power Generation. *Appl. Phys. Lett.* **2013**, *103* (7), 071105–3.

(128) Kim, T. K.; VanSaders, B.; Moon, J.; Kim, T.; Liu, C.-H.; Khamwannah, J.; Chun, D.; Choi, D.; Kargar, A.; Chen, R.; et al. Tandem Structured Spectrally Selective Coating Layer of Copper Oxide Nanowires Combined with Cobalt Oxide Nanoparticles. *Nano Energy* **2015**, *11*, 247–259.

(129) Yablonovitch, E. Inhibited Spontaneous Emission in Solid-State Physics and Electronics. *Phys. Rev. Lett.* **1987**, *58* (20), 2059–2062.

(130) Celanovic, I.; Jovanovic, N.; Kassakian, J. Two-Dimensional Tungsten Photonic Crystals as Selective Thermal Emitters. *Appl. Phys. Lett.* **2008**, *92* (19), 193101–193103.

(131) Yeng, Y. X. Photonic Crystals for High Temperature Applications. Massachusetts Institute of Technology 2014.

(132) Arpin, K. A.; Losego, M. D.; Cloud, A. N.; Ning, H.; Mallek, J.; Sergeant, N. P.; Zhu, L.; Yu, Z.; Kalanyan, B.; Parsons, G. N.; et al. Three-Dimensional Self-Assembled Photonic Crystals with High Temperature Stability for Thermal Emission Modification. *Nat. Commun.* **2013**, *4*, 2630–2638.

(133) Yeng, Y. X.; Ghebrebrhan, M.; Bermel, P.; Chan, W. R.; Joannopoulos, J. D.; Soljačić, M.; Celanovic, I. Enabling High-Temperature Nanophotonics for Energy Applications. *Proc. Natl. Acad. Sci. U. S. A.* **2012**, *109* (7), 2280–2285.

(134) Rinnerbauer, V.; Ndao, S.; Yeng, Y. X.; Chan, W. R.; Senkevich, J. J.; Joannopoulos, J. D.; Soljačić, M.; Celanovic, I. Recent Developments in High-Temperature Photonic Crystals for Energy Conversion. *Energy Environ. Sci.* **2012**, *5* (10), 8815–8823.

(135) Veronis, G.; Dutton, R. W.; Fan, S. Metallic Photonic Crystals with Strong Broadband Absorption at Optical Frequencies over Wide Angular Range. *J. Appl. Phys.* **2005**, *97* (9), 093104–4.

(136) Heinzel, A.; Boerner, V.; Gombert, A.; Bläsi, B.; Wittwer, V.; Luther, J. Radiation Filters and Emitters for the NIR Based on Periodically Structured Metal Surfaces. *J. Mod. Opt.* **2000**, *47* (13), 2399–2419.

(137) Araghchini, M.; Yeng, Y. X.; Jovanovic, N.; Bermel, P.; Kolodziejski, L. A.; Soljacic, M.; Celanovic, I.; Joannopoulos, J. D. Fabrication of Two-Dimensional Tungsten Photonic Crystals for High-Temperature Applications. *J. Vac. Sci. Technol. B Microelectron. Nanom. Struct.* **2011**, *29* (6), 061402–061404.

(138) Sai, H.; Kanamori, Y.; Yugami, H. High-Temperature Resistive Surface Grating for Spectral Control of Thermal Radiation. *Appl. Phys. Lett.* **2003**, *82* (11), 1685–1687.

(139) Lee, H.-J.; Smyth, K.; Bathurst, S.; Chou, J.; Ghebrebrhan, M.; Joannopoulos, J.; Saka, N.; Kim, S.-G. Hafnia-Plugged Microcavities for Thermal Stability of Selective Emitters. *Appl. Phys. Lett.* **2013**, *102* (24), 241904–241906.

(140) Nam, Y.; Yeng, Y. X.; Lenert, A.; Bermel, P.; Celanovic, I.; Soljačić, M.; Wang, E. N. Solar Thermophotovoltaic Energy Conversion Systems with Two-Dimensional Tantalum Photonic Crystal Absorbers and Emitters. *Sol. Energy Mater. Sol. Cells* **2014**, *122*, 287–296.

(141) Rinnerbauer, V.; Ndao, S.; Xiang Yeng, Y.; Senkevich, J. J.; Jensen, K. F.; Joannopoulos, J. D.; Soljačić, M.; Celanovic, I.; Geil, R. D. Large-Area Fabrication of High Aspect Ratio Tantalum Photonic Crystals for High-Temperature Selective Emitters. *J. Vac. Sci. Technol. B Microelectron. Nanom. Struct.* **2013**, *31* (1), 011802–011807.

(142) Yeng, Y. X.; Chou, J. B.; Rinnerbauer, V.; Shen, Y.; Kim, S.-G.; Joannopoulos, J. D.; Soljačić, M.; Čelanović, I. Omnidirectional Wavelength Selective Emitters/absorbers Based on Dielectric-Filled Anti-Reflection Coated Two-Dimensional Metallic Photonic Crystals. In *SPIE NanoScience +*

Engineering; Campo, E. M., Dobisz, E. A., Eldada, L. A., Eds.; International Society for Optics and Photonics, 2014; p 91700X – 8.

(143) Chou, J. B.; Yeng, Y. X.; Lee, Y. E.; Lenert, A.; Rinnerbauer, V.; Celanovic, I.; Soljačić, M.; Fang, N. X.; Wang, E. N.; Kim, S.-G. Enabling Ideal Selective Solar Absorption with 2D Metallic Dielectric Photonic Crystals. *Adv. Mater.* **2014**, *26* (47), 8041–8045.

(144) Badescu, V. Spectrally and Angularly Selective Photothermal and Photovoltaic Converters under One-Sun Illumination. *J. Phys. D. Appl. Phys.* **2005**, *38* (13), 2166–2172.

(145) Blanco, M. J.; Martín, J. G.; Alarcón-Padilla, D. C. Theoretical Efficiencies of Angular-Selective Non-Concentrating Solar Thermal Systems. *Sol. Energy* **2004**, *76* (6), 683–691.

(146) Shen, Y.; Ye, D.; Celanovic, I.; Johnson, S. G.; Joannopoulos, J. D.; Solja i , M. Optical Broadband Angular Selectivity. *Science (80-.).* **2014**, *343* (6178), 1499–1501.

(147) Perlmutter, M.; Howell, J. R. A Strongly Directional Emitting and Absorbing Surface. *J. Heat Transfer* **1963**, *85* (3), 282–283.

(148) Weinstein, L.; Kraemer, D.; McEnaney, K.; Chen, G. Optical Cavity for Improved Performance of Solar Receivers in Solar-Thermal Systems. *Sol. Energy* **2014**, *108*, 69–79.

(149) Solar, S. SCHOTT PTR®70 Receiver.

(150) Hiller, J.; Mendelsohn, J. D.; Rubner, M. F. Reversibly Erasable Nanoporous Anti-Reflection Coatings from Polyelectrolyte Multilayers. *Nat. Mater.* **2002**, *1* (1), 59–63.

(151) Kennedy, S. R.; Brett, M. J. Porous Broadband Antireflection Coating by Glancing Angle Deposition. *Appl. Opt.* **2003**, *42* (22), 4573–4579.

(152) Moghal, J.; Kobler, J.; Sauer, J.; Best, J.; Gardener, M.; Watt, A. A. R.; Wakefield, G. High-Performance, Single-Layer Antireflective Optical Coatings Comprising Mesoporous Silica Nanoparticles. *ACS Appl. Mater. Interfaces* **2012**, *4* (2), 854–859.

(153) Sood, A. K. Development of Nanostructured Antireflection Coatings for EO/IR Sensor and Solar Cell Applications. *Mater. Sci. Appl.* **2012**, *03* (09), 633–639.

(154) Krause, K. M.; Taschuk, M. T.; Brett, M. J. Glancing Angle Deposition on a Roll: Towards High-Throughput Nanostructured Thin Films. *J. Vac. Sci. Technol. A Vacuum, Surfaces, Film.* **2013**, *31* (3), 031507–031509.

(155) Benz, N. Next Generation Receivers. *nrel.gov*.

(156) Glatzmaier, G. C. Measurement of Hydrogen Purge Rates in Parabolic Trough Receiver Tubes. In *SolarPACES*; Perpignan, France, 2010.

(157) Roesle, M.; Coskun, V.; Steinfeld, A. Numerical Analysis of Heat Loss From a Parabolic Trough Absorber Tube With Active Vacuum System. *J. Sol. Energy Eng.* **2011**, *133* (3), 031015–5.

(158) Li, J.; Wang, Z.; Lei, D.; Li, J. Hydrogen Permeation Model of Parabolic Trough Receiver Tube. *Sol. Energy* **2012**, *86* (5), 1187–1196.

(159) Bredendiek-K�mper, S.; Klewe-Nebenius, H.; Pfennig, G.; Bruns, M.; Ache, H. J. Surface Analytical Characterization of the Hydrogen Getter Material ZrCo. *Fresenius' Zeitschrift f�r Anal. Chemie* **1989**, *335* (7), 669–674.

(160) Petti, D.; Cantoni, M.; Leone, M.; Bertacco, R.; Rizzi, E. Activation of Zr–Co–rare Earth Getter Films: An XPS Study. *Appl. Surf. Sci.* **2010**, *256* (21), 6291–6296.

(161) Dinh, L. N.; Schildbach, M. A.; Herberg, J. L.; Saab, A. P.; Weigle, J. C.; Chinn, S. C.; Maxwell, R. S.; McLean, W. Hydrogen Uptake of DPB Getter Pellets. *J. Nucl. Mater.* **2008**, *382* (1), 51–63.

(162) Balooch, M.; Wang, W.-E.; Kirkpatrick, J. R. Hydrogen Uptake Mechanism of a Silicone-Rubber DEB Getter Mixture. *J. Polym. Sci. Part B Polym. Phys.* **2001**, *39* (4), 425–431.

(163) Dinh, L. N.; Cairns, G. A.; Krueger, R.; Mayer, B. P.; Maxwell, R. S. Aging Aspects of DEB Getters. *J. Nucl. Mater.* **2013**, *442* (1-3), 298–305.

(164) Dinh, L. N.; Cairns, G. A.; Strickland, R. A.; McLean, W.; Maxwell, R. S. Mechanism and Kinetic Modeling of Hydrogenation in the Organic Getter/palladium Catalyst/activated Carbon Systems. *J. Phys. Chem. A* **2015**, *119* (6), 943–951.

(165) Maiti, A.; Dinh, L. N.; Baumann, T. F.; Maxwell, R. S.; Saab, A. P. Kinetics of Hydrogen Uptake by Scavenger Molecules – Insights from Molecular Modeling. *Chem. Phys. Lett.* **2009**, *475* (4-6), 223–226.

(166) Blach, A. E.; Hoa, V. S.; Kwok, C. K.; Ahmed, A. K. W. Rectangular Pressure Vessels of Finite Length. *J. Press. Vessel Technol.* **1990**, *112* (1), 50–56.

(167) Pye, J. D.; Morrison, G. L.; Behnia, M. Modelling of Cavity Receiver Heat Transfer for the Compact Linear Fresnel Reflector. *Manuf. Eng.* **2003**, 1–9.

(168) Natarajan, S. K.; Reddy, K. S.; Mallick, T. K. Heat Loss Characteristics of Trapezoidal Cavity Receiver for Solar Linear Concentrating System. *Appl. Energy* **2012**, *93*, 523–531.

(169) Abbas, R.; Muñoz, J.; Martínez-Val, J. M. Steady-State Thermal Analysis of an Innovative Receiver for Linear Fresnel Reflectors. *Appl. Energy* **2012**, *92*, 503–515.

(170) Baetens, R.; Jelle, B. P.; Gustavsen, A. Aerogel Insulation for Building Applications: A State-of-the-Art Review. *Energy Build.* **2011**, *43* (4), 761–769.

(171) Soleimani Dorcheh, A.; Abbasi, M. H. Silica Aerogel; Synthesis, Properties and Characterization. *J. Mater. Process. Technol.* **2008**, *199* (1-3), 10–26.

(172) Reim, M.; Reichenauer, G.; Körner, W.; Manara, J.; Arduini-Schuster, M.; Korder, S.; Beck, A.; Fricke, J. Silica-Aerogel Granulate – Structural, Optical and Thermal Properties. *J. Non. Cryst. Solids* **2004**, *350*, 358–363.

(173) Nordgaard, A.; Beckman, W. A. Modelling of Flat-Plate Collectors Based on Monolithic Silica Aerogel. *Sol. Energy* **1992**, *49* (5), 387–402.

(174) McEnaney, K.; Ghasemi, H.; Weinstein, L. A.; Kraemer, D.; Chen, G. Aerogel-Based Solar Thermal Receiver. *Submitt. to Sol. Energy* **2015**.

(175) Tillotson, T. M.; Hrubesh, L. W. Transparent Ultralow-Density Silica Aerogels Prepared by a Two-Step Sol-Gel Process. *J. Non. Cryst. Solids* **1992**, *145*, 44–50.

(176) Jensen, K. I.; Schultz, J. M.; Kristiansen, F. H. Development of Windows Based on Highly Insulating Aerogel Glazings. *J. Non. Cryst. Solids* **2004**, *350*, 351–357.

(177) Tabata, M.; Adachi, I.; Ishii, Y.; Kawai, H.; Sumiyoshi, T.; Yokogawa, H. Development of Transparent Silica Aerogel over a Wide Range of Densities. *Nucl. Instruments Methods Phys. Res. Sect. A Accel. Spectrometers, Detect. Assoc. Equip.* **2010**, *623* (1), 339–341.

(178) Adachi, I.; Tabata, M.; Kawai, H.; Sumiyoshi, T. Study of Transparent Silica Aerogel with High Refractive Index. *Nucl. Instruments Methods Phys. Res. Sect. A Accel. Spectrometers, Detect. Assoc. Equip.* **2011**, *639* (1), 222–224.

(179) Ho, C. K.; Pacheco, J. E. Levelized Cost of Coating (LCOC) for Selective Absorber Materials. *Sol. Energy* **2014**, *108*, 315–321.

(180) Ho, C. K.; Iverson, B. D. Review of High-Temperature Central Receiver Designs for Concentrating Solar Power. *Renew. Sustain. Energy Rev.* **2014**, *29*, 835–846.

(181) Segal, A.; Epstein, M. The Optics of the Solar Tower Reflector. *Sol. Energy* **2001**, *69*, 229–241.

(182) Slocum, A. H.; Codd, D. S.; Buongiorno, J.; Forsberg, C.; McKrell, T.; Nave, J.-C.; Papanicolas, C. N.; Ghobeity, A.; Noone, C. J.; Passerini, S.; et al. Concentrated Solar Power on Demand. *Sol. Energy* **2011**, *85* (7), 1519–1529.

(183) Mokhtar, M.; Meyers, S. A.; Armstrong, P. R.; Chiesa, M. Performance of a 100 kW Th Concentrated Solar Beam-Down Optical Experiment. *J. Sol. Energy Eng.* **2014**, *136* (4), 041007–041008.

(184) Vant-Hull, L. Issues with Beam-down Concepts. *Energy Procedia* **2014**, *49*, 257–264.

(185) Hall, A.; Ambrosini, A.; Ho, C. *Solar Selective Coatings for Concentrating Solar Power Central Receivers.*; 2011.

(186) Ho, C. K.; Christian, J. M.; Ortega, J. D.; Yellowhair, J.; Mosquera, M. J.; Andraka, C. E. Reduction of Radiative Heat Losses for Solar Thermal Receivers. In *SPIE Solar Energy + Technology*; Plesniak,

A. P., Pfefferkorn, C., Eds.; International Society for Optics and Photonics, 2014; pp 917506–917510.

(187) Boriskina, S. V.; Clarke, D. R.; Wang, E. N.; Chen, G.; Celanović, I.; Soljačić, M. High-Efficiency Solar Receivers with Spectral and Angular Selectivity. 2015.

(188) Behar, O.; Khellaf, A.; Mohammedi, K. A Review of Studies on Central Receiver Solar Thermal Power Plants. *Renew. Sustain. Energy Rev.* **2013**, *23*, 12–39.

(189) Kim, K.; Siegel, N.; Kolb, G.; Rangaswamy, V.; Moujaes, S. F. A Study of Solid Particle Flow Characterization in Solar Particle Receiver. *Sol. Energy* **2009**, *83* (10), 1784–1793.

(190) Khalsa, S. S. S.; Christian, J. M.; Kolb, G. J.; Röger, M.; Amsbeck, L.; Ho, C. K.; Siegel, N. P.; Moya, A. C. CFD Simulation and Performance Analysis of Alternative Designs for High-Temperature Solid Particle Receivers. In *ASME 2011 5th International Conference on Energy Sustainability, Parts A, B, and C*; ASME, 2011; pp 687–693.

(191) Ho, C.; Christian, J.; Gill, D.; Moya, A.; Jeter, S.; Abdel-Khalik, S.; Sadowski, D.; Siegel, N.; Al-Ansary, H.; Amsbeck, L.; et al. Technology Advancements for Next Generation Falling Particle Receivers. *Energy Procedia* **2014**, *49*, 398–407.

(192) Lenert, A.; Bierman, D. M.; Nam, Y.; Chan, W. R.; Celanović, I.; Soljačić, M.; Wang, E. N. A Nanophotonic Solar Thermophotovoltaic Device. *Nat. Nanotechnol.* **2014**, *9* (2), 126–130.

(193) Kraemer, D.; Poudel, B.; Feng, H.-P.; Caylor, J. C.; Yu, B.; Yan, X.; Ma, Y.; Wang, X.; Wang, D.; Muto, A.; et al. High-Performance Flat-Panel Solar Thermoelectric Generators with High Thermal Concentration. *Nat. Mater.* **2011**, *10* (7), 532–538.

(194) Becker, M. Comparison of Heat Transfer Fluids for Use in Solar Thermal Power Stations. *Electr. Power Syst. Res.* **1980**, *3* (3-4), 139–150.

(195) Mouromtseff, I. E. Water and Forced-Air Cooling of Vacuum Tubes Nonelectronic Problems in Electronic Tubes. *Proc. IRE* **1942**, *30* (4), 190–205.

(196) Bonilla, C.; Baumeister, T.; Dunning, J. *Nuclear Engineering*; McGraw-Hill, 1975.

(197) Lenert, A.; Nam, Y.; Wang, E. N. Heat Transfer Fluids. *Annu. Rev. Heat Transf.* **2012**, *15*, 93–129.

(198) Murakami, Y.; Mikic, B. B. Parametric Optimization of Multichanneled Heat Sinks for VLSI Chip Cooling. *IEEE Trans. Components Packag. Technol.* **2001**, *24* (1), 2–9.

(199) Vignarooban, K.; Xu, X.; Arvay, a.; Hsu, K.; Kannan, a. M. Heat Transfer Fluids for Concentrating Solar Power Systems – A Review. *Appl. Energy* **2015**, *146*, 383–396.

(200) Pacio, J.; Singer, C.; Wetzel, T.; Uhlig, R. Thermodynamic Evaluation of Liquid Metals as Heat Transfer Fluids in Concentrated Solar Power Plants. *Appl. Therm. Eng.* **2013**, *60* (1-2), 295–302.

(201) Cipollone, R.; Cinocca, A.; Gualtieri, A. Gases as Working Fluid in Parabolic Trough CSP Plants. *Procedia Comput. Sci.* **2013**, *19* (Seit), 702–711.

(202) López-González, D.; Valverde, J. L.; Sánchez, P.; Sanchez-Silva, L. Characterization of Different Heat Transfer Fluids and Degradation Study by Using a Pilot Plant Device Operating at Real Conditions. *Energy* **2013**, *54*, 240–250.

(203) Looser, R.; Vivar, M.; Everett, V. Spectral Characterisation and Long-Term Performance Analysis of Various Commercial Heat Transfer Fluids (HTF) as Direct-Absorption Filters for CPV-T Beam-Splitting Applications. *Appl. Energy* **2014**, *113*, 1496–1511.

(204) Valkenburg, M. E. Van; Vaughn, R. L.; Williams, M.; Wilkes, J. S. Thermochemistry of Ionic Liquid Heat-Transfer Fluids. *Thermochim. Acta* **2005**, *425* (1-2), 181–188.

(205) Fredlake, C. P.; Crosthwaite, J. M.; Hert, D. G.; Aki, S. N. V. K.; Brennecke, J. F. Thermophysical Properties of Imidazolium-Based Ionic Liquids. *J. Chem. Eng. Data* **2004**, *49* (4), 954–964.

(206) Pacio, J.; Wetzel, T. Assessment of Liquid Metal Technology Status and Research Paths for Their Use as Efficient Heat Transfer Fluids in Solar Central Receiver Systems. *Sol. Energy* **2013**, *93*, 11–22.

(207) Hirsch, T.; Feldhoff, J. F.; Hennecke, K.; Pitz-Paal, R. Advancements in the Field of Direct Steam Generation in Linear Solar Concentrators—A Review. *Heat Transf. Eng.* **2014**, *35* (3), 258–271.

(208) Raade, J. W.; Padowitz, D. Development of Molten Salt Heat Transfer Fluid With Low Melting Point and High Thermal Stability. *J. Sol. Energy Eng.* **2011**, *133* (3), 031013–031016.

(209) Moens, L.; Blake, D. M. Mechanism of Hydrogen Formation in Solar Parabolic Trough Receivers. *J. Sol. Energy Eng.* **2010**, *132* (3), 031006–031009.

(210) Kearney, D.; Herrmann, U.; Nava, P.; Kelly, B.; Mahoney, R.; Pacheco, J.; Cable, R.; Potrovitza, N.; Blake, D.; Price, H. Assessment of a Molten Salt Heat Transfer Fluid in a Parabolic Trough Solar Field. *J. Sol. Energy Eng.* **2003**, *125* (2), 170–176.

(211) Sohal, M. S.; Sabharwall, P.; Calderoni, P.; Wertsching, A. K.; Grover, S. B.; Grover, B. S. *Conceptual Design of Forced Convection Molten Salt Heat Transfer Testing Loop*; 2010.

(212) Janz, G. J. *Molten Salts Handbook*; Elsevier, 2013.

(213) Kearney, D.; Kelly, B.; Herrmann, U.; Cable, R.; Pacheco, J.; Mahoney, R.; Price, H.; Blake, D.; Nava, P.; Potrovitza, N. Engineering Aspects of a Molten Salt Heat Transfer Fluid in a Trough Solar Field. *Energy* **2004**, *29* (5-6), 861–870.

(214) Prigogine, I. Introduction to Thermodynamics of Irreversible Processes. *New York Interscience, 1967, 3rd ed.* **1967**.

(215) Cordaro, J. G.; Rubin, N. C.; Bradshaw, R. W. Multicomponent Molten Salt Mixtures Based on Nitrate/Nitrite Anions. *J. Sol. Energy Eng.* **2011**, *133* (1), 011014–4.

(216) Bradshaw, R. W.; Siegel, N. P. Molten Nitrate Salt Development for Thermal Energy Storage in Parabolic Trough Solar Power Systems. In *ASME 2008 2nd International Conference on Energy Sustainability, Volume 2*; ASME, 2008; pp 631–637.

(217) Seddon, K. R. Ionic Liquids for Clean Technology. *J. Chem. Technol. Biotechnol.* **1997**, *68* (4), 351–356.

(218) Timofeeva, E. V; Yu, W.; France, D. M.; Singh, D.; Routbort, J. L. Nanofluids for Heat Transfer: An Engineering Approach. *Nanoscale Res. Lett.* **2011**, *6* (1), 1–7.

(219) Mahian, O.; Kianifar, A.; Kalogirou, S. a.; Pop, I.; Wongwises, S. A Review of the Applications of Nanofluids in Solar Energy. *Int. J. Heat Mass Transf.* **2013**, *57* (2), 582–594.

(220) Kasaeian, A.; Eshghi, A. T.; Sameti, M. A Review of the Applications of Nanofluids in Solar Energy. *Int. J. Heat Mass Transf.* **2015**, *43*, 584–598.

(221) Wang, J. J.; Zheng, R. T.; Gao, J. W.; Chen, G. Heat Conduction Mechanisms in Nanofluids and Suspensions. *Nano Today* **2012**, *7* (2), 124–136.

(222) Otanicar, T. P.; Phelan, P. E.; Prasher, R. S.; Rosengarten, G.; Taylor, R. A. Nanofluid-Based Direct Absorption Solar Collector. *J. Renew. Sustain. Energy* **2010**, *2* (3), 033102–033108.

(223) Taylor, R. A.; Phelan, P. E.; Otanicar, T. P.; Adrian, R.; Prasher, R. Nanofluid Optical Property Characterization: Towards Efficient Direct Absorption Solar Collectors. *Nanoscale Res. Lett.* **2011**, *6* (1), 1–11.

(224) Javadi, F. S.; Saidur, R.; Kamalisarvestani, M. Investigating Performance Improvement of Solar Collectors by Using Nanofluids. *Renew. Sustain. Energy Rev.* **2013**, *28*, 232–245.

(225) Pacio, J.; Fritsch, a.; Singer, C.; Uhlig, R. Liquid Metals as Efficient Coolants for High-Intensity Point-Focus Receivers: Implications to the Design and Performance of next-Generation CSP Systems. *Energy Procedia* **2013**, *49*, 647–655.

(226) Frazer, D.; Stergar, E.; Cionea, C.; Hosemann, P. Liquid Metal as a Heat Transport Fluid for Thermal Solar Power Applications. *Energy Procedia* **2013**, *49*, 627–636.

(227) Warrier, G. R.; Ju, Y. S. Es2014-6611 Development of High Temperature Liquid Metal Heat Transfer. **2014**, 1–15.

(228) Energy, S. U. S. D. of. Concentrating Solar Power Program Review 2013. **2013**.

(229) Muñoz-Antón, J.; Rubbia, C.; Rovira, A.; Martínez-Val, J. M. Performance Study of Solar Power Plants with CO2 as Working Fluid. A Promising Design Window. *Energy Convers. Manag.* **2015**, *92*, 36–46.

(230) Cau, G.; Cocco, D.; Tola, V. Performance and Cost Assessment of Integrated Solar Combined Cycle Systems (ISCCSs) Using CO2 as Heat Transfer Fluid. *Sol. Energy* **2012**, *86* (10), 2975–2985.

(231) Dostal, V.; Hejzlar, P.; Driscoll, M. J. The Supercritical Carbon Dioxide Power Cycle: Comparison to Other Advanced Power Cycles. *Nucl. Technol.* **2006**, *154* (3), 283–301.

(232) Neises, T.; Turchi, C. A Comparison of Supercritical Carbon Dioxide Power Cycle Configurations with an Emphasis on CSP Applications. *Energy Procedia* **2014**, *49*, 1187–1196.

(233) Padilla, R. V.; Soo Too, Y. C.; Benito, R.; Stein, W. Exergetic Analysis of Supercritical CO2 Brayton Cycles Integrated with Solar Central Receivers. *Appl. Energy* **2015**, *148*, 348–365.

(234) Hischier, I. Experimental and Numerical Analyses of a Pressurized Air Receiver for Solar-Driven Gas Turbines. *J. Sol. Energy Eng.* **2012**, *134* (2), 021003–021008.

(235) Bader, R.; Barbato, M.; Pedretti, A.; Steinfeld, A. An Air-Based Cavity-Receiver for Solar Trough Concentrators. *J. Sol. Energy Eng.* **2010**, *132* (3), 031017–7.

(236) Biencinto, M.; González, L.; Zarza, E.; Díez, L. E.; Muñoz-Antón, J. Performance Model and Annual Yield Comparison of Parabolic-Trough Solar Thermal Power Plants with Either Nitrogen or Synthetic Oil as Heat Transfer Fluid. *Energy Convers. Manag.* **2014**, *87*, 238–249.

(237) Vargaftik, N. *Handbook of Physical Properties of Liquids and Gases : Pure Substances and Mixtures*; Begell: New York N.Y., 1996.

(238) Zarza, E.; Valenzuela, L.; León, J.; Hennecke, K.; Eck, M.; Weyers, H. D.; Eickhoff, M. Direct Steam Generation in Parabolic Troughs: Final Results and Conclusions of the DISS Project. *Energy* **2004**, *29* (5-6), 635–644.

(239) Zarza, E.; Rojas, M. E.; González, L.; Caballero, J. M.; Rueda, F. INDITEP: The First Pre-Commercial DSG Solar Power Plant. *Sol. Energy* **2006**, *80* (10), 1270–1276.

(240) ABENGOA SOLAR Annual report 2011.

(241) Feldhoff, J. F.; Benitez, D.; Eck, M.; Riffelmann, K.-J. Economic Potential of Solar Thermal Power Plants With Direct Steam Generation Compared With HTF Plants. *J. Sol. Energy Eng.* **2010**, *132* (4), 041001–041009.

(242) Barton, J. P.; Infield, D. G. Energy Storage and Its Use With Intermittent Renewable Energy. *IEEE Trans. Energy Convers.* **2004**, *19* (2), 441–448.

(243) Izquierdo, S.; Montañés, C.; Dopazo, C.; Fueyo, N. Analysis of CSP Plants for the Definition of Energy Policies: The Influence on Electricity Cost of Solar Multiples, Capacity Factors and Energy Storage. *Energy Policy* **2010**, *38* (10), 6215–6221.

(244) Bauer, T.; Steinmann, W.-D.; Laing, D.; Tamme, R. THERMAL ENERGY STORAGE MATERIALS AND SYSTEMS. *Annu. Rev. Heat Transf.* **2012**, *15* (15), 131–177.

(245) Kuravi, S.; Trahan, J.; Goswami, D. Y.; Rahman, M. M.; Stefanakos, E. K. Thermal Energy Storage Technologies and Systems for Concentrating Solar Power Plants. *Prog. Energy Combust. Sci.* **2013**, *39* (4), 285–319.

(246) IBRAHIM, H.; ILINCA, A.; PERRON, J. Energy Storage systems—Characteristics and Comparisons. *Renew. Sustain. Energy Rev.* **2008**, *12* (5), 1221–1250.

(247) Mills, A.; Wiser, R. *Changes in the Economic Value of Variable Generation at High Penetration Levels : A Pilot Case Study of California*; 2012.

(248) Lilliestam, J.; Bielicki, J. M.; Patt, A. G. Comparing Carbon Capture and Storage (CCS) with Concentrating Solar Power (CSP): Potentials, Costs, Risks, and Barriers. *Energy Policy* **2012**, *47*, 447–455.

(249) Rosen, M. A. Appropriate Thermodynamic Performance Measures for Closed Systems for Thermal Energy Storage. *J. Sol. Energy Eng.* **1992**, *114* (2), 100–105.

(250) Jegadheeswaran, S.; Pohekar, S. D.; Kousksou, T. Exergy Based Performance Evaluation of Latent Heat Thermal Storage System: A Review. *Renew. Sustain. Energy Rev.* **2010**, *14* (9), 2580–2595.

(251) Modi, A.; Pérez-Segarra, C. D. Thermocline Thermal Storage Systems for Concentrated Solar Power Plants: One-Dimensional Numerical Model and Comparative Analysis. *Sol. Energy* **2014**, *100*, 84–93.

(252) Yang, Z.; Garimella, S. V. Cyclic Operation of Molten-Salt Thermal Energy Storage in Thermoclines for Solar Power Plants. *Appl. Energy* **2013**, *103*, 256–265.

(253) Bauer, T.; Breidenbach, N.; Pfleger, N.; Laing, D. Overview of Molten Salt Storage Systems and Material Development for Solar Thermal Power Plants. In *Proceedings of the 2012 National Solar Conference for (SOLAR 2012)*; Denver, CO, 2012.

(254) Herrmann, U.; Kelly, B.; Price, H. Two-Tank Molten Salt Storage for Parabolic Trough Solar Power Plants. *Energy* **2004**, *29* (5-6), 883–893.

(255) Kearney, D.; Price, H. Assessment of Thermal Energy Storage for Parabolic Trough Solar Power Plants. In *Solar Energy*; ASME, 2004; pp 675–681.

(256) Brosseau, D.; Kelton, J. W.; Ray, D.; Edgar, M.; Chisman, K.; Emms, B. Testing of Thermocline Filler Materials and Molten-Salt Heat Transfer Fluids for Thermal Energy Storage Systems in Parabolic Trough Power Plants. *J. Sol. Energy Eng.* **2005**, *127* (1), 109–116.

(257) Liu, M.; Saman, W.; Bruno, F. Review on Storage Materials and Thermal Performance Enhancement Techniques for High Temperature Phase Change Thermal Storage Systems. *Renew. Sustain. Energy Rev.* **2012**, *16* (4), 2118–2132.

(258) Cabeza, L. F.; Sole, C.; Castell, A.; Oro, E.; Gil, A. Review of Solar Thermal Storage Techniques and Associated Heat Transfer Technologies. *Proc. IEEE* **2012**, *100* (2), 525–538.

(259) Medrano, M.; Gil, A.; Martorell, I.; Potau, X.; Cabeza, L. F. State of the Art on High-Temperature Thermal Energy Storage for Power Generation. Part 2—Case Studies. *Renew. Sustain. Energy Rev.* **2010**, *14* (1), 56–72.

(260) Geyer, M. A. Thermal Storage for Solar Power Plants. In *Solar Power Plants*; Springer Berlin Heidelberg, 1991; pp 199–214.

(261) Tufeu, R.; Petitet, J. P.; Denielou, L.; Le Neindre, B. Experimental Determination of the Thermal Conductivity of Molten Pure Salts and Salt Mixtures. *Int. J. Thermophys.* **1985**, *6* (4), 315–330.

(262) Tian, Y.; Zhao, C. Y. A Review of Solar Collectors and Thermal Energy Storage in Solar Thermal Applications. *Appl. Energy* **2013**, *104*, 538–553.

(263) Laing, D.; Steinmann, W.-D.; Tamme, R.; Richter, C. Solid Media Thermal Storage for Parabolic Trough Power Plants. *Sol. Energy* **2006**, *80* (10), 1283–1289.

(264) Pierson, H. O. *Handbook of Carbon, Graphite, Diamonds and Fullerenes: Processing, Properties and Applications*; William Andrew, 2012.

(265) Tamme, R.; Bauer, T.; Buschle, J.; Laing, D.; Müller-Steinhagen, H.; Steinmann, W.-D. Latent Heat Storage above 120°C for Applications in the Industrial Process Heat Sector and Solar Power Generation. *Int. J. Energy Res.* **2008**, *32* (3), 264–271.

(266) Steinmann, W.-D.; Eck, M. Buffer Storage for Direct Steam Generation. *Sol. Energy* **2006**, *80* (10), 1277–1282.

(267) Solucar. *10 MW Solar Thermal Power Plant for Southern Spain*; 2006.

(268) Peng, Q.; Yang, X.; Ding, J.; Wei, X.; Yang, J. Design of New Molten Salt Thermal Energy Storage Material for Solar Thermal Power Plant. *Appl. Energy* **2013**, *112*, 682–689.

(269) MacFarlane, D. R.; Tachikawa, N.; Forsyth, M.; Pringle, J. M.; Howlett, P. C.; Elliott, G. D.; Davis, J. H.; Watanabe, M.; Simon, P.; Angell, C. A. Energy Applications of Ionic Liquids. *Energy Environ. Sci.* **2014**, *7* (1), 232–250.

(270) Moens, L.; Blake, D. M.; Rudnicki, D. L.; Hale, M. J. Advanced Thermal Storage Fluids for Solar Parabolic Trough Systems. *J. Sol. Energy Eng.* **2003**, *125* (1), 112–116.

(271) Laing, D.; Bahl, C.; Bauer, T.; Fiss, M.; Breidenbach, N.; Hempel, M. High-Temperature Solid-Media Thermal Energy Storage for Solar Thermal Power Plants. *Proc. IEEE* **2012**, *100* (2), 516–524.

(272) Khare, S.; Dell'Amico, M.; Knight, C.; McGarry, S. Selection of Materials for High Temperature Sensible Energy Storage. *Sol. Energy Mater. Sol. Cells* **2013**, *115*, 114–122.

(273) Hale, M. *Survey of Thermal Storage for Parabolic Trough Power Plants*; 2000.

(274) Warerkar, S.; Schmitz, S.; Goettsche, J.; Hoffschmidt, B.; Reißel, M.; Tamme, R. Air-Sand Heat Exchanger for High-Temperature Storage. *J. Sol. Energy Eng.* **2011**, *133* (2), 021010–021017.

(275) Iniesta, A.; Martínez, M.; Delclos, T. Gravity-Fed Combined Solar Receiver/storage System Using Sand Particles as Heat Collector, Heat Transfer and Thermal Energy Storage Media. *SolarPACES …* **2014**.

(276) Bai, F.; Xu, C. Performance Analysis of a Two-Stage Thermal Energy Storage System Using Concrete and Steam Accumulator. *Appl. Therm. Eng.* **2011**, *31* (14-15), 2764–2771.

(277) Energy, G. Graphite Energy http://www.graphiteenergy.com/.

(278) Mehling, H.; Cabeza, L. F. *Heat and Cold Storage with PCM*; Heat and Mass Transfer; Springer Berlin Heidelberg: Berlin, Heidelberg, 2008.

(279) Hoshi, A.; Mills, D. R.; Bittar, A.; Saitoh, T. S. Screening of High Melting Point Phase Change Materials (PCM) in Solar Thermal Concentrating Technology Based on CLFR. *Sol. Energy* **2005**, *79* (3), 332–339.

(280) Kenisarin, M. M. High-Temperature Phase Change Materials for Thermal Energy Storage. *Renew. Sustain. Energy Rev.* **2010**, *14* (3), 955–970.

(281) Ge, Z.; Ye, F.; Cao, H.; Leng, G.; Qin, Y.; Ding, Y. Carbonate-Salt-Based Composite Materials for Medium- and High-Temperature Thermal Energy Storage. *Particuology* **2014**, *15*, 77–81.

(282) Wang, X.; Liu, J.; Zhang, Y.; Di, H.; Jiang, Y. Experimental Research on a Kind of Novel High Temperature Phase Change Storage Heater. *Energy Convers. Manag.* **2006**, *47* (15-16), 2211–2222.

(283) Steinmann, W.-D.; Tamme, R. Latent Heat Storage for Solar Steam Systems. *J. Sol. Energy Eng.* **2008**, *130* (1), 011004–011005.

(284) Ji, H.; Sellan, D. P.; Pettes, M. T.; Kong, X.; Ji, J.; Shi, L.; Ruoff, R. S. Enhanced Thermal Conductivity of Phase Change Materials with Ultrathin-Graphite Foams for Thermal Energy Storage. *Energy Environ. Sci.* **2014**, *7* (3), 1185–1192.

(285) Zhao, C. Y.; Wu, Z. G. Heat Transfer Enhancement of High Temperature Thermal Energy Storage Using Metal Foams and Expanded Graphite. *Sol. Energy Mater. Sol. Cells* **2011**, *95* (2), 636–643.

(286) Petrasch, J.; Klausner, J. Integrated Solar Thermochemical Cycles for Energy Storage and Fuel Production. *Wiley Interdisc. Rev. Energy Environ.* **2012**, *1* (3), 347–361.

(287) Pardo, P.; Deydier, A.; Anxionnaz-Minvielle, Z.; Rougé, S.; Cabassud, M.; Cognet, P. A Review on High Temperature Thermochemical Heat Energy Storage. *Renew. Sustain. Energy Rev.* **2014**, *32*, 591–610.

(288) Steinfeld, A. THERMOCHEMICAL PRODUCTION OF SYNGAS USING CONCENTRATED SOLAR ENERGY. *Annu. Rev. Heat Transf.* **2012**, *15* (15), 255–275.

(289) Weber, R.; Dorer, V. Long-Term Heat Storage with NaOH. *Vacuum* **2008**, *82* (7), 708–716.

(290) Lovegrove, K.; Luzzi, A.; Soldiani, I.; Kreetz, H. Developing Ammonia Based Thermochemical Energy Storage for Dish Power Plants. *Sol. Energy* **2004**, *76* (1-3), 331–337.

(291) Azpiazu, M. N.; Morquillas, J. M.; Vazquez, A. Heat Recovery from a Thermal Energy Storage Based on the Ca(OH)2/CaO Cycle. *Appl. Therm. Eng.* **2003**, *23* (6), 733–741.

(292) Schaube, F.; Kohzer, A.; Schütz, J.; Wörner, A.; Müller-Steinhagen, H. De- and Rehydration of Ca(OH)2 in a Reactor with Direct Heat Transfer for Thermo-Chemical Heat Storage. Part A: Experimental Results. *Chem. Eng. Res. Des.* **2013**, *91* (5), 856–864.

(293) Schaube, F.; Wörner, A.; Tamme, R. High Temperature Thermochemical Heat Storage for Concentrated Solar Power Using Gas–Solid Reactions. *J. Sol. Energy Eng.* **2011**, *133* (3), 031006–031007.

(294) Felderhoff, M.; Bogdanović, B. High Temperature Metal Hydrides as Heat Storage Materials for Solar and Related Applications. *Int. J. Mol. Sci.* **2009**, *10* (1), 325–344.

(295) Aihara, M.; Nagai, T.; Matsushita, J.; Negishi, Y.; Ohya, H. Development of Porous Solid Reactant for Thermal-Energy Storage and Temperature Upgrade Using Carbonation/decarbonation Reaction. *Appl. Energy* **2001**, *69* (3), 225–238.

(296) Meier, A.; Bonaldi, E.; Cella, G. M.; Lipinski, W.; Wuillemin, D.; Palumbo, R. Design and Experimental Investigation of a Horizontal Rotary Reactor for the Solar Thermal Production of Lime. *Energy* **2004**, *29* (5-6), 811–821.

(297) Price, H. Assessment of Parabolic Trough and Power Tower Solar Technology Cost and Performance Forecasts. *Natl. Renew. Energy Lab. Golden, CO* **2003**.

(298) Dunham, M. T.; Iverson, B. D. High-Efficiency Thermodynamic Power Cycles for Concentrated Solar Power Systems. *Renew. Sustain. Energy Rev.* **2014**, *30*, 758–770.

(299) Deng, H.; Boehm, R. F. An Estimation of the Performance Limits and Improvement of Dry Cooling on Trough Solar Thermal Plants. *Appl. Energy* **2011**, *88* (1), 216–223.

(300) Bejan, A. Models of Power Plants That Generate Minimum Entropy While Operating at Maximum Power. *Am. J. Phys.* **1996**, *64* (8), 1054–1059.

(301) Weitzel, P. S. Steam Generator for Advanced Ultra Supercritical Power Plants 700C to 760C. In *ASME 2011 Power Conference, Volume 1*; ASME, 2011; pp 281–291.

(302) Turchi, C. S.; Ma, Z.; Neises, T. W.; Wagner, M. J. Thermodynamic Study of Advanced Supercritical Carbon Dioxide Power Cycles for Concentrating Solar Power Systems. *J. Sol. Energy Eng.* **2013**, *135* (4), 041007–7.

(303) Chiesa, P.; Macchi, E. A Thermodynamic Analysis of Different Options to Break 60% Electric Efficiency in Combined Cycle Power Plants. In *Volume 1: Turbo Expo 2002*; ASME, 2002; pp 987–1002.

(304) Kongtragool, B.; Wongwises, S. A Review of Solar-Powered Stirling Engines and Low Temperature Differential Stirling Engines. *Renew. Sustain. Energy Rev.* **2003**, *7* (2), 131–154.

(305) Yeo, W. H.; Fry, A. T.; Purbolaksono, J.; Ramesh, S.; Inayat-Hussain, J. I.; Liew, H. L.; Hamdi, M. Oxide Scale Growth and Presumed Exfoliation in a 700°C or Higher Steam Condition: A Simulation Study for Future Operations of Ultra-Supercritical Power Plants. *J. Supercrit. Fluids* **2014**, *92*, 215–222.

(306) Iverson, B. D.; Conboy, T. M.; Pasch, J. J.; Kruizenga, A. M. Supercritical CO2 Brayton Cycles for Solar-Thermal Energy. *Appl. Energy* **2013**, *111*, 957–970.

(307) Turchi, C. *10 MW Supercritical CO2 Turbine Test*; Golden, CO (United States), 2014.

(308) Cheang, V. T.; Hedderwick, R. A.; McGregor, C. Benchmarking Supercritical Carbon Dioxide Cycles against Steam Rankine Cycles for Concentrated Solar Power. *Sol. Energy* **2015**, *113*, 199–211.

(309) Dersch, J.; Geyer, M.; Herrmann, U.; Jones, S. A.; Kelly, B.; Kistner, R.; Ortmanns, W.; Pitz-Paal, R.; Price, H. Trough Integration into Power Plants—a Study on the Performance and Economy of Integrated Solar Combined Cycle Systems. *Energy* **2004**, *29* (5-6), 947–959.

(310) Spelling, J.; Favrat, D.; Martin, A.; Augsburger, G. Thermoeconomic Optimization of a Combined-Cycle Solar Tower Power Plant. *Energy* **2012**, *41* (1), 113–120.

(311) Kribus, A.; Zaibel, R.; Carey, D.; Segal, A.; Karni, J. A Solar-Driven Combined Cycle Plant. *Sol. Energy* **1998**, *62* (2), 121–129.

(312) SALEH, B.; KOGLBAUER, G.; WENDLAND, M.; FISCHER, J. Working Fluids for Low-Temperature Organic Rankine Cycles. *Energy* **2007**, *32* (7), 1210–1221.

(313) Kalina, A. I. Combined-Cycle System With Novel Bottoming Cycle. *J. Eng. Gas Turbines Power* **1984**, *106* (4), 737–742.

(314) Ho, T.; Mao, S. S.; Greif, R. Comparison of the Organic Flash Cycle (OFC) to Other Advanced Vapor Cycles for Intermediate and High Temperature Waste Heat Reclamation and Solar Thermal Energy. *Energy* **2012**, *42* (1), 213–223.

(315) McEnaney, K.; Kraemer, D.; Chen, G. Direct Heat-to-Electricity Conversion of Solar Energy. *Annu. Rev. Heat Transf.* **2012**, 179–230.

(316) Goldsmid, H. J. *Applications of Thermoelectricity*; Methuen: London, 1960.

(317) Rowe, D. M. Thermoelectrics, an Environmentally-Friendly Source of Electrical Power. *Renew. Energy* **1999**, *16* (1-4), 1251–1256.

(318) Rowe, D. M. CRC Handbook of Thermoelectrics. *New York* **1995**, *16* (1-4), 1251–1256.

(319) Goldsmid, H. J. Principles of Thermoelectric Devices. *Br. J. Appl. Phys.* **1960**, *11* (6), 209–217.

(320) Biswas, K.; He, J.; Blum, I. D.; Wu, C.-I.; Hogan, T. P.; Seidman, D. N.; Dravid, V. P.; Kanatzidis, M. G. High-Performance Bulk Thermoelectrics with All-Scale Hierarchical Architectures. *Nature* **2012**, *489* (7416), 414–418.

(321) Poudel, B.; Hao, Q.; Ma, Y.; Lan, Y.; Minnich, A.; Yu, B.; Yan, X.; Wang, D.; Muto, A.; Vashaee, D.; et al. High-Thermoelectric Performance of Nanostructured Bismuth Antimony Telluride Bulk Alloys. *Science (80-.).* **2008**, *320* (5876), 634–638.

(322) Joshi, G.; Lee, H.; Lan, Y.; Wang, X.; Zhu, G.; Wang, D.; Gould, R. W.; Cuff, D. C.; Tang, M. Y.; Dresselhaus, M. S.; et al. Enhanced Thermoelectric Figure-of-Merit in Nanostructured P-Type Silicon Germanium Bulk Alloys. *Nano Lett.* **2008**, *8* (12), 4670–4674.

(323) Hsu, K. F.; Loo, S.; Guo, F.; Chen, W.; Dyck, J. S.; Uher, C.; Hogan, T.; Polychroniadis, E. K.; Kanatzidis, M. G. Cubic AgPb(m)SbTe(2+m): Bulk Thermoelectric Materials with High Figure of Merit. *Science* **2004**, *303* (5659), 818–821.

(324) Nolas, G. S.; Morelli, D. T.; Tritt, T. M. SKUTTERUDITES: A Phonon-Glass-Electron Crystal Approach to Advanced Thermoelectric Energy Conversion Applications. *Annu. Rev. Mater. Sci.* **1999**, *29* (1), 89–116.

(325) Zebarjadi, M.; Esfarjani, K.; Dresselhaus, M. S.; Ren, Z. F.; Chen, G. Perspectives on Thermoelectrics: From Fundamentals to Device Applications. *Energy Environ. Sci.* **2012**, *5* (1), 5147–5162.

(326) Kraemer, D.; Chen, G. High-Accuracy Direct ZT and Intrinsic Properties Measurement of Thermoelectric Couple Devices. *Rev. Sci. Instrum.* **2014**, *85* (4), 045107–045112.

(327) Rowe, D. M.; Min, G. Evaluation of Thermoelectric Modules for Power Generation. *J. Power Sources* **1998**, *73* (2), 193–198.

(328) Kraemer, D.; Sui, J.; McEnaney, K.; Zhao, H.; Jie, Q.; Ren, Z. F.; Chen, G. High Thermoelectric Conversion Efficiency of MgAgSb-Based Material with Hot-Pressed Contacts. *Energy Environ. Sci.* **2015**, *8* (4), 1299–1308.

(329) Telkes, M. Solar Thermoelectric Generators. *J. Appl. Phys.* **1954**, *25* (6), 765–777.

(330) McEnaney, K.; Kraemer, D.; Ren, Z.; Chen, G. Modeling of Concentrating Solar Thermoelectric Generators. *J. Appl. Phys.* **2011**, *110* (7), 074502–074508.

(331) Baranowski, L. L.; Snyder, G. J.; Toberer, E. S. Concentrated Solar Thermoelectric Generators. *Energy Environ. Sci.* **2012**, *5* (10), 9055–9067.

(332) Baranowski, L. L.; Warren, E. L.; Toberer, E. S. High-Temperature High-Efficiency Solar Thermoelectric Generators. *J. Electron. Mater.* **2014**.

(333) Chávez Urbiola, E. A.; Vorobiev, Y. Investigation of Solar Hybrid Electric/thermal System with Radiation Concentrator and Thermoelectric Generator. *Int. J. Photoenergy* **2013**, *2013* (4), 704087–7.

(334) Kraemer, D.; McEnaney, K.; Liu, W.-S.; Jie, Q.; Cao, F.; Weinstein, L. A.; Ren, Z.; Chen, G. High-Efficiency Segmented Solar Thermoelectric Generators with Optical Concentration. *Submitt. to Nat. Mater.* **2015**.

(335) Chan, W. R.; Bermel, P.; Pilawa-Podgurski, R. C. N.; Marton, C. H.; Jensen, K. F.; Senkevich, J. J.; Joannopoulos, J. D.; Soljacic, M.; Celanovic, I. Toward High-Energy-Density, High-Efficiency, and Moderate-Temperature Chip-Scale Thermophotovoltaics. *Proc. Natl. Acad. Sci. U. S. A.* **2013**, *110* (14), 5309–5314.

(336) Li, W.; Guler, U.; Kinsey, N.; Naik, G. V.; Boltasseva, A.; Guan, J.; Shalaev, V. M.; Kildishev, A. V. Plasmonics: Refractory Plasmonics with Titanium Nitride: Broadband Metamaterial Absorber (Adv. Mater. 47/2014). *Adv. Mater.* **2014**, *26* (47), 7921–7921.

(337) Datas, A.; Algora, C. Development and Experimental Evaluation of a Complete Solar Thermophotovoltaic System. *Prog. Photovoltaics Res. Appl.* **2013**, *21* (5), 1025–1039.

(338) Shimizu, M.; Kohiyama, A.; Yugami, H. 10% Efficiency Solar Thermophotovoltaic Systems Using Spectrally Controlled Monolithic Planar Absorber/Emitters. *SPIE Photonics Eur.* **2014**, *9140*, 91400P.